University of Bremen

Reconstruction of late Quaternary sedimentary environments at the southern Mendeleev Ridge (Arctic Ocean)

A thesis submitted in order to obtain a Doctoral degree in Earth Sciences

Dissertation zur Erlangung
des akademischen Grades eines Doktors der Naturwissenschaften:
Doctor rerum naturalium (**Dr. rer. nat.**)
An der Fakultät für Geowissenschaften

By

Evgenia A. Bazhenova

Supervisors: **Prof. Dr. Rüdiger Stein**
Alfred Wegener Institute for Polar and Marine Research, Bremerhaven

Prof. Dr. Georgy A. Cherkashov
Faculty of Geology, St. Petersburg State University, Russia
All-Russia Research Institute for Geology and Mineral Resources
of the World Ocean (VNIIOkeangeologia)

Date of colloquium: 09.11.2012

Abstract

The late Pleistocene history of the Arctic comprised cyclical changes in the extension of land-based ice sheets and sea-ice cover that affected sedimentary environments in the Arctic Ocean. This PhD thesis focuses on sediment records from the Mendeleev Ridge spanning the last 200 ka. Over this time period, variable sedimentation patterns were described and possible implications for reconstruction of glacial/interglacial paleoenvironments were provided. One of the main goals of this study was to identify mineralogical and inorganic-geochemical tracers in marine sediments that could be used for discrimination of sediment provenance and consequently for reconstruction of sediment pathways.

In *Chapter 5* possibility of provenance discrimination based on bulk mineral composition of surface sediments is discussed. This study compares the results from two software packages, RockJock and QUAX, for quantification of mineral assemblages from the X-Ray diffraction (XRD) data. Comparison with published overviews on the mineral composition of Arctic Ocean surface sediments demonstrates that in provenance studies bulk mineral composition of sediments should be used along with other indicators for source areas.

In *Chapter 6* stratigraphy for 4 cores recovered along a transect at ca. 77°36'N across the Mendeleev Ridge during the ARK-XXIII/3 Expedition of RV "Polarstern" was revised using paleomagnetic parameters (inclination and paleointensity) supported by AMS ^{14}C datings and micropaleontological evidences. Changes of sedimentary settings from the Mendeleev Ridge towards the East Siberian Sea margin were documented for the last 200 ka. As evidenced by grain-size and mineralogical data, there were several events of intensified sediment discharge at the Mendeleev Ridge possibly linked to paleoenvironmental changes in North America and Eurasia.

Chapter 7 describes provenance investigations using the isotopic composition of radiogenic lead (Pb) and neodymium (Nd) of detrital fraction in core PS72/340-5 at the eastern flank of the Mendeleev Ridge. Obtained results were compared with marine surface sediment data and values for the circum-Arctic subaerial provinces. Late Quaternary sediment supply variability was analyzed using the mixing model constrained by two tracers: $^{207}Pb/^{206}Pb$ and εNd. Our results confirm that over the last 200 ka dolomite-rich pink layers at the southern Mendeleev Ridge were deposited during events associated with intensified iceberg transport from North America. On the whole, sedimentation was mostly controlled by terrigenous input from the Chukchi and East Siberian Seas whereas sediment supply from the Laptev Sea area remained less important and relatively constant at the studied location.

Zusammenfassung

Der spätquartäre Wechsel von Glazialen und Interglazialen in der Arktis besitzte einen bedeutenden Einfluss auf die unterschiedlichen Sedimentationsprozesse im Arktischen Ozean. Die vorliegende Arbeit rekonstruiert die Entwicklungen der letzten 200.000 Jahre durch Bearbeitung eines Profils von Sedimentkernen, die auf der „Polarstern"-Expedition ARK-XXIII/3 (Arctic-2008) in der Umgebung des Mendeleew-Rückens gewonnen wurden. Das Hauptziel dieser Arbeit war es, die Herkunftsgebiete des terrigenen Materials anhand der spezifischen Mineralvergesellschaftungen beziehungsweise geochemischen Parameter in Sedimenten zu identifizieren.

In der erste Studie (*Kapitel 5)* wurde die Gesamtmineralogie der Oberflächensedimente im Amerasischen Becken untersucht. Die Ergebnisse der Röntgendiffraktometeranalysen wurden mittels den zwei Softwarepaketen, RockJock und QUAX, bewertet. Der Vergleich mit veröffentlichten Übersichten auf den Mineralvergesellschaftungen von Oberflächensedimenten der Region demonstriert, dass die Gesamtmineralogie zusammen mit anderen Hinweisen auf Herkunftsgebiete verwendet werden sollte.

In der zweite Studie (*Kapitel 6)* wurde die Stratigraphie der untersuchten Kerne mittels Variationen gesteinsmagmatischer Parameter in Sedimenten, der absoluter AMS-^{14}C-Datierung, dem Vorkommen und den Vergesellschaftungen von benthischen Foraminiferen erstellt. Damit wurden die unterschiedliche hochglazialen/interglazialen Bedingungen und Transportprozessen für die letzten 200.000 Jahre in der Umgebung des Mendeleew-Rückens beschrieben.

In der dritte Studie (*Kapitel 7)* wurden die potentiellen Liefergebiete auf der Auswertung der geochemischen Signaturen (^{207}Pb/^{206}Pb and εNd) festgestellt. Diese Studie zeigt, dass in den letzten 200.000 Jahren erhöhte Einträge vom eisbergtransportierten Material mit dem Leitmineral Dolomit aus dem Kanadischen Arktischen Archipel auf dem Mendeleew-Rücken erfolgten. Generell wurde die Sedimentationsprozesse durch Sedimentzufuhr mit Chukchi/Ostsibirische-See-Signatur kontrolliert.

Acknowledgements

This page is to express my sincere thanks to the many people that have provided help during my PhD study at the Alfred Wegener Institute in Bremerhaven in 2009-2012. First I would like to thank my supervisor in Bremerhaven, Prof. Dr. Rüdiger Stein, who invited me to participate in the ARK-XXIII/3 Expedition onboard "Polarstern" in 2008, consequently to write my master thesis and afterwards to do a PhD study at the AWI. He helped me over these years through continuous discussions and suggestions, as well as encouraged me to try and learn different approaches and methods of research. I would also like to thank my supervisor from St. Petersburg, Prof. Dr. Georgy A. Cherkashov, who supported my PhD study through cooperation and critical discussions and helped me to stay in touch with the scientific community in Russia.

Jens Matthiessen (AWI) and Seung-Il Nam (KOPRI) are thanked for friendly scientific discussions and new ideas for my research. Christoph Vogt (University of Bremen) shared a lot of knowledge on mineralogical analysis and marine geology of the Arctic with me and spent time on the joint manuscript providing plenty of critical comments, which is greatly appreciated. Alexey Krylov (VNIIO) is thanked for numerous scientific debates, contribution to my research through new ideas, and his deep interest in the Arctic geomarine research which inspired me to keep the motivation during the hard times in Bremerhaven. I am very thankful to Nathalie Fagel who invited me for a research stay at the University of Liege and initiated our joint work on the isotopic composition of radiogenic Pb and Nd. I greatly appreciate the wiliness of Leonid Polyak (Ohio State University) to discuss different issues on the Arctic Ocean paleoceanography.

Fellow PhD students from the AWI, Uni Bremen, Hamburg and Kiel are thanked for making me company during the various parts of these long three years. I especially owe many thanks to David Naafs, for discussions, critics, help and support, and everything else.

I am undoubtedly grateful to my family for support throughout my whole life. Special thanks to my friends from Russia who stayed in permanent contact with me and helped me to survive these three years away from home.

AWI provided a very good laboratory for sedimentological and mineralogical investigations. Rita Fröhlking is especially thanked for guidance and help in the lab. This PhD study was conducted in the frame of the Helmholtz Graduate School for Polar and Marine Research (POLMAR) that also provided travel support for participation in many conferences in these 3 years and financed a 3-month research stay at the University of Liege in 2012. Additional support for participation in conferences and measurements came from the host Department for Marine Geology and Paleontology at the AWI. ECORD travel grant gave me an opportunity to take part in the IODP-Canada Summer School 2010. Participation in grants of the Otto-Schmidt-Laboratory (2011, 2012) and of the Russian Foundation for Basic Research (2012) provided additional help in research activities and scientific mobility.

Table of contents

1 General introduction and outline

The late Pleistocene history of the Arctic comprised cyclical changes in the extension of land-based ice sheets and sea-ice cover that affected sedimentary environments in the Arctic Ocean. This PhD thesis focuses on sediment records spanning the last 200 ka. Studied cores were recovered at the southern Mendeleev Ridge during the ARK-XXIII/3 Expedition of RV "Polarstern". For the studied time interval, variable sedimentation patterns at the Mendeleev Ridge were described and possible implications for reconstruction of glacial/interglacial paleoenvironments were provided. One of the main goals of this study was to identify tracers in marine sediments that could be used for discrimination of source areas for terrigenous material and consequently for reconstruction of sediment pathways.

In the first three chapters of this thesis a general introduction to the topic is provided. *Chapter 2* gives an overview about the oceanographic setting in the Arctic Ocean. *Chapter 3* introduces the materials and methods used in this study. *Chapter 4* provides an overview of the up-to-date state of knowledge on the Arctic glacial/interglacial history. This introductive part of the thesis is followed by three chapters (*Ch. 5, Ch. 6, Ch. 7*) that contain the manuscripts in preparation which present the main results related to the research objectives.

Chapter 5: "Bulk mineral composition of surface sediments in the Arctic Ocean revisited", in preparation for *Letters* in *Marine Geology*.

Chapter 6: "Study of core records from the southern Mendeleev Ridge: stratigraphy revised using paleomagnetic data and implications for glacial/interglacial variability", in preparation for *Quaternary Science Reviews*.

Chapter 7: "Provenance discrimination in sediments from the Mendeleev Ridge: new insights from the radiogenic Pb and Nd signature of detrital fraction", in preparation for *Geochimica et Cosmochimica Acta*.

In these manuscripts research questions stated below will be addressed.

Q1: Is there any mineralogical tracer in Arctic Ocean sediments which can be used to determine the sediment source area? Can results from published studies be compared?

In *Chapter 5*, possibility of provenance discrimination based on bulk mineral composition of surface sediments is discussed. This study compares the results from two software packages, RockJock and QUAX, for quantification of mineral assemblages from the X-Ray diffraction (XRD) data. We show that a quite good correlation between RockJock and QUAX results is observed for non-clay minerals while contents of clay minerals should be

reported cautiously as it is difficult to distinguish some of these minerals without special treatment. In summary, results of the two methods can be compared when the relative proportions of mineral contents are used. Comparison with published overviews on the mineral composition of Arctic Ocean surface sediments demonstrates that in provenance studies bulk mineral composition of sediments should be used along with other indicators for source areas.

Q2: How did sedimentary settings at the Mendeleev Ridge changed over the last 200 ka?

In *Chapter 6*, stratigraphy for core records is revised. As evidenced by grain-size and mineralogical data, there were several events of intensified sediment discharge at the Mendeleev Ridge possibly linked to paleoenvironmental changes in North America and Eurasia. However additional information on the ice-rafted debris provenance is needed to differentiate between potential sediment source areas.

Q3: How did the sediment provenance in Arctic Ocean sediments change over the last 200 ka? Did the ice rafted debris from North America reach the Eurasian continental margin and shelf seas?

In *Chapter 7*, new insights into the source discrimination from the radiogenic lead and neodymium signature of marine sediments are provided. The results indicate that over the last 200 ka dolomite-rich pink layers at the southern Mendeleev Ridge were deposited during events associated with intensified iceberg transport from North America. On the whole, sedimentation was mostly controlled by terrigenous input from the Chukchi and East Siberian Seas whereas sediment supply from the Laptev Sea area remained less important and relatively constant at the studied location.

To conclude, *Chapter 8* summarizes the main conclusions and provides an outlook on the possible future investigations.

2 Arctic Ocean: oceanographic setting

The Arctic Ocean is surrounded by the North American and Eurasian land masses and is remarkable for the vast continental shelf areas that make up 53% of its total area. Shelf seas of northern Europe and Asia have a similar shape, with typical depths of 0 to 50 m (Fig. 1). The East Siberian and Laptev Seas together with the Chukchi Sea form a large flat shallow shelf province composing as much as 22% of the entire Arctic Ocean area but only 1% of the volume. This implies that Arctic Ocean circulation might be very sensitive to eustatic sea-level changes (Jakobsson, 2002).

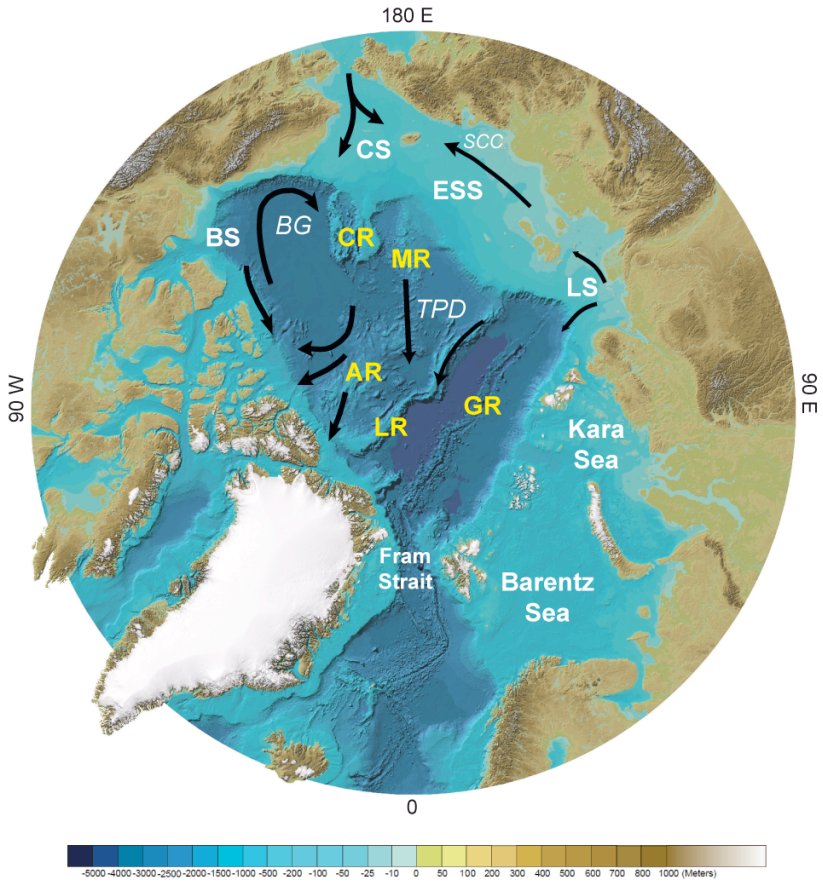

Figure 1. Bathymetric map of the Arctic Ocean, IBCAO (Jakobsson et al., 2008). Black arrows mark the directions of major surface current systems (here the main focus is on the Amerasian Basin, see text): *BG* – Beaufort Gyre, *TPD* – Transpolar Drift, *SCC* – Siberian Coastal Current. Names of shelf seas are indicated in white colour: CS – Chukchi Sea, ESS – East Siberian Sea, LS – Laptev Sea, KS – Kara Sea, BS – Beaufort Sea. Major geomorphologic features are indicated in yellow font: CR – Chukchi Rise, MR – Mendeleev Ridge, AR – Alpha Ridge, LR – Lomonosov Ridge, GR – Gakkel Ridge.

Beyond the shelf breaks are the relatively steep continental slopes coming to the flat abyssal plains. The central Arctic Ocean is divided into deep basins by three main ridge systems (Fig. 1). Gakkel Ridge is parallel to the shelf break of northern Eurasia. The next elevated geomorphologic feature, Lomonosov Ridge, divides the Arctic Ocean into two parts: the Amerasian Basin and Eurasian Basins. Our study area, Mendeleev Ridge is the largest submarine system in the Arctic Ocean that together with the Alpha Ridge stretches from the Canadian Continental Margin northwest of Ellesmere Island to the Eurasian Continental Margin north of Wrangel Island. It is a morphologically complex feature with numerous seamounts and sea valleys with depths varying from more than 2000 to 740 m below sea level (Jakobsson et al., 2003).

The present-day current pattern in the Arctic Ocean (Fig. 1) is determined by interaction of Atlantic and Pacific saline water masses together with the freshwater inflow from rivers draining the Arctic hinterland. Warm Atlantic waters follow the shelf break of the Eurasian seas submerging due to their high salinity and then follow the bathymetry to the deep basins (Schlosser et al., 1995). Pacific water masses enter the Arctic Ocean via the Bering Strait and then penetrate into the Chukchi and Beaufort Seas. Currently, the front between Atlantic and Pacific components in subsurface waters is located along the Mendeleev Ridge (Macdonald et al., 2000, and references therein). There are two main systems of oceanic surface currents. In the Canadian Basin, the surface oceanic circulation is dominated by the Beaufort Gyre (e.g. Polyak and Jakobsson, 2011). The second large system, Transpolar Drift, leads to the movement of sea-ice away from the Siberian coast, across the Arctic basin, and south through the Fram Strait (Rudels et al., 2004). The Siberian Coastal Current, forced by winds, river outflows and ice melt, flows from the ESS eastward (Weingartner et al., 1999).

As the oceanic circulation is strongly coupled to bathymetry (Huh et al., 1997; Schlosser et al., 1995) and sea-level changes (Jakobsson, 2002), sediment cores taken from the ridge systems that provide demarcation between water masses can serve as a good archive of sedimentary paleoenvironments in the Arctic Ocean. Core locations at ridges also enable better recovery of longer sedimentary records due to the general offshore decrease in sedimentation rates (Backman et al., 2004; Polyak et al., 2009).

3 Materials and methods

This research is based on Arctic Ocean marine sediment cores recovered during the ARK-XXIII/3 Expedition of German RV "Polarstern" in 2008. Here we used 4 cores from the "southern" transect at ca. 77°36'N cored across the Mendeleev Ridge towards the ESS continental margin (Fig. 2; see Table 1 for coordinates).

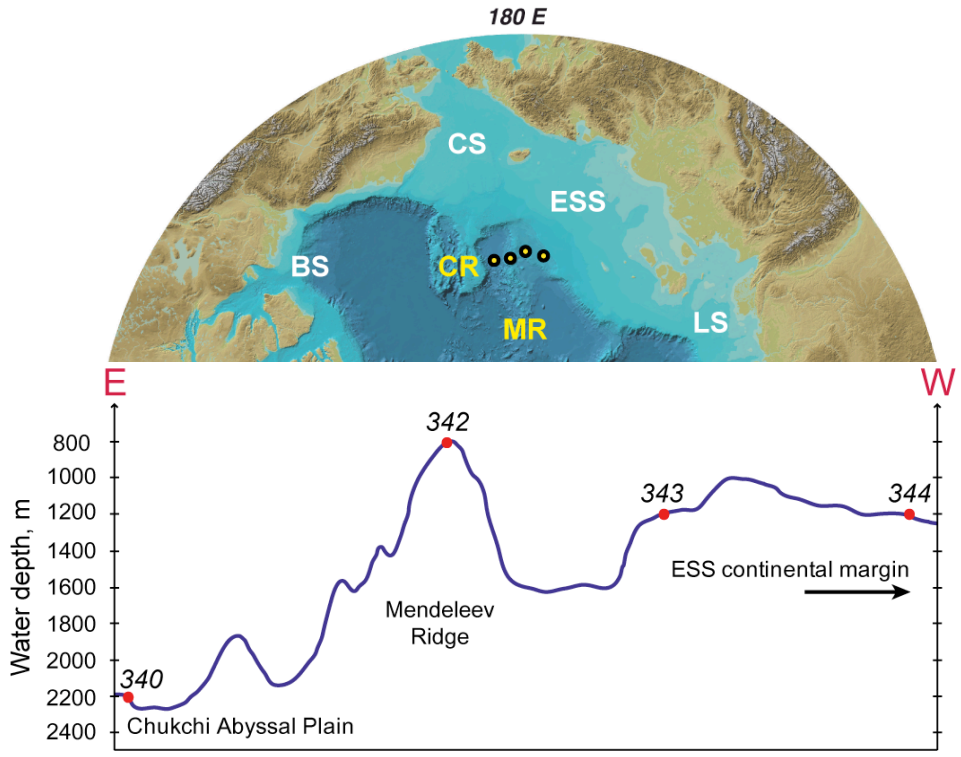

Figure 2. Bathymetric profile showing the depths of coring sites from the ARK-XXIII/3 Expedition used in this study: 344 - PS72/344-3, 343 – PS72/343-1, 342 – PS72/342-1, 340 – PS72/340-5. Inlay map shows these 4 coring locations at the Mendeleev Ridge. Names of shelf seas are indicated in white colour: CS – Chukchi Sea, ESS – East Siberian Sea, LS – Laptev Sea, BS – Beaufort Sea.

Table 1. Coring sites of the ARK-XXIII/3 Expedition used in this study

Core ID	PS72/340-5	PS72/342-1	PS 72/343-1	PS 72/344-3
Position	77° 36.31' N 171° 29.09' W	77° 36.01' N 177° 20.62' W	77° 18.33' N 179° 2.99' E	77° 36.62' N 174° 32.37' E
Water depth, m	2349	820	1227	1257
Recovery, cm	809	320	704	820
Gear	Kastenlot*	Gravity corer	Gravity corer	Kastenlot

*Square barrel gravity corer

3.1 Shipboard measurements

Standard descriptions and measurements on split core halves were performed by the shipboard Geology Group. Changes in sediment colour were visually described using the Munsell Colour Chart (1974), as well as spectral reflectance was measured at 1-cm intervals with a hand-held spectrophotometer Minolta CM 2002 at wave lengths from 400 to 700 nm (10nm steps). Output files contain the L*a*b* colour space that is also referred to as CIELAB space (Commission Internationale de l´Éclairage L*a*b colour space 1976). Lightness L* (grey scale) is recorded from 0 % (black) to 100% (white), the red-green colour space a* from -4 (green) to 16 (red), and the yellow-blue colour space b* from 0 (blue) to 40 (yellow). Logging was performed using a GEOTEK Multi-Sensor-Core-Logger, when sediment density, p-wave velocity, and magnetic susceptibility were measured at 1-cm intervals. Discrete shear strength measurements were conducted on fresh core halves according to the lithology at 5- to 10-cm intervals. Slabs for the X-ray radiography were taken to estimate the IRD contents and to study sediment structures. Details on the shipboard measurements are given in the ARK-XXIII/3 Cruise Report (Jokat, 2009). If not stated below, all the other measurements were performed at the Alfred Wegener Institute in Bremerhaven, starting with digital imaging of all the cores. Below a brief overview of methods applied by the author during the PhD study will be given, more details and descriptions of approaches used in the joint studies will be provided in *Chapters 5-7*.

In this study inorganic sediment properties were investigated. Samples were taken from core halves every 5-10 cm according to changes in lithology (colour and grain size) and additionally at 1 cm in the coarse-grained intervals. Samples were frozen and dried in the freeze-dryer. All the further measurements were performed on dry samples.

3.2 Grain-size analysis

Grain-size distribution in sediments was analyzed in several steps. Firstly, coarse fraction (>63 μm) was isolated from the bulk sample via wet sieving. Sand, gravel and pebble particles were separated via dry sieving. Grain-size distribution in the fine fraction (<63 μm) was analyzed using Micrometrics Sedigraph 5100 facility at the Otto-Schmidt-Laboratory (AARI, St.Petersburg, Russia). Prior to the measurements, 10%-H_2O_2 was added to the samples to remove the organic matter. Grain-size distributions of fine fraction were determined over 0.5–63 μm range, measuring distribution of silt (2-63 μm) and capturing the silt-clay transition (2 μm). After that, contents of clay (< 2 μm) were calculated by distracting the relative amount of coarse-grained fraction and silt from the bulk sample.

3.3 Mineralogical analysis

For all the 4 studied cores, mineralogical analysis was performed on bulk sediments by the X-ray diffraction (XRD) method. Measurements were run on the Philips PW 3020 diffractometer equipped with Co kα-radiation, graphite monochromator and automatic divergence slit. XRD patterns were obtained in the range of 5 to 65 degrees two-theta with 0.02 two-theta steps and 2 seconds count time per step. Dry powder samples were mixed together with internal standard (corundum Al_2O_3) at the weight ratio 4:1, which enabled further quantification of mineral contents performed using the Microsoft Excel-based program RockJock (RJ) Vers. 11 (details are described by Eberl, 2003). As required for the RJ calculations, X-Ray intensities were converted into the Cu kα-radiation wavelength and fixed divergence slit mode by using MacDiff Vers. 4.2.6 routines (for details see Petschick et al., 1996). After visual check of the diffractograms, minerals that are likely to be present are chosen from the list of standards (Fig. 3).

No.	Mineral	Present? (1 = yes)	AutoShift? (1 = Yes)	Report as: (1 = No report; 2 = Non-Clay; 3 = Clay)	The usual suspects (1 = yes)
1	Quartz	1	0	2	1
2	Kspar (ordered Microcline)	1	0	2	1
3	Kspar (intermediate microcline)	0	0	2	1
4	Kspar (sanidine)	0	0	2	1
5	Kspar (orthoclase)	0	0	2	1
6	Kspar (anorthoclase)	0	0	2	0
7	Plagioclase (albite, var. cleavelandite)	1	0	2	1
8	Plagioclase (oligoclase; NC)	0	0	2	1
9	Plagioclase (oligoclase; Norway)	0	0	2	0
10	Plagioclase (andesine)	0	0	2	1
11	Plagioclase (labradorite)	0	0	2	1
12	Plagioclase (bytownite)	0	0	2	0
13	Plagioclase (anorthite)	1	0	2	0
14	Calcite	1	0	2	1
15	Calcite (Mg-rich)	0	0	2	0
16	Aragonite	0	0	2	0
17	Dolomite	1	0	2	1
18	Dolomite (Fe-rich)	0	0	2	0
19	Ankerite	0	0	2	0
20	Magnesite	0	0	2	0
21	Siderite	0	0	2	0
22	Halite	1	0	2	0

Figure 3. Fragment of the list of mineral standards located in the Input sheet of the RockJock program.

The program fits the XRD patterns of standard minerals (calculated pattern) to the measured pattern by varying the fraction of each mineral using the Solver function in Excel (Fig. 4). After that weight percentages of minerals present in the sample are calculated based on comparison of integrated intensities with the integrated intensity of internal standard. As each mineral is analyzed independently, the weight percentages should sum up to 100%.

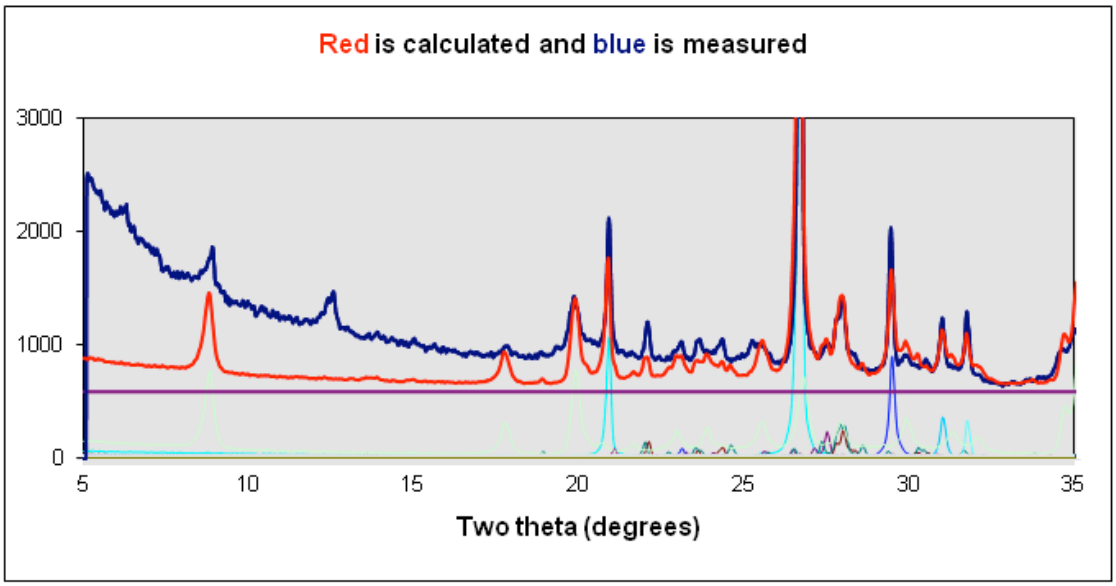

Figure 4. Chart from the FullPattern sheet of the RockJock program showing the measured (blue) and calculated (red) XRD paterns. Note the large inconsistency in the low-angle region that contains characteristic peaks for clay minerals.

During the calculation procedure, it was found out that contents of clay minerals, such as micas and smectite, should be reported together, as clay minerals can often give a false-positive reading in RockJock and it is difficult to distinguish these minerals without special treatment. Therefore, downcore data on clay mineral assemblages obtained from the bulk XRD measurements were not discussed in this thesis.

3.4 Radiogenic isotope analysis

Isotope geochemical analysis for provenance discrimination was tested on the core PS72/340-5 for which the most detailed age model was provided. Isotope ratios of radiogenic lead (Pb) and neodymium (Nd) were measured on the detrital fraction of clay size (< 2 μm). Sample preparation was carried out in the AGEs laboratory of the University of Liege (Belgium) under the supervision of Prof. Dr. N. Fagel (head of the lab). Firstly, samples were treated with HCl 0.1N to remove biogenic carbonates and calcinated at 550 °C to destroy the organic matter. After that chemical separation was performed in the clean lab following the analytical protocol defined by Weis et al. (2006). Dry sediment samples were digested using a mixture of three acids: HF, HNO_3 and HCl. Obtained dissolutions were run through three different columns with varying adsorbents and eluents to extract the individual components: Pb and Nd eluates. Isotopic composition of Pb and Nd was measured on a Nu Plasma MC-ICP-MS instrument at the Université Libre de Bruxelles (Belgium).

4 Arctic glacial history of the last 200 ka: an overview

The late Pleistocene history of the Arctic region comprises cyclical changes in the extension of the land-based ice sheets and sea-ice cover that affected sedimentary environments in the Arctic Ocean. In the last 200 ka, large parts of North America and Europe were covered with ice sheets in glacial times corresponding to MIS 6 and 4-2 (Fig. 5). In the Canadian Arctic, ice also extended onto the shelf areas except for Alaska (England et al., 2009). In northern Eurasia, ice sheet advanced onto the shelves of the Barents Sea and Kara Sea (Svendsen et al., 2004). Only NE Russia is believed to have remained ice-free (e.g. Gualtieri et al., 2003). During the LGM, configuration of ice sheets in North America was similar, whereas in Siberia large ice sheet did not reach so far east as before. However in NE Russia there were glaciers restricted to mountain ranges (Stauch and Gualtieri, 2008). Lack of detailed onshore investigations and inconsistency in dating of glacial advances make it difficult to differentiate between the extent of the LGM and earlier glaciations (Zamoruyev, 2004).

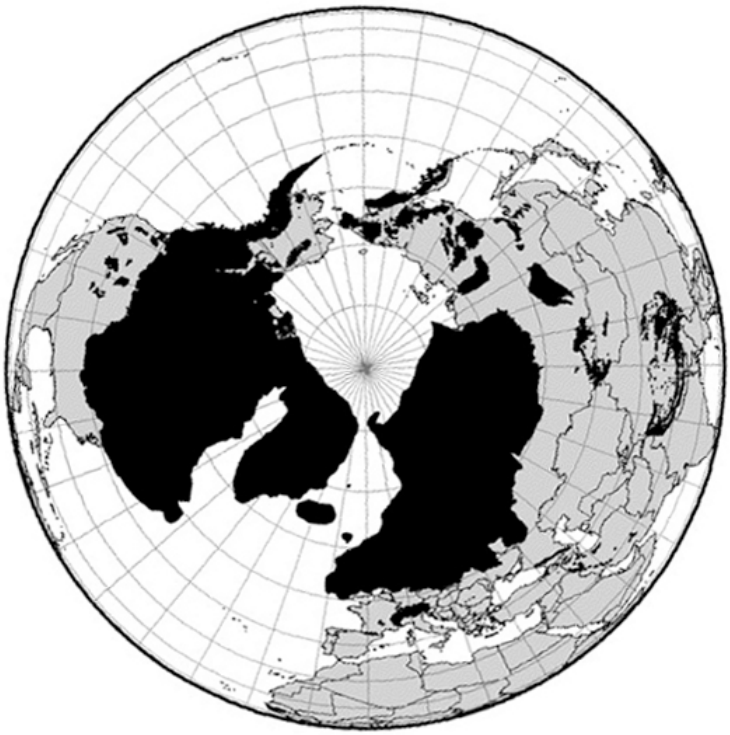

Figure 5. Circum-Arctic map showing the extent of the Pleistocene glacial maximum (corresponding to MIS 6) in the Northern Hemisphere (summarized by Ehlers and Gibbard, 2007).

During glacial times, sea-level drops caused exposure of shallow Arctic shelves, reduced oceanic circulation and water exchange with the Atlantic and the Pacific Oceans. Along with more severe ice conditions in the Arctic Ocean, this had a significant effect on

sedimentary environments (Knies et al., 2000; Polyak and Jakobsson, 2011; Spielhagen et al., 2004; 2011). The most dramatic events occurred when large ice sheets advanced to the broad continental shelves of the Arctic and subarctic seas. These advances are evidenced by geophysical data from Greenland, Barentz, Chukchi and Canadian margins, which demonstrate that Quaternary glacial ice, in the form of ice shelves or large tabular icebergs, scoured many regions of the Arctic seafloor (Fig. 6). These scoured surfaces include isolated topographic highs that are found in modern water depths of up to 1000 m (Jakobsson et al., 2010; O'Regan et al., 2011; Polyak et al., 2007; 2001).

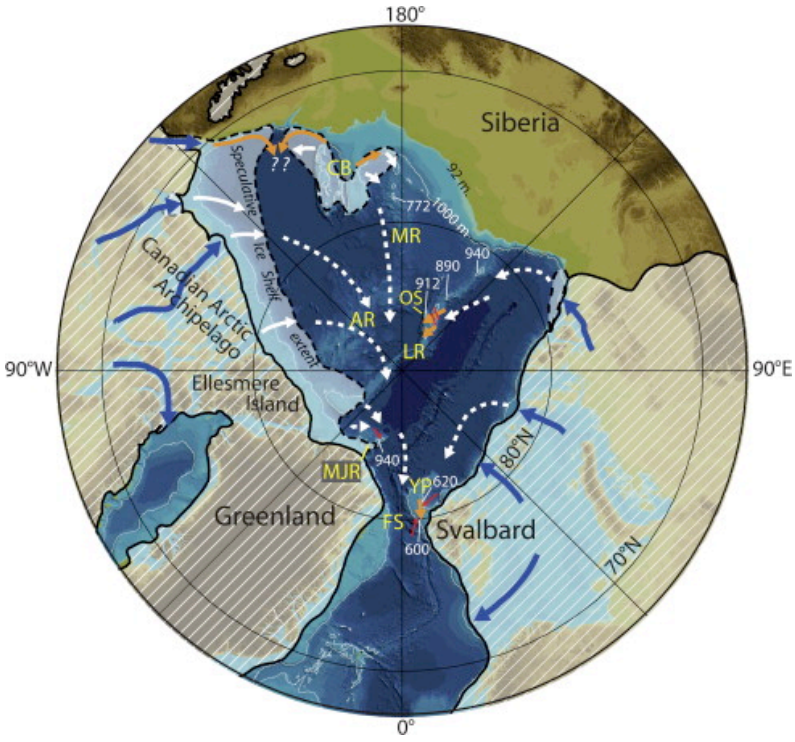

Figure 6. Circum-Arctic map showing tentative reconstruction of MIS 6 ice shelves (Jakobsson et al., 2010). Orange arrows indicate ice flow inferred from geophysical mapping and white arrows hypothesized ice flow. The portrayed bathymetry is derived by lowering the estimated sea level drop during MIS 6 of 92 m (Rabineau et al., 2006) from the IBCAO (Jakobsson et al., 2008). The Eurasian Late Saalian Ice Sheet (MIS 6) is inferred from the reconstruction by the QUEEN project (Svendsen et al., 2004). The North American Ice Sheet shown is the Late Wisconsinan by Dyke et al. (2002), updated to include Banks and Melville Islands as ice covered (England et al., 2009).

Similar erosional events may have occurred on the southern part of the Mendeleev Ridge, as reflected in a prominent diamicton recorded at the water depths of 800-900 m by the acoustic parasound survey (Stein et al., 2010). The same campaign alone the ESS continental margin identified lineations in seafloor morphology which could potentially represent iceberg scours. Existence of an ice sheet in MIS 6 was also proposed on the New Siberian Islands (Basilyan et al., 2010).

Build-up and disintegration of ice sheets in the Arctic hinterland were accompanied by increased iceberg discharge to the Arctic Ocean. Therefore, the history of iceberg transport of terrigenous material is reflected by the ice-rafted debris (IRD) abundance in marine sediment cores as illustrated in Figure 7 (Spielhagen et al., 2004). The highest IRD contents are consistent with late Pleistocene glaciations during MIS 6 (190-130 ka), MIS 5b (90-80 ka), and during transitions MIS 5/4 (75 ka) and MIS 4/3 (65-50 ka).

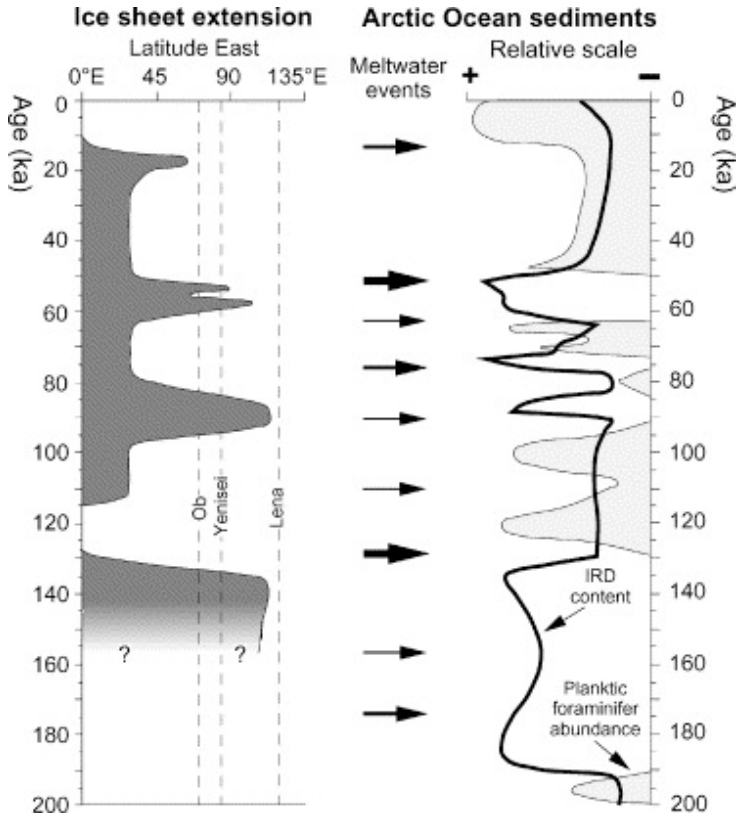

Figure 7. Comparison of reconstructions of the eastward extension of ice sheets during the past 150 ka (Svendsen et al., 2004) with results from central Arctic deep-sea sediment cores (figure from Spielhagen et al., 2004).

IRD has a broad definition. In general, particles that have size larger than 63 μm are assumed to be transported by ice as the open ocean currents rarely have velocities capable to keep grains of this size in suspension (McCave et al., 1995). IRD composition (petrography of large-size dropstones) was intensively studied for determination of potential source areas and further reconstructions of trajectories of iceberg drifting (e.g. Bischof et al., 1996; Bischof and Darby, 1997; Phillips and Grantz, 2001). On the other hand, heavy mineral composition of the fine sand fraction provide important information on the trajectories of sea-ice drift (Behrends et al., 1999; Krylov et al., 2008). In addition, terrigenous sediment composition is a good proxy for development of stratigraphic correlations as it is not much affected by diagenetic processes (Clark et al., 1980; Polyak et al., 2009; Stein et al., 2010).

5 Bulk mineral composition of surface sediments in the Arctic Ocean revisited: testing different quantitative techniques for evaluation of the X-Ray diffraction data

E. A. Bazhenova, H.Zou, C. Vogt, R. Stein, J. Matthiessen

Spatial and temporal variations in mineral composition of marine sediments may be used to reconstruct sediment pathways, namely the ocean paleocirculation and trajectories of sea-ice and iceberg movement. On the one side, provenance studies in the Arctic Ocean are often complicated due to the lack of information about the bedrock geology in the North American and Eurasian hinterlands. On the other side, existing literature data cannot be compared directly when different grain-size fractions and measurement procedures are utilized for estimation of the mineral contents. In this study we used surface sediments from the Arctic Ocean to compare two techniques, RockJock and QUAX, for quantification of mineral assemblages from the X-Ray diffraction (XRD) data. Measurements were performed on dry bulk powder samples using the internal corundum standard. We show that a quite good correlation between RockJock and QUAX results is observed for non-clay minerals while contents of clay minerals should be reported cautiously as it is difficult to distinguish some of these minerals without special treatment. In summary, results of the two methods can be compared when the relative proportions of mineral contents are used. Comparison with published overviews on the mineral composition of Arctic Ocean sediments shows that for provenance studies bulk mineral composition of sediments should be used along with other indicators for source areas, for example, geochemical fingerprints.

5.1 Introduction

Identification of source areas for the material transported from the North American and Eurasian hinterland gives important information about the surface circulation patterns in the Arctic Ocean. Landmasses surrounding the Arctic Ocean comprise terraines of variable geological age and tectonic setting, therefore characterized by different mineralogical and chemical signature. Mineralogical composition of sediments is determined by that of the rocks in the source area and is also influenced by processes of transportation of terrigenous material carried from the shelf zones into the deep ocean by oceanic currents, sea-ice and icebergs (e.g. Lisitzin, 2002).

As a result of numerous mineralogical studies (e.g. Belov and Lapina, 1961; Darby et al., 2011; Darby et al., 1989; Kosheleva and Jashin, 1999; Krylov et al., 2008; Stein et al., 1994; Vogt et al., 2001; Wahsner et al., 1999) source areas for terrigenous material coming to the Arctic Ocean were described based on the distribution of bulk, clay and heavy minerals (Fig. 10). However these data cannot be easily produced and combined for interpretation as they are obtained by usage of different methods and size fractions. For example, variations in heavy mineral composition of the fine sand fraction may provide important information on the sea-ice dynamics as well as trajectories of sea-ice drift (Behrends et al., 1999; Krylov et al., 2008). Open-water conditions are marked by fine-grained sediments dominated by clay minerals (Vogt et al., 2001). Clay mineral composition is usually based on the semi-quantitative estimations after Biscaye (1965), when contents of the main clay minerals (illite, chlorite, smectite, kaolinite) in the fraction < 2 μm are retrieved from XRD diagrams and normalized to 100%. Such procedures often cause underestimation of other mineral assemblages.

While looking for unique methodology, it is now common to use software for evaluation of mineral assemblages from the XRD data. In this study we tested if bulk mineral assemblages can be used for provenance discrimination in the Arctic Ocean sediments, providing the comparison between quantitative estimations from two software packages, namely RockJock (Eberl, 2003) and QUAX (Emmermann and Lauterjung, 1990; Vogt et al., 2002).

5.2 Oceanographic setting

The present-day current pattern in the Arctic Ocean (Fig. 8) is determined by interaction of Atlantic and Pacific saline water masses together with the freshwater inflow from rivers draining the Arctic hinterland. Currently, the front between Atlantic and Pacific

components in subsurface waters is located along the Mendeleev Ridge (Macdonald et al., 2000, and references therein). The Transpolar Drift leads to the movement of sea-ice away from the Siberian coast, across the Arctic basin, and south through the Fram Strait (Rudels et al., 2004). The Siberian Coastal Current, forced by winds, river outflows and ice melt, flows from the ESS eastward (Weingartner et al., 1999). Pacific water masses enter the Arctic Ocean via the Bering Strait and then penetrate into the Chukchi and Beaufort Seas. In the Canadian Basin, the surface oceanic circulation is dominated by the Beaufort Gyre (e.g. Polyak and Jakobsson, 2011).

The permanent sea-ice cover in the central Arctic Ocean caused by high river runoff and net precipitation is mainly controlled by the interaction of warm Atlantic and cold polar water masses as well as by the seasonal variability leading to sea-ice melt (e.g. Spielhagen et al., 2011). The surface waters of the Arctic Ocean receive the voluminous river runoff that keeps the salinity low and thus maintains the sea-ice cover. The Arctic rivers transport large amounts of dissolved and particulate material onto the shelves where it is accumulated or further transported by different mechanisms (sea ice, icebergs, turbidity currents, etc.). Thus, river-derived material contributes in major proportions to the entire sedimentary and chemical budgets of the Arctic Ocean (e.g. Lisitzin, 2002). Furthermore, the different rivers carry suspension loads characterized by different mineralogical and geochemical tracers, dependant on the geology of the hinterland, which can be used as indicators for specific source areas and reconstruction of sediment pathways (Stein, 2008, and references therein).

5.3 Materials and methods

We used surface samples from the central Arctic Ocean recovered in the expeditions of the research vessel “Polarstern” ARK-XXIII/3 (Jokat, 2009) and ARK-XXVI/3 (2011), as well as from cruises RUSALCA-2009 to the Chukchi Sea (RUSALCA, 2009) and ISSS-2008 to the East Siberian Sea (Dudarev, 2008). Locations are shown in Figure 8 (coordinates of sampling locations are available at http://doi.pangaea.de/10.1594/PANGAEA.792555). In total, 78 samples were analyzed.

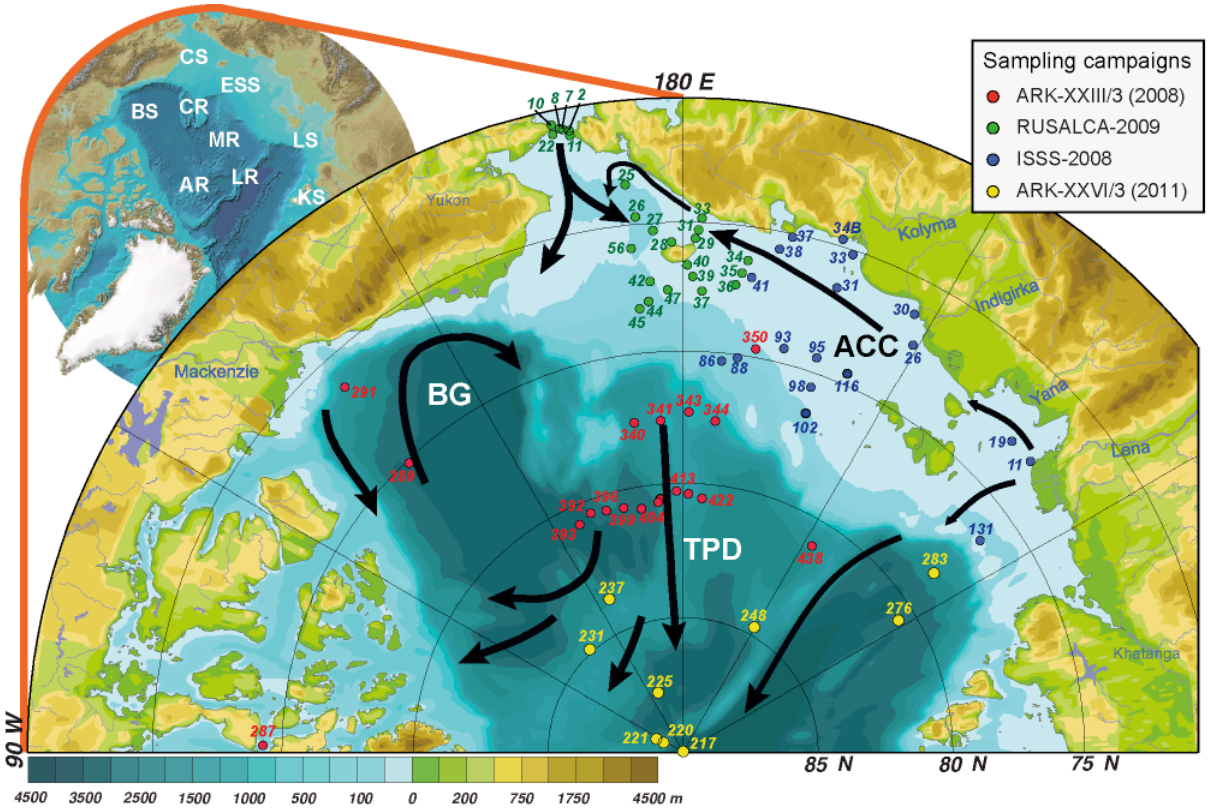

Figure 8. Locations of surfaces samples from the Arctic Ocean marked according to the different cruises specified in the legend. Black arrows mark the directions of major surface current systems: Beaufort Gyre (BG), Transpolar Drift (TPD), Arctic Coastal Current (ACC). Bathymetry and the circum-polar inlay map are from IBCAO (Jakobsson et al., 2008). CS – Chukchi Sea, ESS – East Siberian Sea, LS – Laptev Sea, KS – Kara Sea, BS – Beaufort Sea, CR – Chukchi Rise, MR – Mendeleev Ridge, AR – Alpha Ridge, LR – Lomonosov Ridge.

Mineralogical analysis was performed on bulk sediments by the X-ray diffraction (XRD) method following preparation and experimental setup developed for usage of the RockJock software Vers. 11 (Eberl, 2003). Dry powder samples were mixed together with internal standard (corundum) in the proportion 4:1, which enabled further quantification of mineral contents. XRD patterns were obtained in the range of 5 to 65 degrees two-theta with 0.02 two-theta steps and 2 seconds count time per step. Initially the measurements were run on the Philips PW 3020 diffractometer equipped with Co kα-radiation, graphite monochromator and automatic divergence slit. All diffractograms were checked visually for the characteristic peaks of minerals (d-values): quartz - 4.26 Å, K-feldspar - 3.24 Å, plagioclase - 3.19 Å, calcite - 3.03 Å, dolomite – 2.88 Å, pyroxenes - 2.98-3.00 Å, amphiboles – 8.27-8.59 Å; illite and micas – 4.47 and 10 Å, smectite and montmorillonite – 5.2 and 7.07 Å, kaolinite and chlorite group - 7 Å, separated by the peaks for kaolinite at 3.57-3.58 Å and for chlorite at 3.53-3.54 Å (e.g. Biscaye, 1965; Darby, 1971; Darby, 1975; Elverhoi and Ronningsland, 1978). Prior to the RJ calculations, X-Ray intensities were converted into the Cu kα-radiation wavelength and

fixed divergence slit mode by using MacDiff Vers. 4.2.6 routines (for details see Petschick et al., 1996). RJ runs were carried out using the automatic background correction. Minerals that are likely to be present in the samples have to be chosen manually from the list of standards. After the calculation, graphs and degree of fit were checked to compare the calculated and measured X-Ray intensities. Additionally, raw XRD data were processed using the QUAX (Quantitative Phase-Analysis with X-ray Powder Diffraction) software (Emmermann and Lauterjung, 1990) to test the consistency of both methods. During the QUAX procedures, peaks (d-values) are recognized by the software. Integrated intensities of peaks are then compared to those of standards in the database. Based on this comparison, the most prominent minerals in the sample are listed according to the decreasing probability of their presence. After that an XRD pattern is calculated with the best fit to the measured intensities. The residual intensities are assigned to less abundant minerals and a list of accessory minerals is provided (for more details see Vogt et al., 2002).

5.4 Results

Results of quantification of mineral assemblages obtained using the RockJock and QUAX software packages are available at http://doi.pangaea.de/10.1594/PANGAEA.792555. Quantification of mineral phases revealed the common non-clay minerals to be represented by quartz, plagioclase, K-feldspar, calcite and dolomite. Main clay minerals identified are micas (including illite), kaolinite and chlorite. During the calculation procedure, it was found out that contents of clay minerals, such as micas (including illite) and smectite, should be added together when reported, as clay minerals can often give a false-positive reading in RockJock and it is difficult to distinguish these minerals without special treatment (Eberl, 2003). That is why the low-angle region of the XRD patterns should be examined carefully prior to the calculation. Normalized results of the quantitative RJ analysis are shown as pie diagrams in Figure 10a. Detection limit is 1-2 wt% depending on the mineral group, and measurement errors in RJ are approximately ± 4 relative weight percent (wt%) of the mineral amount present. However, errors can become larger as the minerals in samples are different from the ones used as standards (Eberl, 2003). Among the accessory minerals pyroxenes, amphiboles, garnet, rutile, magnetite and epidote were observed. However it is difficult to quantify these mineral phases based on the bulk analysis due to their low contents, so we are only able to use their presence to help identify the mineralogical provinces in surface sediments.

5.5 Discussion

5.5.1 Comparison between RJ and QUAX results

Comparison between RJ and QUAX results is shown in Fig. 9. Here a quite good correlation is observed for non-clay minerals, such as dolomite and plagioclase. Samples from the shelf seas (i.e. RUSALCA Cruise) seem to cause more problems with correlation for quartz and phyllosilicates, as the background for these XRD patterns is relatively higher, most probably due to larger amounts of amorphous material in the zones with higher bioproductivity. In RJ calculations, the quartz contents were in many cases underestimated as it was visually seen from the mismatch of the calculated and measured quartz peaks. However, it was not possible to correct the position of peaks manually as the program is automated. Underestimation of the quartz contents can probably explain the increased clay mineral sum, as shown by the quartz/phyllosilicate ratios. As XRD results are normalized to 100%, the closed sum issue has to be keep in mind when comparing the absolute numbers of mineral contents (e.g. Andrews and Eberl, 2011). In summary, results of the two methods can be compared when the relative proportions of mineral contents are used.

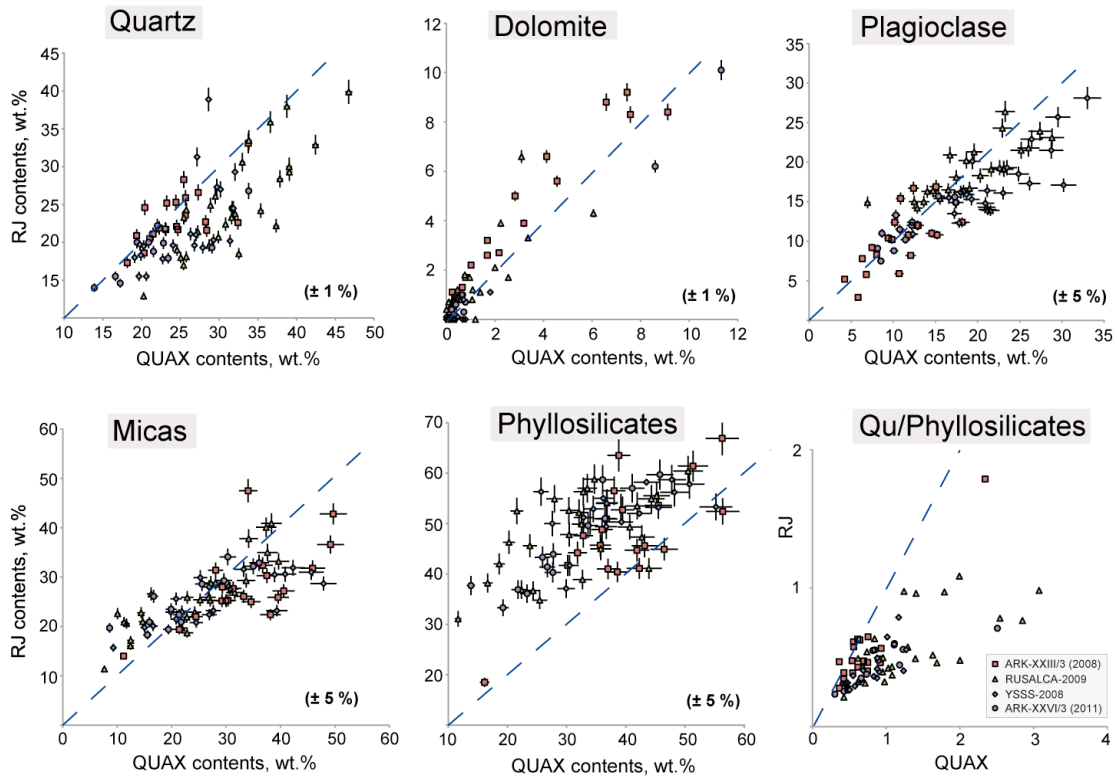

Figure 9. Plots showing the bivariant relationship between normalized mineral contents obtained using the RockJock and QUAX software. Values in brackets indicate the 2s-relative error for the QUAX results (Vogt et al., 2002). For the RJ results, this error is taken for ± 4 % according to the RJ manual (Eberl, 2003). Note that here contents of micas include illite and smectite (see text for details). Dashed lines show the one-to-one correlation.

The different reference mineral standard sets can be the major influence on the results. Not only Eberl (2003) and Andrews & Eberl (2007; 2012) illustrated the development and important improvements of RockJock to its current version, the whole set of reference minerals was documented as raw measurements in the RockJock spreadsheets and therefore, easily accessible. For QUAX, the initial status of reference minerals sets was given by Vogt (1997), while improvements as well as entering and testing of new mineral standards were described by Vogt et al. (2002). Since then continuous additions have been done especially in the clay mineral section. The current number of approximately 250 accepted reference minerals in QUAX has been reached by, in particular, adding and editing the source materials from the Reynolds Cup's measurements using the results spreadsheets distributed to members of this biannual laboratory contest (e.g. Omotoso et al., 2006). The corundum addition in our measurements for the RockJock analysis allows for correction of diffractogram positions and of course a test of the precision of the corundum weight percentage determination (± 1.5 % for all samples). On the other hand, addition of internal standards reduces the content of the original mineral assemblage and might lead to decrease of minor mineral contents below detection limits.

5.5.2 Bulk mineral assemblages: implications for provenance studies

Based on the results of quantitative estimations of mineral assemblages from the bulk XRD data, we would like to discuss the possibility to use these data for provenance studies.

Dolomite was described to be a common mineral in surface samples of the Beaufort Sea (Fig. 10c), as shown by microscopic and petrographic studies performed on the coarse fraction (e.g. Belov and Lapina, 1961; Bischof et al., 1996). Vast carbonate province of Cambrian-Devonian age outcropping on the Canadian Arctic Archipelago (Fig. 10c) is considered to be the main source for dolomites in the Arctic Ocean sediments (Dalrymple and Maass, 1987; Darby et al., 1989). Our results indicate enrichment in dolomite along the Alpha-Mendeleev Ridge and in the adjacent areas. Presence of dolomite in the ESS surface samples can be explained by either transport with sea ice and/or currents from the Beaufort Sea or by input from the Siberian sources. Thick Paleozoic carbonate strata were described on the Wrangel, Kotelniy Islands and Severnaya Zemlya archipelago as well as in the Kolyma and Olenek river valleys (Gordeev and Sidorov, 1993; Petrov et al., 1995). Nevertheless, western Laptev Sea, ESS, and Southern Lomonosov Ridge surface sediments do not contain much dolomite (see Fig. 8; Müller and Stein, 2000; Viscosi-Shirley et al., 2003a; Viscosi-Shirley et al., 2003b; Vogt, 1997) while glacial samples from the central Lomonosov Ridge and samples

from the Morris Jesup Rise cores close to North Greenland do contain high contents of dolomite in the coarse fraction which is suggested to be transported by icebergs as shown by Nørgaard-Pedersen et al. (2007; 1998), Vogt (1996; 1997), Behrends et al. (1999). Therefore, additional mineralogical and geochemical evidence should be found to confirm the origin of dolomite in the central Arctic Ocean sediments.

Kaolinite was suggested to be a possible indicator for enhanced transport from the Canadian Basin as higher amounts of kaolinite are consistent with dolomite maxima in cores from the Amerasian Basin (Dalrymple and Maass, 1987; Darby et al., 1989) and northern Mendeleev Ridge (Krylov et al., 2012). As shown already long ago, kaolinite occurs in some Mezozoic and Cenozoic units along the North America coast from Alaska to the Mackenzie River delta (Clark et al., 1980; Darby, 1975; Naidu et al., 1982; Naidu and Mowatt, 1983). Oligocene weathering surfaces were found on the Banks Island (Kim and Slobodin, 1991), and elevated concentrations of kaolinite were reported from around Ellef Ringnes Island (Darby et al., 2011). In our samples, kaolinite was also found in sediments from the Beaufort Sea and in the Bering Strait (Fig. 10b), which is consistent with the described kaolinite-rich province.

As shown by our results, kaolinite is also present in samples from the western Laptev Sea shelf. In the Eurasian Basin, there are some sources of Triassic and Jurassic kaolinite-bearing rocks in the Barentz Sea as well as the Mezozoic sediments on the Franz Joseph Land (Nürnberg et al., 1995; Vogt, 1997, and references therein). In the Laptev Sea region, Miocene kaolinite and kaolinite-illite clays occur on the Bolshevik Island, between the Anabar and Olenek Rivers, in the Lena River delta, near the Laptev Strait (Kim and Slobodin, 1991). Kaolinite was also observed in the eastern part of the ESS close to the Wrangel Island, where it could be transported from the potential source areas by currents and/or sea ice. From this perspective, it seems difficult to use kaolinite presence alone for provenance discrimination.

Amphibole. Although it was not possible to quantify the amount of amphibole from the bulk patterns, this mineral can be possibly used as indicator for sediment input from the Siberian shelves as shown in Fig. 10c, where amphibole-bearing locations from this study are marked with red circles. High amounts of amphiboles were recorded in sediments from the Laptev, East Siberian and western Chukchi seas (Behrends et al., 1999; Stein and Korolev, 1994) and in the adjacent parts of Mendeleev and Lomonosov ridges where they can be delivered by sea ice (Krylov et al., 2008). This distribution pattern may be of importance for paleoreconstructions in the Amerasian Basin but more detailed microscopic studies on the heavy mineral composition of sediments are needed.

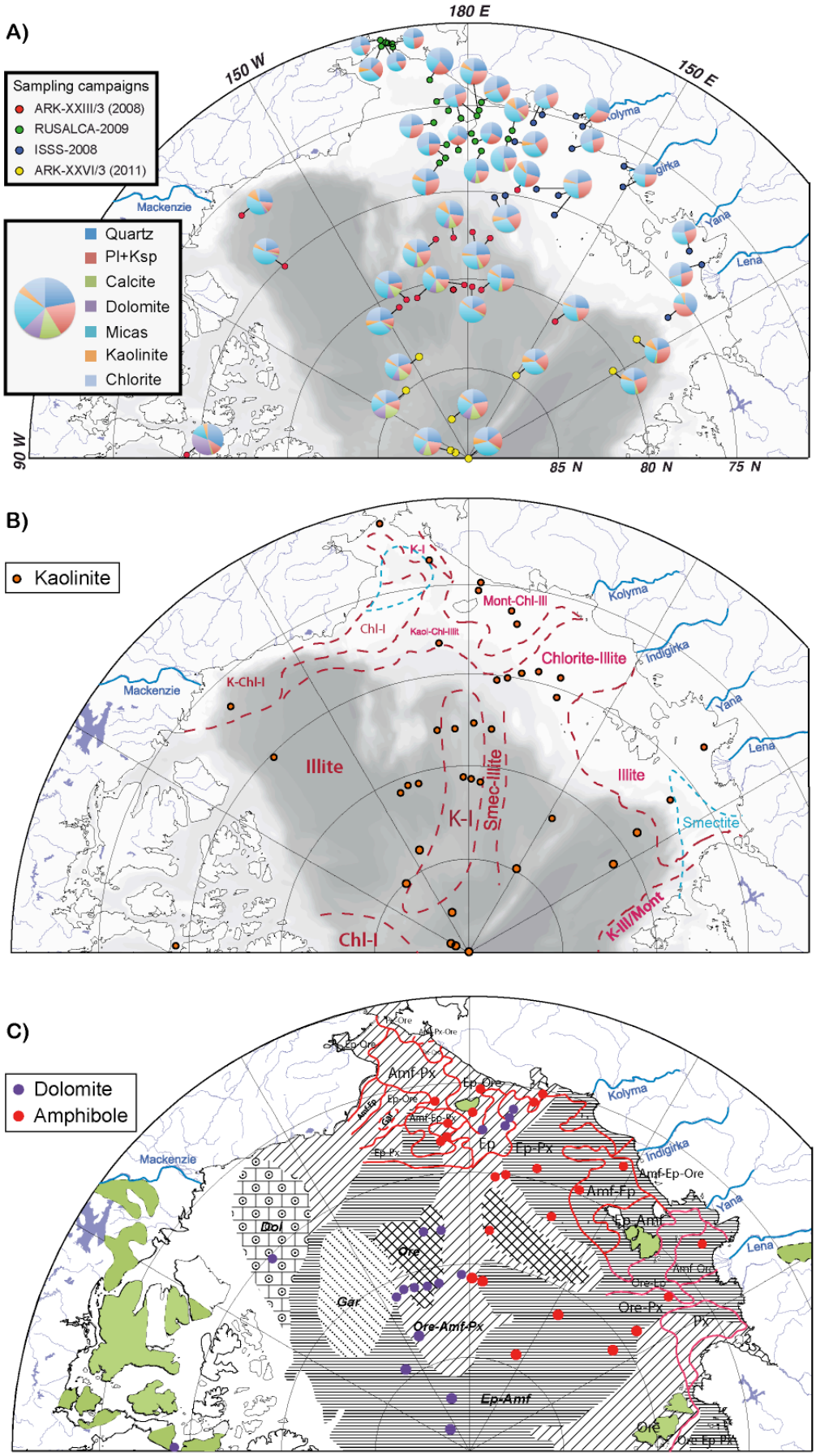
A)
Sampling campaigns
ARK-XXIII/3 (2008)
RUSALCA-2009
ISSS-2008
ARK-XXVI/3 (2011)
Quartz
Pl+Ksp
Calcite
Dolomite
Micas
Kaolinite
Chlorite
180 E
150 W
150 E
90 W
85 N
80 N
75 N
Mackenzie
Kolyma
Indigirka
Yana
Lena
B)
Kaolinite
K-I
Mont-Chl-Ill
Chl-I
Kaol-Chl-Illit
Chlorite-Illite
K-Chl-I
Illite
Smec-Illite
Smectite
K-Ill/Mont
C)
Dolomite
Amphibole
Amf-Px
Ep-Ore
Amf-Ep-Px
Ep
Ep-Px
Amf-Ep-Ore
Amf-Ep
Ep-Amf
Dol
Ore
Gar
Ore-Amf-Px
Ore-Px
Px
Ore-Ep-Px

Figure 10. A) Results of quantitative mineralogical analysis performed using the RockJock software, summed up to 100 wt% and plotted as pie diagrams. Here we added together the contents of micas and smectite (see text for more details).
B) Distribution of clay minerals in the Arctic Ocean surface samples, compiled for the Beaufort Sea and Alpha-Mendeleev Ridge (Clark et al., 1980, and references therein), Chukchi Sea (Clark et al., 1980; Kosheleva and Jashin, 1999; Viscosi-Shirley et al., 2003a), ESS (Kosheleva and Jashin, 1999), Laptev Sea (Kosheleva and Jashin, 1999; Wahsner et al., 1999). Locations from this study where kaolinite was identified are marked with orange circles.
C) Locations from this study are marked with violet circles indicating the presence of dolomite and with red circles for findings of amphiboles. Provinces show distribution of accessory minerals in the fine sand fraction of surface samples, determined by means of immersion microscopy. Provinces marked with red lines are from the detailed work of Kosheleva and Jashin (1999). Areas filled with black-and-white patterns are from earlier work by Belov and Lapina (1961), name of provinces written in *italics*. Early Paleozoic carbonate provinces on land are marked with green, locations are from geological maps compiled by Trettin (1991) and Petrov et al. (1995).

5.6 Conclusions

In this study we used surface sediments from the Arctic Ocean to compare two techniques, RockJock and QUAX, for quantification of mineral assemblages from the bulk XRD data. We show that a quite good correlation between RockJock and QUAX results is observed for non-clay minerals while contents of clay minerals should be reported cautiously as it is difficult to distinguish them without special treatment. In summary, results of the two methods can be compared when the relative proportions of mineral contents are used.

Comparison with published overviews on the mineral composition of Arctic Ocean sediments shows that for provenance studies bulk mineral composition of sediments should be used along with other indicators for source areas, for example, geochemical fingerprints (e.g. Darby et al., 2011; Viscosi-Shirley et al., 2003a).

5.7 Acknowledgements

This study was carried out within the PhD project of EB supported by the Helmholtz Research School for Polar and Marine Research (POLMAR). We are very thankful to L. Polyak (Ohio State University, USA) and E. Gusev (VNIIO, St. Petersburg, Russia) who kindly shared the sediment material from the ISSS-2008 and RUSALCA-2009 cruises, respectively.

5.8 Supplementary material

Coordinates of sampling locations, as well as results of quantification of mineral assemblages obtained using the RockJock and QUAX software packages are available at http://doi.pangaea.de/10.1594/PANGAEA.792555.

6 Study of core records from the southern Mendeleev Ridge: stratigraphy revised using paleomagnetic data and implications for glacial/interglacial variability

E. A. Bazhenova, T. Frederichs, J. Wollenburg, S. Kostygov, R. Stein, F. Niessen

Stratigraphy for 4 cores recovered along a transect at ca. 77°36'N across the Mendeleev Ridge was revised using paleomagnetic parameters (inclination and paleointensity) supported by AMS ^{14}C datings and micropaleontological (foraminiferal) evidences. Inclination data revealed 6 excursions of reversed polarity which were correlated to the Mono Lake (33 ka), Laschamp (41 ka), North Greenland Sea (70 ka), Blake (120 ka), Iceland Basin (188 ka) and Pringle Fall (211 ka) events. For age-depth estimations, paleointensity was tuned to the GLOPIS-75 and PISO-1500 global stacks. However additional age constraints are needed to locate MIS 6/5, 5/4 and 4/3 boundaries. Changes in accumulations rates, grain-size distribution and provenance of ice-rafted debris were documented from the Mendeleev Ridge towards the East Siberian Sea continental margin. As evidenced by grain-size and mineralogical data, there were several events of intensified sediment discharge at the Mendeleev Ridge possibly linked to paleoenvironmental changes in the circum-Arctic hinterland during the last 200 ka. Glaciations in North America corresponding to MIS 6 and 4-2 are reflected in the presence of pink (dolomite-rich) layers in cores along the studied transect. Additional information on the IRD provenance is needed to differentiate between sediment source areas in Eurasia, that was also partially covered with ice sheets during these times.

6.1 Introduction

Quaternary history of the Arctic Ocean features multiple dramatic changes associated with land-based glaciations in the Arctic. Consequent sea-level fluctuations caused exposure of shallow Arctic shelves, partially covered by ice sheets, reduced oceanic circulation and water exchange with the Atlantic and the Pacific Oceans. Along with more severe ice conditions in the Arctic Ocean, this had a dramatic effect on sedimentary environments (Knies et al., 2000; Polyak and Jakobsson, 2011; Spielhagen et al., 2004). Despite its importance in the global climate system, there are only few age-calibrated marine geologic records reflecting the evolution of glacial cycles through the Pleistocene in the Amerasian Basin of the Arctic Ocean. Due to the perennial sea-ice cover, biological productivity in the Arctic Ocean is relatively low as compared to lower latitudes. Therefore, sediments largely lack biostratigraphically useful calcareous and siliceous microfossils (Backman et al., 2004; Cronin et al., 2008; O'Regan et al., 2008). Large extension of the sea-ice cover also affects sedimentation rates in the Arctic Ocean, that are mainly controlled by input of terrigenous material from the adjacent land. Therefore, the pattern of sedimentation rates is determined by bathymetry and sources and transport pathways of sediment (e.g. Backman et al., 2004; Huh et al., 1997; Polyak et al., 2009; Sellen et al., 2010). Due to generally low sedimentation rates in the central Arctic Ocean, it is difficult to get high-resolution paleomagnetic inclination excursion records. Normally, cores contain a thick upper section of normal polarity. Time constraints for the reversed interval below vary as additional chronostratigraphic markers are needed to assign specific age to the inclinations (e.g. Jakobsson et al., 2000; Nowaczyk et al., 2001; Stoner et al., 1995). Furthermore, inclination components carried by magnetic minerals can be overprinted by diagenetic alterations which are common in the Arctic Ocean sediments (Channell and Xuan, 2009; Xuan et al., 2012).

Here we use a core transect at ca. 77°36'N across the southern Mendeleev Ridge to revise the shipboard stratigraphy proposed by Stein et al. (2010) using paleomagnetic and new litho- and biostratigraphic data. Obtained stratigraphic framework is used to analyze sedimentation patterns along the transect and to provide possible implications for reconstruction of late Quaternary glacial/interglacial paleoenvironments close to the East Siberian Sea continental margin.

6.2 Oceanographic setting

The present-day current pattern in the eastern Arctic Ocean is dominated by the interaction of Atlantic water inflow with its counterpart, the Transpolar Drift, with its cold and low-saline polar water outflow (Fig. 11). In the Canadian Basin the oceanic circulation is dominated by the Beaufort Gyre (Rudels et al., 2004). The permanent sea-ice cover in the central Arctic Ocean caused by high river runoff and net precipitation is mainly controlled by the interaction of warm Atlantic and cold polar water masses as well as by the seasonal variability leading to sea-ice melt (e.g. Spielhagen et al., 2011). The Arctic rivers transport large amounts of dissolved and particulate material onto the shelves (Stein, 2008, and references therein) where it settles down or get carried farther by the Arctic Coastal Current, forced by winds, river outflows and ice melt (Weingartner et al., 1999) and driven eastward by the Coriolis force (Schlosser et al., 1995). The Transpolar Drift system governs the overall motion of sea-ice in the eastern Arctic Ocean and leads to a movement of sea-ice away from the Siberian coast, across the Arctic basin, and south through the western side of the Fram Strait.

6.3 Materials and methods

This research is based on Arctic Ocean marine sediment cores recovered during the ARK-XXIII/3 Expedition of RV "Polarstern" in 2008. Here we used 4 cores from the "southern" transect at ca. 77°36'N across the Mendeleev Ridge (for core locations see Fig. 11 and Table 2): PS72/340-5 (Chukchi Abyssal Plain), PS72/342-1, PS72/343-1 (Mendeleev Ridge), and PS72/344-3 (ESS continental margin).

Table 2. Coring sites of the ARK-XXIII/3 Expedition used in this study

Core ID	PS72/340-5	PS72/342-1	PS 72/343-1	PS 72/344-3
Position	77° 36.31' N 171° 29.09' W	77° 36.01' N 177° 20.62' W	77° 18.33' N 179° 2.99' E	77° 36.62' N 174° 32.37' E
Water depth, m	2349	820	1227	1257
Recovery, cm	809	320	704	820

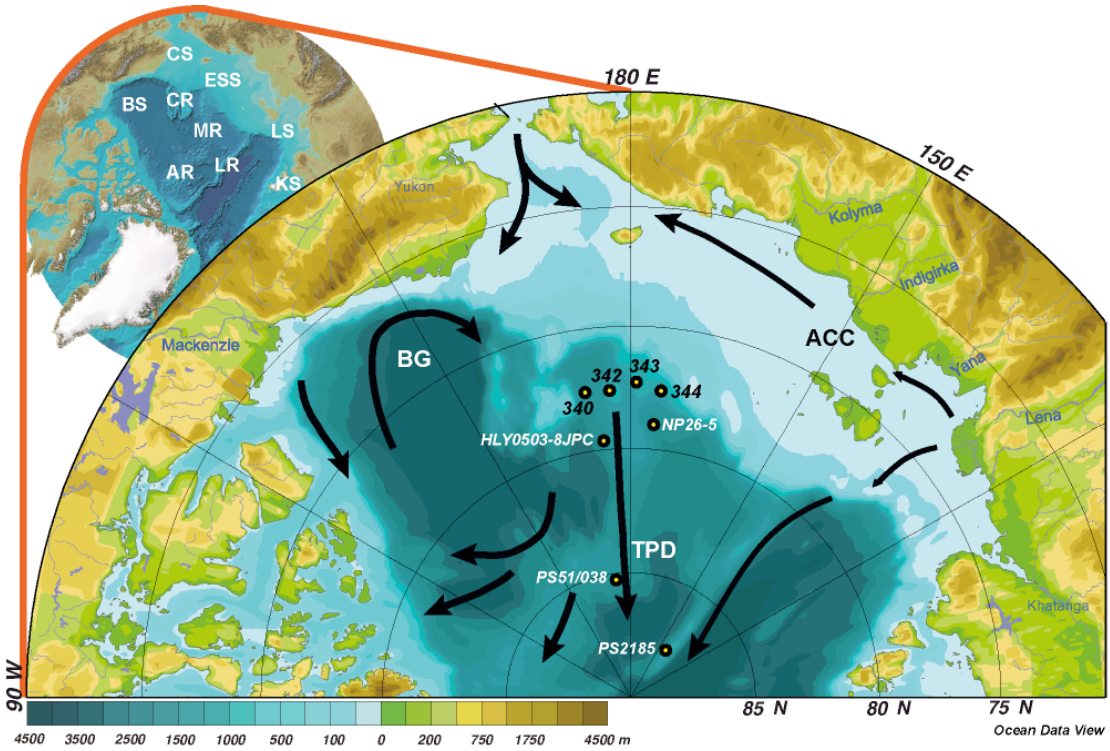

Figure 11. Locations of cores used in this study (coordinated listed in Table 2), as well as of cores used for comparison: HLY0503-8JPC (Adler et al., 2009); NP26-5 (Polyak et al., 2004); PS51/038, PS2185 (Spielhagen et al., 2004). Black arrows mark the directions of major surface current systems: BG – Beaufort Gyre, TPD – Transpolar Drift, ACC – Arctic Coastal Current (for details see text).
Inlay map shows the Arctic Ocean (CS – Chukchi Sea, ESS – East Siberian Sea, LS – Laptev Sea, KS – Kara Sea, BS – Beaufort Sea, CR – Chukchi Rise, MR – Mendeleev Ridge, AR – Alpha Ridge, LR – Lomonosov Ridge), bathymetry used on both maps is IBCAO (Jakobsson et al., 2008).

All the cores were taken by gravity corer. Standard descriptions and measurements were performed by the ARK-XXIII/3 shipboard Geology Group. Changes in sediment colour and lithology were visually described, followed by spectral reflectance (lightness) measurements at 1-cm intervals with a hand-held spectrophotometer Minolta CM 2002. Lightness L* (grey scale) is recorded from 0 % (black) to 100% (white) as described for the L*a*b CIELAB colour space (Commission Internationale de l´Éclairage 1976). Logging was performed using a GEOTEK Multi-Sensor-Core-Logger, when sediment density, p-wave velocity, and magnetic susceptibility were measured at 1-cm intervals. Details on the shipboard measurements are given in the ARK-XXIII/3 Cruise Report (Jokat, 2009). If not stated below, all the other measurements were performed at the Alfred Wegener Institute in Bremerhaven, starting with digital imaging of all the cores.

Grain-size analysis. Coarse fraction (>63 μm) was isolated via wet sieving. Sand and gravel (grain sizes of 0.063-0.125, 0.125-0.250, 0.250-0.500, 0.5-2 mm and > 2 mm) were separated via dry sieving. Grain-size distribution in the fine fraction (<63 μm) was analyzed

using a Micromeritics Sedigraph 5100 facility at the Otto-Schmidt-Laboratory (Arctic and Antarctic Research Institute, St.Petersburg, Russia). Each sample was tested three times to gain statistically significant data. The output grain-size data represents a set of mass concentrations for the grain sizes from 0.5 to 63 μm measured with increasing step of 0.3 to 3 μm. The cumulative data were recalculated to get absolute weight percentages of size classes. Analytical details and errors are described by Stein (1985), McCave et al. (1995) and Bianchi et al. (1999).

Mineralogical analysis was performed on bulk sediments by the X-ray diffraction (XRD) method following preparation and experimental setup developed for usage of the RockJock software Vers. 11 (Eberl, 2003). Dry powder samples were mixed together with internal standard (corundum) in the proportion 4:1, which enabled further quantification of mineral contents. XRD patterns were obtained in the range of 5 to 65 degrees two-theta with 0.02 two-theta steps and 2 seconds count time per step. Initially the measurements were run on the Philips PW 3020 diffractometer equipped with Co kα-radiation, graphite monochromator and automatic divergence slit. Prior to the RJ calculations, X-Ray intensities were converted into the Cu kα-radiation wavelength and fixed divergence slit mode by using MacDiff Vers. 4.2.6 routines (for details see Petschick et al., 1996). RJ runs were carried out using the automatic background correction. After the calculation, graphs and degree of fit were checked to compare the calculated and measured X-Ray intensities.

Paleomagnetic measurements. Samples for geomagnetic investigations (comprising determination of intensity and direction of the Earth's magnetic field in the past) were taken at 5-cm intervals from fresh split halves of core PS72/340-5 with 2.2 cm×2.2 cm×1.8 cm cubic plastic boxes, generally avoiding sandy layers. Additional samples were taken after the first round of measurements to prove inclination changes, which corresponded to fine-grained layers except for the lowermost part of the core. All discrete samples were analyzed in the paleomagnetic laboratory at the Department of Geosciences, University of Bremen. Palaeomagnetic directions and magnetization intensities of natural remanent magnetization (NRM), anhysteretic remanent magnetization (ARM) generated in a peak alternating field of 100 mT and a biasing DC field of 40 μT as well as isothermal remanent magnetization (IRM) generated in a DC field of 100 mT were measured on a cryogenic magnetometer (model 2G Enterprises 755 HR). Natural remanent magnetisation (NRM) was measured on each sample before these were subjected to a systematic demagnetisation treatment involving 16 steps for each sample with a maximum alternating field intensity of 100 mT. A detailed vector analysis

was applied to the results (Kirschvink, 1980) in order to determine the characteristic remanent magnetisation (ChRM). Samples showing no systematic demagnetisation pattern were rejected. Inclination data were assumed to be reliable only if the following criteria were fulfilled: 1) MAD (mean angular deviation) < 10°; 2) maximum intensity of NRM (natural remanent magnetization) > 1 mA/m; 3) MDF (median destructive field) of NRM <50 mT. Due to the fact that the remanence vectors of samples from high latitudes are mostly represented by their vertical component, we present and discuss only results referring to inclination data. Relative paleointensity (RPI) was calculated as ratios NRM20mT / ARM20mT, NRM20mT / IRM20mT using an AF demagnetisation level of 20 mT for each type of remanence as well as NRM/κ. Magnetic grain-size proxy κ_{ARM}/κ was calculated using the ARM and magnetic susceptibility values.

Additional low-temperature measurements as described by Channell and Xuan (2009) were performed on several samples showing normal as well as reversed polarity using a Quantum Design MPMS XL-7. This was done in order to rule out the presence of titanomaghemite which might carry a chemical remanent magnetization (CRM) that is partially self-reversed relative to the detrital remanent magnetization (DRM) carried by the host titanomagnetite and thus pretending negative inclinations. The results yielded no differences between samples with normal and reversed inclination data and thus gave no evidence for the presence of titanomaghemite. However, further high-temperature measurements (thermal cycling and thermal demagnetization) according to Channell and Xuan (2009), which could confirm these results, were not performed due to technical limitations.

Radiocarbon dating. All measurements were performed on the *Neogloboquadrina pachyderma* tests at the Leibniz Laboratory for Radiometric Dating and Isotope Research (University of Kiel). Obtained radiocarbon ages (years BP) were calibrated using the Fairbanks0107 program available at http://radiocarbon.ldeo.columbia.edu (Fairbanks et al., 2005). Older ages were calibrated using the CalPal07 online tool at www.calpal-online.de (Danzeglocke et al., 2007). Standard marine reservoir correction of 440 years was applied prior to calibration, however, actual reservoir age in the Arctic Ocean varies with time and can exceed 1400 yr (e.g. Hanslik et al., 2010).

Total organic carbon (TOC) contents were determined by a carbon-sulfur analyzer Leco CS-125. Before the measurements, carbonate was dissolved by HCl acid. For calibration of the instrument an external standard was used with the carbon content of 0,817±0,004.

6.4 Results

6.4.1 Lithology, TOC contents

Description of core lithologies is compiled from the shipboard core descriptions and colour scanning records (for details see the ARK-XXIII/3 Cruise Report by Jokat, 2009), estimations of the coarse-grained subfractions after wet sieving and sedigraph grain-size analysis of the < 63 μm fraction (this study). In general, various horizontally bedded mud lithofacies dominate in cores. There is also a number of diamictons with higher contents of coarse-grained material, marked by maxima in wet bulk density and p-wave velocity which could be potentially used as acoustic reflectors for correlation in the shipboard parasound records (Matthiessen et al., 2010). Wet bulk density values show distinct minima corresponding to the brown units, which are characterized by peaks in magnetic susceptibility (MS; shown in Fig. 25). Peaks in density record are mainly consistent with coarse-grained layers where there is also a strong increase in the MS signal.

The colour scanning records display distinct alterations of the sediment colour (Fig. 26). According to the commonly used stratigraphy for the Arctic Ocean cores (Jakobsson et al., 2000), we identify 'brown' units which are characterized by pronounced minima in lightness (L*) values. These lows are consistent with higher a* values (not shown here), indicating 'redness' of the reflectance spectra. Brown units are normally coarser than 'grey' units, which are of darker olive to grey colours, very fine-grained, usually laminated and strongly bioturbated. Grey units can be clearly seen in cores PS72/343-1 (Fig. 14) and PS72/344-3 (Fig. 15) as well as in the upper part of core PS72/340-5 (Fig. 12), where they are consistent with the highest TOC contents. Intermediate units are characterized by greyish, yellowish- and olive-brown colours.

Distribution of coarse grain sizes in the 4 cores is not uniform. On the whole, amount of the > 250 μm fraction decreases from east to west, from 25 wt% in core PS72/340-5 to 2.5 wt% in PS72/344-3. The same tendency was observed for the > 0.5 and > 2 mm fractions, and dolomite contents, which peak in the 'pinkish' layers as will be shown in Fig. 27. Dropstones of larger sizes were found in all the cores, ranging from 1 cm (PS72/344-3) to 10 cm (PS72/340-5) in diameter. Pebble-sized dropstones were described in details by Krylov et al. in the ARK-XXIII/3 Cruise Report (Jokat, 2009). In general, occurrence of dropstones is not bound to the highest sand peaks (63-125 μm).

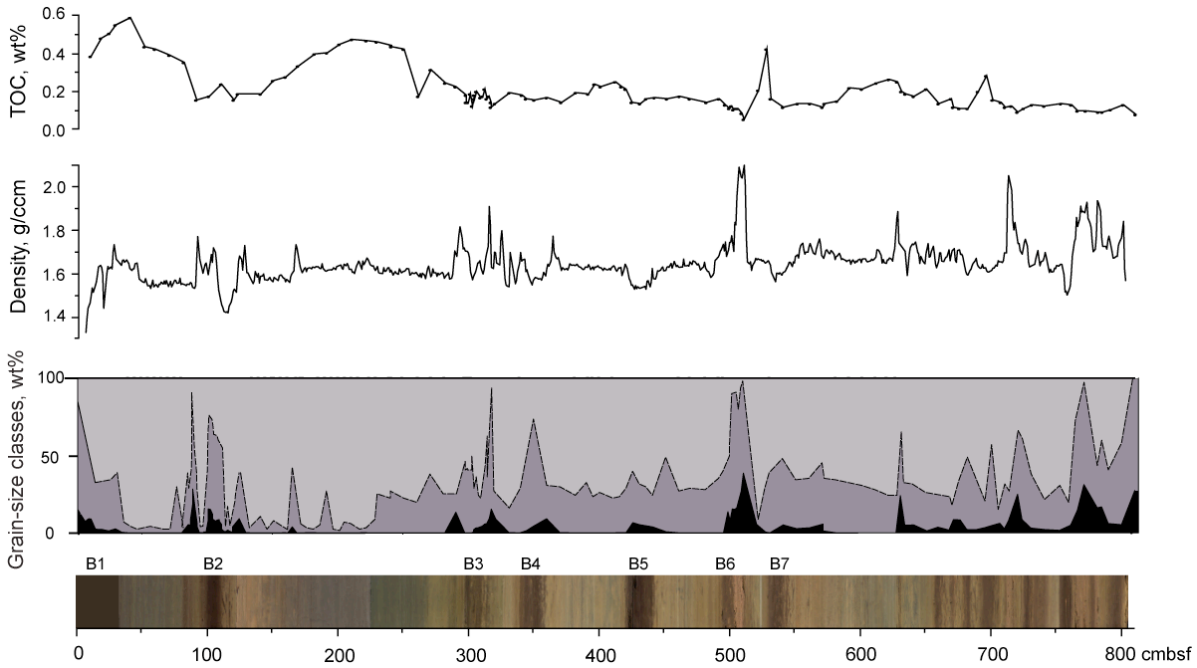

Figure 12. Core PS72/340-5: 1) spliced core images from digital line scanner, brown units are indicated as B1-B7; 2) grain-size distribution: contents of coarse fraction (> 63 μm; in black), silt (2-63 μm; dark grey), and clay (< 2 μm; light grey); 3) MSCL density, g/ccm; 4) total organic carbon (TOC), wt%.

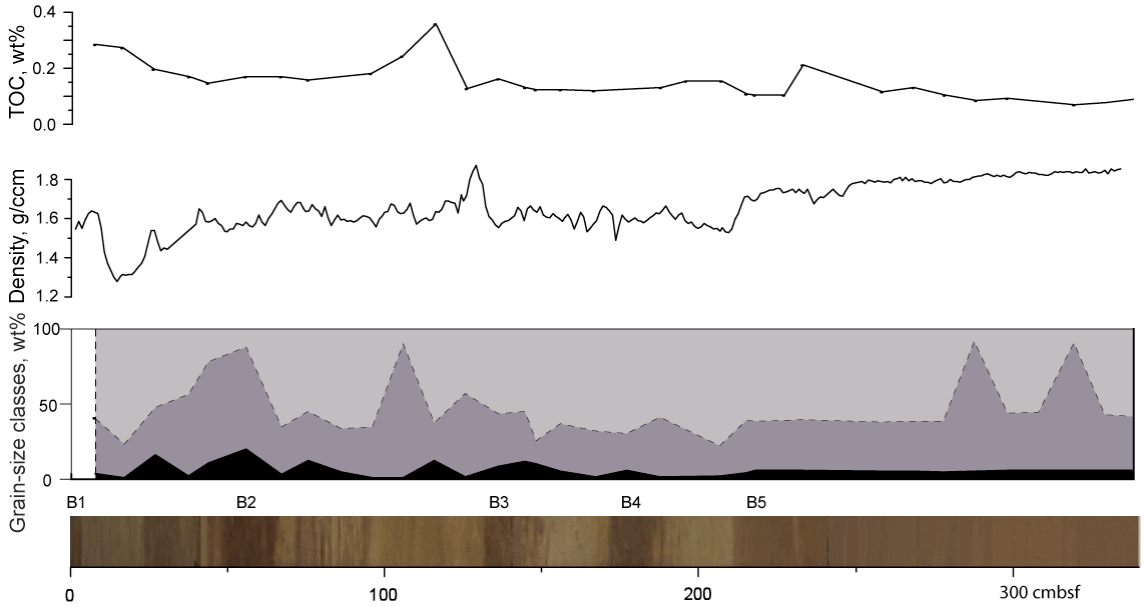

Figure 13. Core PS72/342-1: 1) spliced core images from digital line scanner, brown units are indicated as B1-B5; 2) grain-size distribution: contents of coarse fraction (> 63 μm; in black), silt (2-63 μm; dark grey), and clay (< 2 μm; light grey); 3) MSCL density, g/ccm; 4) total organic carbon (TOC), wt%.

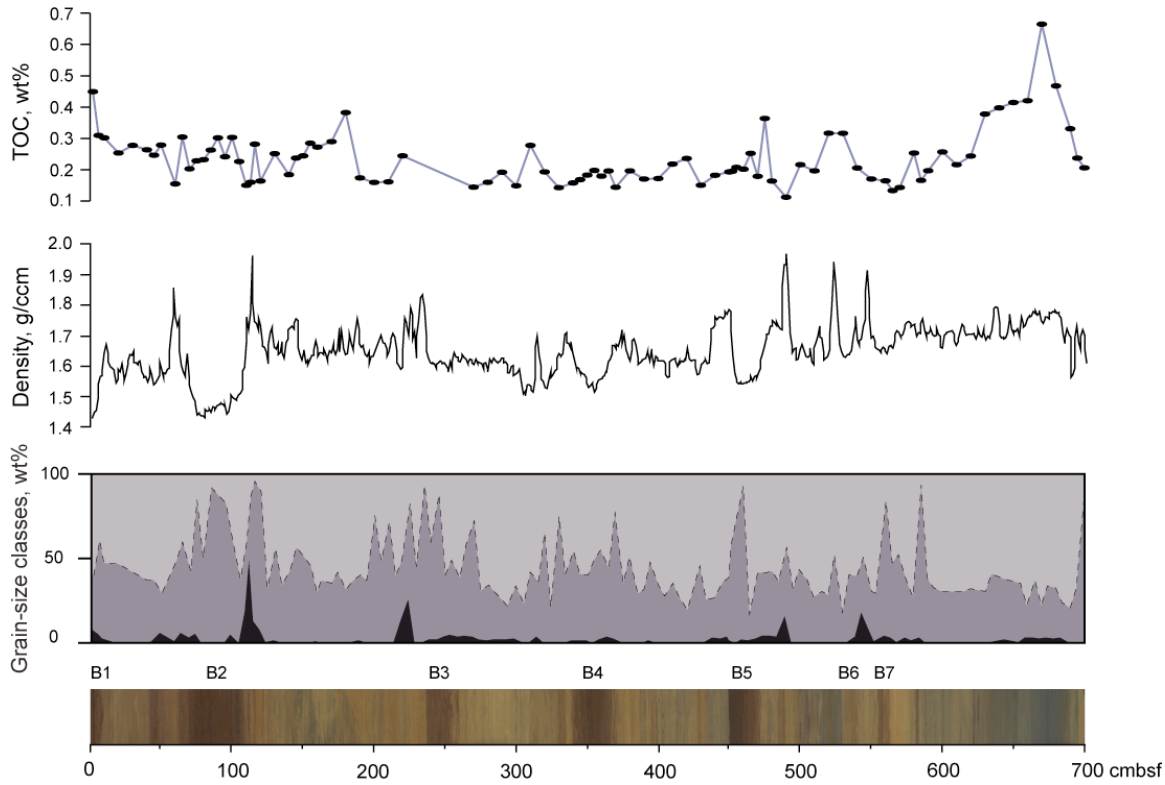

Figure 14. Core PS72/343-1, ESS continental margin: 1) spliced core images from digital line scanner, brown units are indicated as B1-B7; 2) grain-size distribution: contents of coarse fraction (> 63 μm; in black), silt (2-63 μm; dark grey), and clay (< 2 μm; light grey); 3) MSCL density, g/ccm; 4) total organic carbon (TOC), wt%.

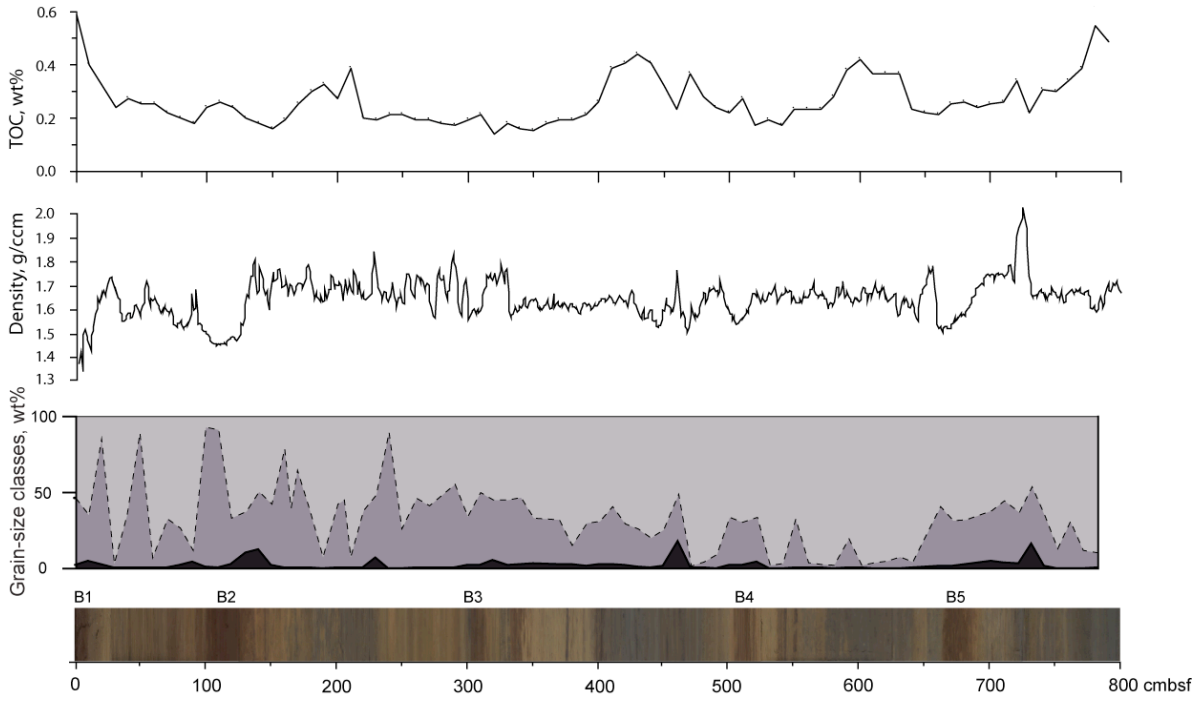

Figure 15. Core PS72/344-3: 1) spliced core images from digital line scanner, brown units are indicated as B1-B7; 2) grain-size distribution: contents of coarse fraction (> 63 μm; in black), silt (2-63 μm; dark grey), and clay (< 2 μm; light grey); 3) MSCL density, g/ccm; 4) total organic carbon (TOC), wt%.

6.4.2 Sediment texture

Sedigraph measurements were carried out on the < 63 μm fraction, isolated by wet sieving. Weight percentages of grain-size classes 1-63 μm were obtained, then merged together and normalized along with the amount of the coarse fraction (> 63 μm) to determine the contents of silt (2-63 μm) and clay (< 2 μm). Distribution of these 3 main classes is plotted against the scanned images of the 4 cores in Figures 9 to 12. After that the relative proportion of sand, silt and clay was displayed in the ternary diagrams (Fig. 16) to help classify the sediment types. In all the cores, most of the samples occur along the clay to silt axis. Therefore, most of the sediments can be classified as clay, silty clay and clayey silt.

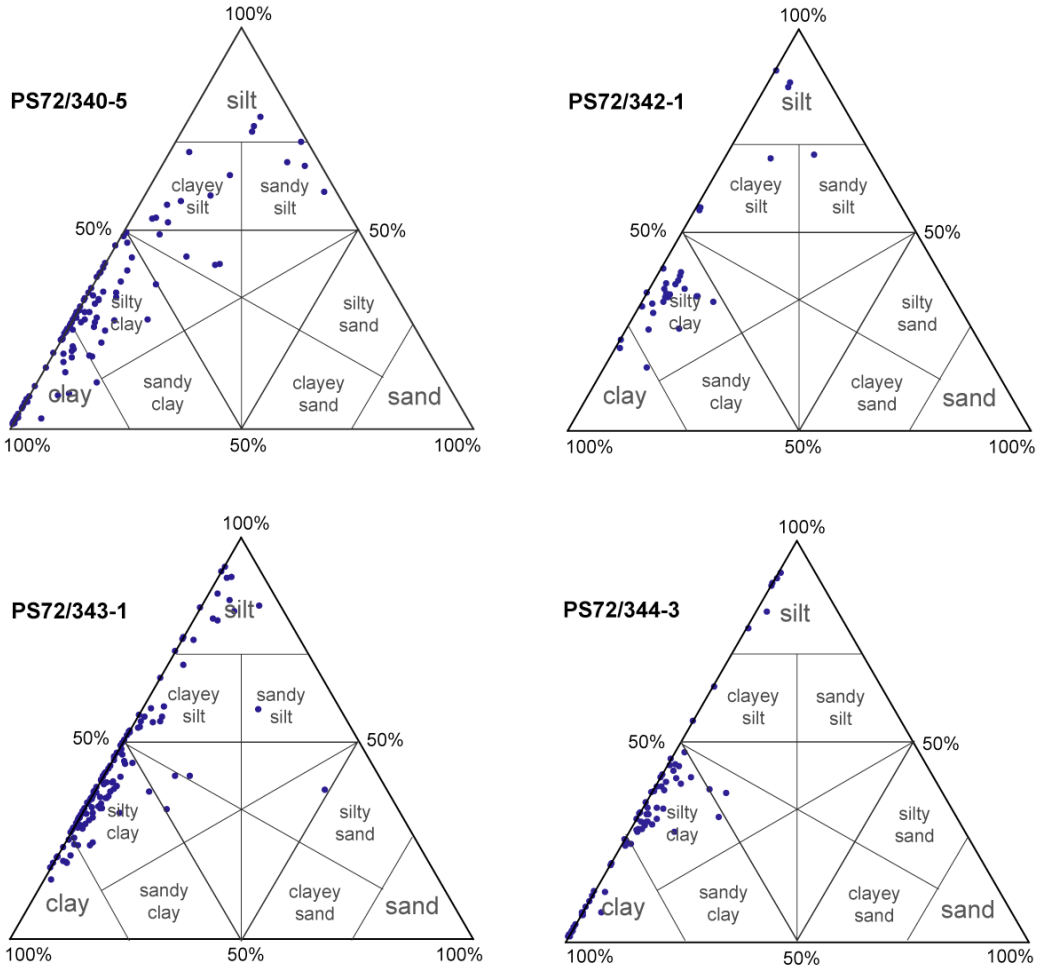

Figure 16. Relative proportion of sand, silt and clay in cores from the Mendeleev Ridge displayed in ternary diagrams.

In the ternary diagrams, there is also a number of values that are shifted to the coarser field. Strong correlation is observed between the silt and clay distribution, which disappears when the silt contents are higher than 40%. There is no clear correlation between the sand and silt distribution.

We use additional plots displaying the bivariant relationship between the sorting and skewness parameters (Fig. 17). Due to similarities in the grain-size distribution in cores PS72/340-5 and PS72/344-3 versus the cores PS72/342-1 and PS72/343-1, here we plot results only for one example from each group. Sediments in cores of the first group are commonly finer as compared to the cores from the Mendeleev Ridge. Based on the sorting values, calculated as the standard deviation, we can distinguish only a small group of values higher than 1.62 (moderately sorted) that are different from the common well-sorted distribution (sorting values lower than 1.62). Skewness values allow us to estimate the asymmetry of the distribution, in our case changing from symmetrical (-0.43 to 0.43) to very coarse skewed (> 1.43) (Blott and Pye, 2001).

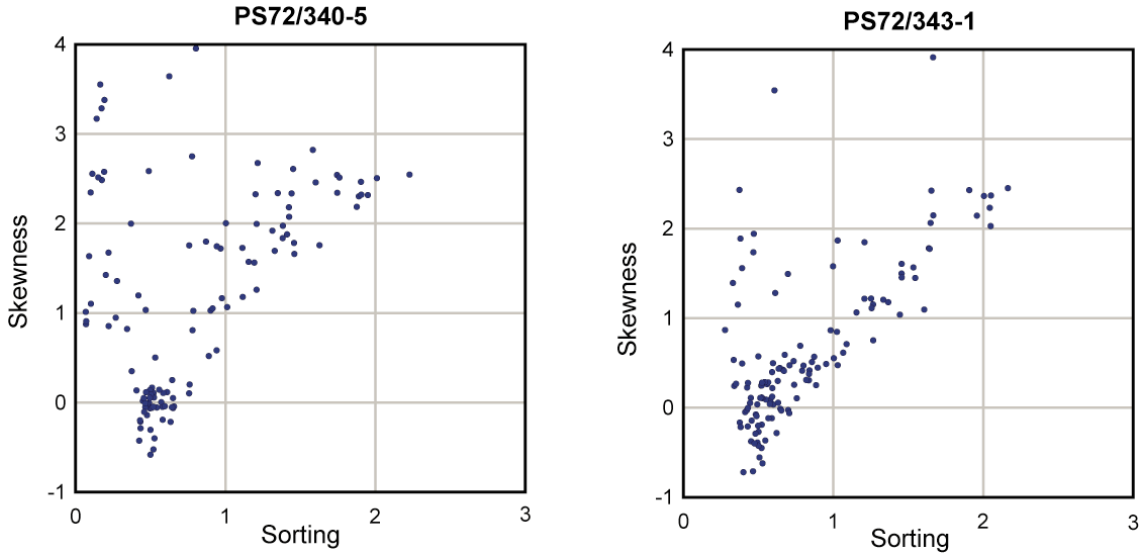

Figure 17. Plots showing the bivariant relationship between the sorting and skewness values in cores PS72/340-5 and PS72/343-1. See text for more details on the grain-size statistical parameters.

6.4.3 Paleomagnetic measurements

Paleomagnetic measurements were carried out on discrete samples from core PS72/340-5. Inclination pattern (Fig. 18) demonstrates that there were several intervals of reversed polarity. These intervals were additionally subsampled to prove the presence of inclination drops, which corresponded to fine-grained layers except for the lowermost part of the core. Based on that, one could reject the single reversed inclinations at 325 and 455 cm (between B3 and B4; and B5 and B6, respectively) as they are represented only by one data point each.

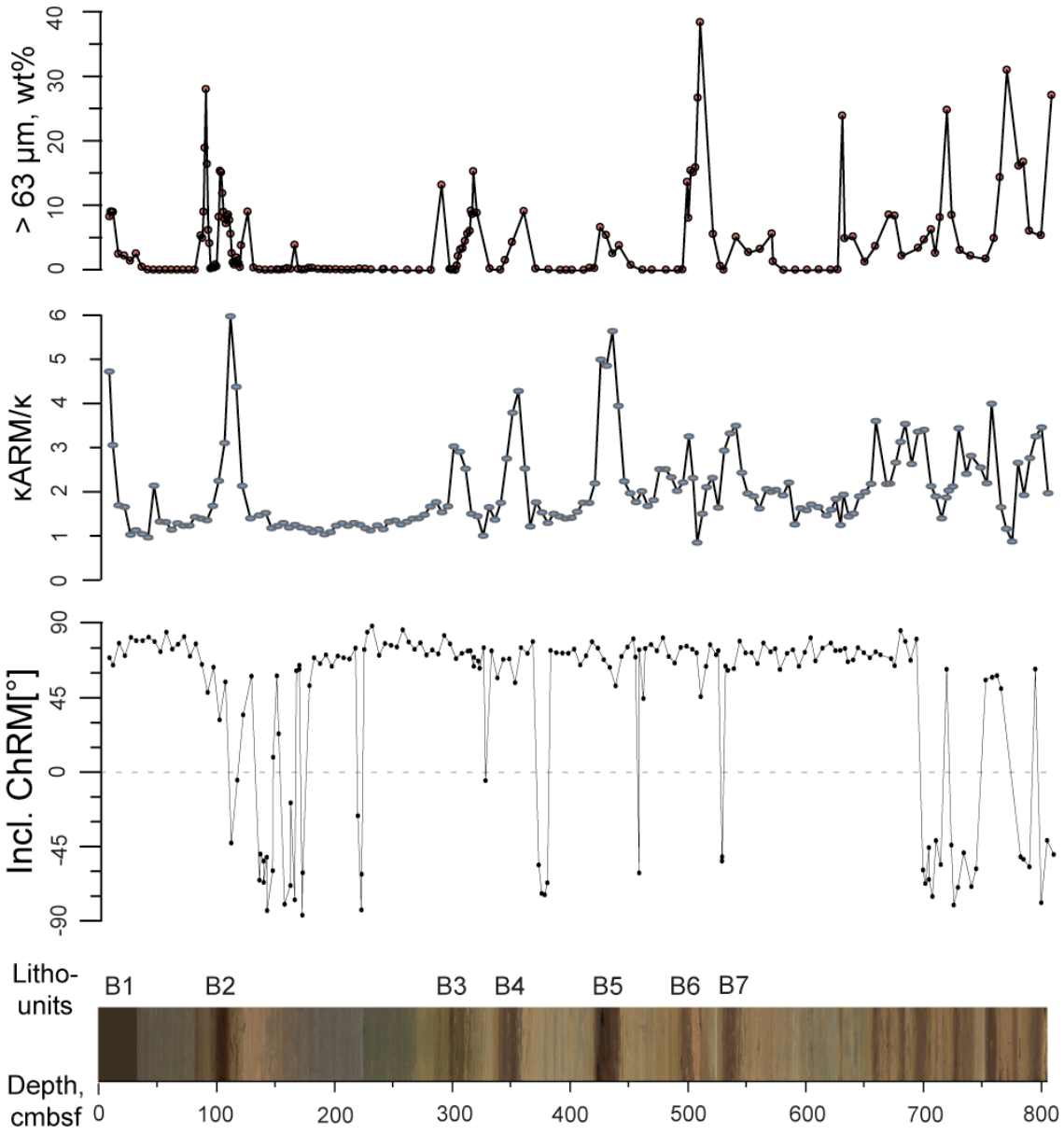

Figure 18. Paleomagnetic parameters in core PS72/340-5: inclination, κ_{ARM}/κ (magnetic grain size); and contents of coarse fraction (>63 µm). Brown lithounits are indicated as B1-B7.

Magnetic grain-size parameter (κ_{ARM}/κ) shows maxima at brown layers. Correlation between κ_{ARM}/κ and sand contents indicates that magnetic grain size in core PS72/340-5 is dependant on the IRD input. However most of the inclinations are not consistent with peaks in κ_{ARM}/κ (except for the one at 121 cm, corresponding to B2), therefore the inclination component should be independent from the grain-size distribution. In the reversed interval at 120-170 cm sediment is slightly bioturbated. In the lowermost part of the core, long interval of reversed polarity is present which could be correlated to many of the Lomonosov and Mendeleev Ridge cores using additional proxies, as will be discussed in *Chapter 6.5* (*Discussion*).

6.4.4 Radiocarbon dating

AMS-^{14}C dates obtained for 5 samples from cores PS72/340-5 and PS72/342-1 are given in Table 3. Age reservoir correction and calibration were applied as described in *Chapter 6.3* (*Methods*). In samples KIA 43286 and KIA 42640, the ^{14}C concentration was lower than the 2σ standard measurement error. This resulted in the radiocarbon ages, calculated with 98% probability that the real age is older.

Table 3. Radiocarbon ages in core PS72/340-5 and PS72/342-1

Lab number	Depth, cm	Radiocarbon age ± 1 σ, yrBP	Calendar age ± 1 σ, yrBP	Unit
KIA 39133	4	6660 ± 35	7142 ± 55*	B1
KIA 39134	20	9425 ± 50	10175 ± 59*	B1
KIA 43285	89.5	43950 + 2640 / -1990	47953 ± 2932**	B2
KIA 42640	100.5	> 46750	n/a	B2
KIA 43286	62	> 46450	n/a	B2[(2)]

All measurements were performed on the *Neogloboquadrina pachyderma* tests at the Leibniz Laboratory (University of Kiel).
* Ages calibrated using the Fairbanks0107 program (Fairbanks et al., 2005).
** Ages calibrated using the CalPal07 program (Danzeglocke et al., 2007), error used for the calculation **1σ**=2640.
[(2)] Sample from core PS72/342-1.

6.4.5 Microfaunal investigations

PS72/340-5. Coarse fraction isolated via wet sieving was studied and after that the core was extensively subsampled around the intervals enriched in foraminifers. These intervals appeared to be generally consistent with brown units B1-B7 (Table 6).

Table 4. Foraminiferal findings in core PS72/340-5

Depth, cmbsf	Faunal findings	Unit
16	drop in *C. wuellerstorfi* and *Epistominella spp.*	base of B1
93-102	peak in *C. wuellerstorfi* and *Epistominella spp.*	B2
300-309	peak in *C. wuellerstorfi* and *Epistominella spp.*	B3
347-355	peak in *C. w.*, *E. spp.*, *O. tener*, *C. subglobosum* (agglutinates), single *B.aculeata*	B4
423-430	peak in *C. subglobosum*, no calcareous forams	B5
515-525	peak in *C. wuellerstorfi*, *C. trullisata (agglutinates)*; last *B. arctica* maximum	B7
525	drop in *C.w., B.arctica, C.subgl., Ep. spp.*; drop in δ18O values	B7

PS72/342-1. Fraction 125-250 μ m was analyzed by means of optical binocular Olympus SZX-12 at the Otto-Schmidt-Laboratory (Arctic and Antarctic Research Institute, St.Petersburg, Russia). Samples were split into 2 to 32 parts when needed to get enough material for counting statistically significant number of foraminifera shells (300 to 600 individuals). Average number of shells in most samples fits the requirements of statistical significance.

The core contains only calcareous forms of benthic foraminifera which are generally well preserved in studied intervals. Absolute abundance graph shows four peaks well correlated with the brown units (Fig. 19). The most notable abundance maximum was observed at 52 - 62 cm (B2) with clearly dominating *Cassidulina teretis* and increased amounts of accessory species *Nonion sp*. (10 shells/g) and *Triloculina tricarinata* (15 shells/g). The upper part of the core is marked with another abundance peak at 2 - 12 cm (B1). Relative abundances are not as high as in previously mentioned intervals but faunal composition looks very similar to the B2 unit. *C. teretis* and *Oridorsalis tener* dominate here. Assemblage also includes accessory species *T. tricarinata* (6 shells/g), *Nonion sp.* (4 shells/g), *Cassidulina reniforme* (3 shells/g) and *Pyrgo murrhina* (3 shells/g).

The second significant maximum is found at 136 - 152 cm (B3). Here we observe the first occurrence of dominant species *Bulimina aculeata* which dominates together with *O. tener*. Among accessory species we may distinguish *Quinqueloculina sp.* (42 shells/g) and *Melonis barleeanum* (4 shells/g) which is very rare throughout the core and here reaches its maximum.

The last observed abundance peak corresponds to 162 - 182 cm (B4) and shows quite high numbers of three dominate species such as *C. teretis*, *O. tener* and *B. aculeata* with almost absent accessory species. These three main species were also found in B5 but much less abundant. The last occurrence of very rare benthic foraminifera shells was captured at 272 cm depth in the upper part of the diamicton unit.

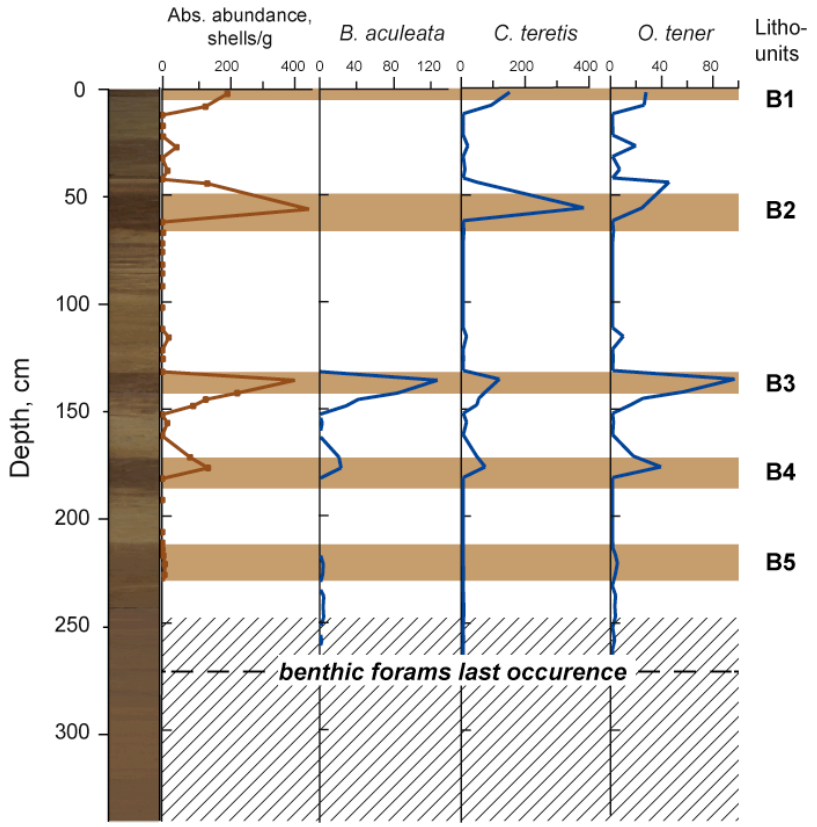

Figure 19. Core PS72/342-1: lithology, planktic and benthic foraminifera absolute abundances (shells per gram dry sediment), relative abundances (shells/g) of selected benthic foraminifera (dominant species, 20-50%). Brown bars indicate sediment brown units B1-B5. Diamicton interval is hatched.

PS72/344-3. Microscopy of the coarse fraction (> 63 μm) was performed in the Otto-Schmidt-Laboratory using the microscope Olympus SZX-12 at 5-60x magnification of the objective and at 10x magnification of the ocular. The coarse fraction is dominated by inorganic terrigenous components. The studied sedimentary section is typically barren of microfossils except for the uppermost 'brown' layers B1 and B2 which contain abundant planktic and benthic forams as well as occasional remains of ostracodes, diatoms, sponge spicules and crinoids (Table 5 and Fig. 20).

The subsurface B1 layer is enriched in the planktic species *Neogloboquadrina pachyderma*, indicating the influence of warm Atlantic currents (Jones, 1994). Benthic assemblages are dominated by the cosmopolitan Atlantic benthic species *Cibicidoides wuellerstorfi* with small numbers of *Milionella subrotunda* and *Dentalina albatrossi* that currently inhabit shelf zones of the Pacific Ocean (Jones, 1994; Loeblich and Tappan, 1987).

Table 5. Micropaleontological findings in the coarse fraction (> 63 µm) in core PS72/344-3

Interval, cm	Planktic forams	Benthic forams	Other findings
0-1	*Neogloboquadrina pachyderma*	*Cibicidoides wuellerstorfi*, *Milionella subrotunda*, *Dentalina albatrossi*	diatoms, sponge spicules, ostracodes
9-11	*N. pachyderma*	*C. wuellerstorfi*, *D. albatrossi*	diatoms, sponge spicules, ostracodes
89-91	*N. pachyderma*	*C. wuellerstorfi*	diatoms, ostracodes
99-101	*N. pachyderma*	*C. wuellerstorfi, O. tenera, Pullenia quinqueloba*	Diatoms, ostracods, crionoids

B2 layer assemblages are characterized by relatively less abundance of *N. pachyderma* whereas the cosmopolitan benthic species *C. wuellerstorfi* is prevailing. At the depth ~ 100 cm insignificant amounts of *Oridorsalis tener* and *Pullenia quinqueloba* (Jones, 1994) were found. Lower in the core no microfauna was observed. However, the B3 unit contains carbonate grains with partly dissolved surface.

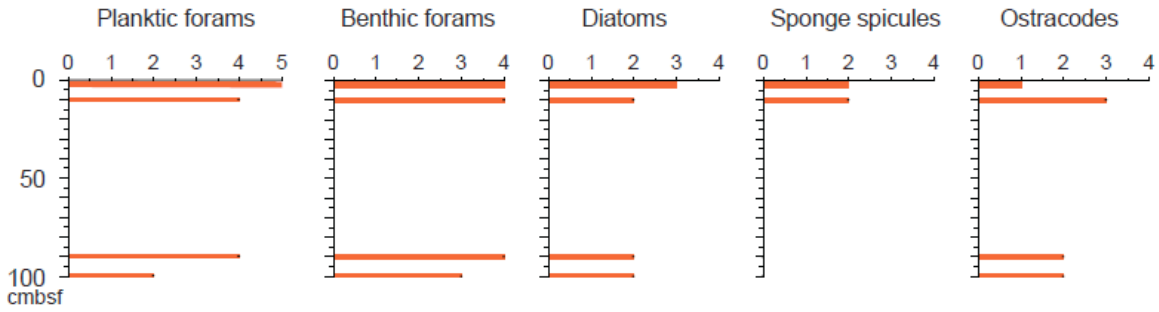

Figure 20. Downcore distribution of microfaunal findings in PS72/344-3, units B1 and B2. Occurence: 0 - none; 1 - very rare; 2 - rare; 3 - common; 4 - abundant; 5 - dominant.

6.5 Discussion

6.5.1 Age model

To constrain the age model, several approaches were tested, mostly on core PS72/340-5. However no perfect final chronology was established and additional absolute dating is needed to verify the proposed stratigraphical framework which is based on combination of paleomagnetic and biostratigraphic data as well as several calibrated radiocarbon ages.

Inclination data of PS72/340-5 show a long interval of reversed polarity below 700 cm in the core, which can be correlated to many cores from the Arctic Ocean. This polarity transition was once interpreted as a reversal, namely the Brunhes-Matuyama boundary (e.g. Clark et al., 1980). However based on high amount of normal polarity data and new biostratigraphic markers, i.e. coccolith assemblages correlated to MIS 5, the reversed polarity zones were suggested to represent excursions (e.g. Jakobsson et al., 2000; Nowaczyk et al., 2001). In core PS72/340-5, most of the reversed inclinations were taken for reliable except for the ones at 325 and 455 cm. Another possible exception could be the first inclination drop corresponding to B2 (for proposed explanation see *Ch. 6.4.3*, *Results*). Remained reversed inclinations were considered as the globally documented geomagnetic events: Mono Lake (ML) - 33 ka, Laschamp (L) - 41 ka, North Greenland Sea (NGS) - 70 ka, Blake (B) - 120 ka, Iceland Basin (IB) - 188 ka, and Pringle Falls (PF) - 211 ka (Roberts, 2008, and references therein).

Depths were assigned to the listed excursions with the help of the foraminiferal findings (Table 6). Units B1-B3 were treated as interglacials based on the high abundances of the cosmopolitan Atlantic benthic species *Cibicidoides wuellerstorfi.* In general, high planktic foraminiferal abundances indicate interglacial/interstadial periods with restricted sea ice cover and open water leads at least during summer. However foraminiferal preservation in the Arctic Ocean is influenced by diagenetic factors such as long-term pore water dissolution and the diluting effect of the dominant terrigenous material flux, therefore making the preservation effect dependant on sedimentation rates. Consequently, the faunal abundance can not be taken alone as a proxy for planktic productivity and sea–ice conditions (Cronin et al., 2008; Norgaard-Pedersen et al., 1998; O'Regan et al., 2008).

Benthic species *Bulimina aculeata* peaks in unit B4 in cores NP26-5 (Polyak et al., 2004) and HLY0503-8JPC (Adler et al., 2009) where it is assigned to MIS 5a, also in core PS2185 from the Lomonosov Ridge (J. Wollenburg, *unpubl. data*). However in core HLY0503-8JPC, unit B4 could be also correlated to MIS 4 as suggested by Backman et al.

(2009) based on the coccolith assemblages. In core PS72/340-5, there was only a single *B. aculeata* found in B4. In core PS72/342-1, there are two prominent peaks in the *B. aculeata* abundances corresponding to B3 and B4 (see Fig. 19). At the same time, dominant species in PS72/340-5 and PS72/344-4 - *C. wuellerstorfi* - is almost absent in PS72/342-1 samples and agglutinated shells either. On the other side, a quite correlation was achieved between PS72/342-1, PS72/340-5 and HLY0503-8JPC using inorganic sediment proxies as will be shown below. Therefore, biostratigraphic correlation between cores from different water depths should be done cautiously, taking into consideration different environmental settings (including depth and water mass circulation) at the studied locations (Polyak et al., 2004, and references therein). Other paleoproductivity proxies such as TOC contents should also be considered as potentially biased due to the postdepositional alterations. Arctic Ocean sediments receive organic carbon from terrestrial runoff, aeolian deposits and marine biological productivity. In the Eurasian shelf seas, TOC found in sediments is predominantly of terrestrial origin as derived from the Siberian hinterland (Stein et al., 1994). However, this can be a result of degradation of the major part of marine organic matter in sediments as proved by biomarker studies in the East Siberian Sea (Vetrov et al., 2008). TOC fluxes are also influenced by changes in mass accumulation rates (density of sediment multiplied by linear sedimentation rates, Knies et al., 2000). Therefore, the TOC variability in the studied cores does not necessarily indicate directly the glacial/interglacial variations in paleoproductivity when TOC peaks in grey sediment units are associated with colder stages as explained by higher preservation of organic matter (Henrich, 1989; Knies et al., 2000; Vogt et al., 2001).

Table 6. Stratigraphic boundaries in core PS72/340-5 based on microfaunal findings

Unit	Faunal findings in core PS72/340-5	MIS	Core
base of B1	drop in *C. wuellerstorfi* and *Epistominella spp.*	MIS 1/2	
B2	peak in *C. wuellerstorfi* and *Epistominella spp.*	MIS 3.1 or 3.3	
B3	peak in *C. wuellerstorfi* and *Epistominella spp.*	MIS 5.1 or earlier	
B4	peak in *C. w.*, *E. spp.*, *O. tener*, *C. subglobosum* (agglutinates), single *B. aculeata*	MIS 5.1* / MIS 4**	HLY0503-8JPC, NP26-5
B5	peak in *C. subglobosum*, no calcareous forams	MIS 5.1	PS2185***
B7	peak in *C. wuellerstorfi*, *C. trullisata (agglutinates)*; last *B. arctica* maximum	MIS 5.5	NP26-5
base of B7	drop in *C.w., B.arctica, C.subgl., Ep. spp.*	MIS 5/6	

*Polyak et al. (2004), Adler et al. (2009); **Backman et al. (2009); ***J. Wollenburg (*unpubl. data*)

Calibrated radiocarbon dates (Table 3) and ages of excursions were used as tie points for tuning of relative paleointensity variations in core PS72/340-5 to the global stack. We used the high-resolution global geomagnetic paleointensity curve for the past 75 kyr GLOPIS-75 (Laj et al., 2004), combined with the youngest part of synthetic paleointensity stack PISO-1500 (Channell et al., 2009) which integrates 13 records into a composite curve. Tuning was performed using the best-match dynamic programming algorithm (Lisiecki and Lisiecki, 2002), while minima in paleointensity values should be consistent with the reversed inclinations. Obtained data points were used to rescale the paleointensity values in order to plot the age-depth curve (black curve, Fig. 21). For comparison, additional run was made without using any magnetic excursions as tie points (green curve). On the whole, the curve resulting from tuning is similar to the no-tie curve. The long interval of reversed inclinations between 100 and 170 cm core depth is the most difficult to interpret. Here the sedimentation rates seem to be quite high, probably enlarging the log-in depth where the paleomagnetic signal is fixed.

Another possible solution would be to set the NGS event (70 ka) to 215 cm and Blake event (120 ka) to 365 cm (Fig. 22). Then the inclination minima at 520 cm could be referred to as the Fram Strait event (155-165 ka), which is not considered to be globally reliable according to Roberts (2008) but was repeatedly found in the Arctic Ocean sediments (Nowaczyk et al., 2001, and references therein). This would result in lower sedimentation rates and larger mismatch with the no-tie curve in comparison to the first model. However similar age model when B5 corresponds to MIS 6 was obtained by tuning of manganese records to the global benthic oxygen isotope stack (L. Polyak, pers. comm.).

The last calibrated radiocarbon date does not fit either of the proposed age-depth curves. Some explanations were proposed in literature to explain the old radiocarbon ages estimated in the Arctic Ocean cores. In Figure 23, the age-depth distribution in several cores from the Mendeleev Ridge is shown. In general, very few data points are available for MIS 2 (14-29 ka) which should be characterized by severe ice conditions and consequent low bioproductivity. Older radiocarbon ages are mostly reversed and restricted to the top of B2 unit which features high contents of dolomite. Detrital carbonates can bias the ^{14}C composition in foraminiferal tests through contamination with fine-grained carbonate and/or through the accompanying release of hard water containing dissolved old carbonate (for more details see Polyak et al., 2009, and references therein).

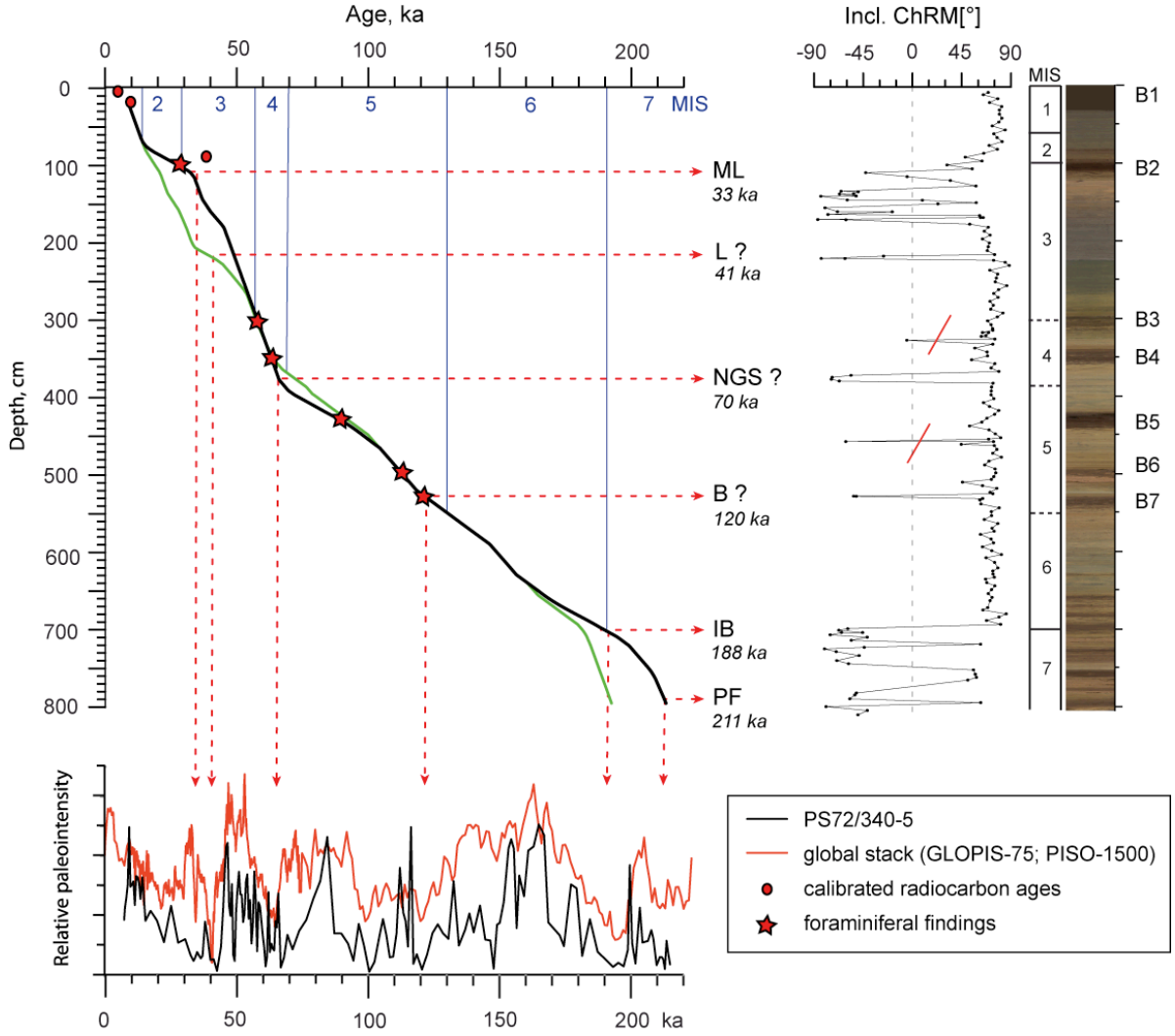

Figure 21. Age model **1** of core PS72/340-5 based on the paleomagnetic data. Calibrated radiocarbon (calendar) ages are given in Table 2, foraminiferal findings used as biostratigraphic markers are listed in Table 5. Ages of MIS boundaries are based on the LR04 stack (Lisiecki and Raymo, 2005).
Relative paleointensity variations in core PS72/340-5 were tuned to the global stack: 1) GLOPIS-75 for the last 75 ka (Laj et al., 2004), and 2) PISO-1500 for the last 1500 ka (Channell et al., 2009). Red arrows mark the minima in paleointensity corresponding to the excursions proposed (ML – Mono Lake, L – Laschamp, NGS – North Greenland Sea, B – Blake, IB – Iceland Basin, PF – Pringle Falls). Ages of excursions (Roberts, 2008, and references therein) were used as tie points. Age-depth curve (black) was obtained using the tuned record. Green curve shows the alternative tuning results obtained without using tie points (no-tie curve).

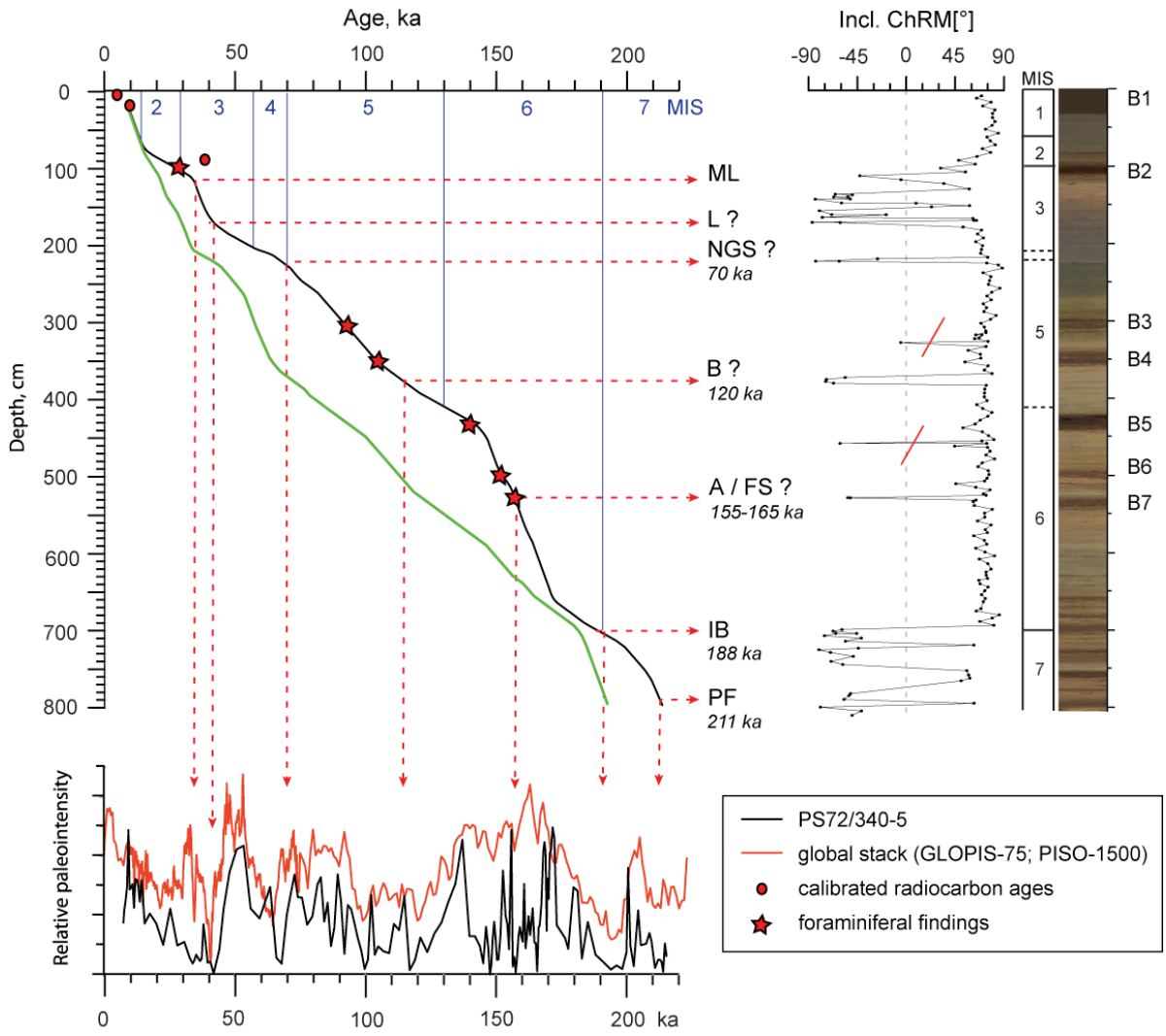

Figure 22. Age model **2** of core PS72/340-5 based on the paleomagnetic data. Calibrated radiocarbon (calendar) ages are given in Table 2, foraminiferal findings used as biostratigraphic markers are listed in Table 5. Ages of MIS boundaries are based on the LR04 stack (Lisiecki and Raymo, 2005).
Relative paleointensity variations in core PS72/340-5 were tuned to the global stack: 1) GLOPIS-75 for the last 75 ka (Laj et al., 2004), and 2) PISO-1500 for the last 1500 ka (Channell et al., 2009). Red arrows mark the minima in paleointensity corresponding to the excursions proposed (ML – Mono Lake, L – Laschamp, NGS – North Greenland Sea, B – Blake, A / FS – Albuquerque / Fram Strait, IB – Iceland Basin, PF – Pringle Falls). Age-depth curve (black) was obtained using the tuned record. Green curve shows the alternative tuning results obtained without using tie points (no-tie curve).

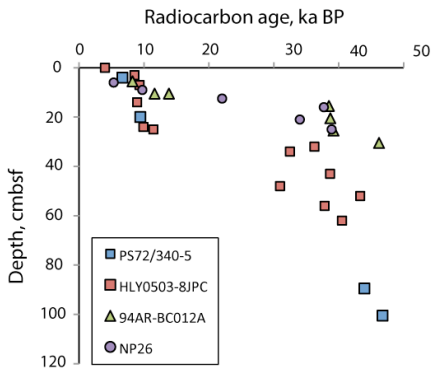

Figure 23. Distribution of uncalibrated radiocarbon ages in cores from the Mendeleev Ridge: PS72/340-5 (this study), HLY0503-8JPC (Kaufman et al., 2008); 94AR-BC012A (Cronin et al., 2010), NP26-32/5 (Polyak et al., 2004). No reservoir correction was applied due to its uncertainty in the Arctic Ocean.

For correlation with other sediment records from the Mendeleev Ridge area, we compared the downcore variations of lightness, coarse-fraction contents (>63 μm) and magnetic susceptibility in cores PS72/340-5 and HLY0503-8JPC (Adler et al., 2009), dated by AMS ^{14}C and amino acid racemization (AAR) methods. The correlation results show a quite good consistency of the two records (Fig. 24), demonstrating coarsening in the carbonate-rich pink layers, brown units and adjacent zones. Magnetic susceptibility peaks normally correspond to the brown units, except for the prominent MS maximum within MIS 6 sediments which looks consistent with high amount of coarse-grained material.

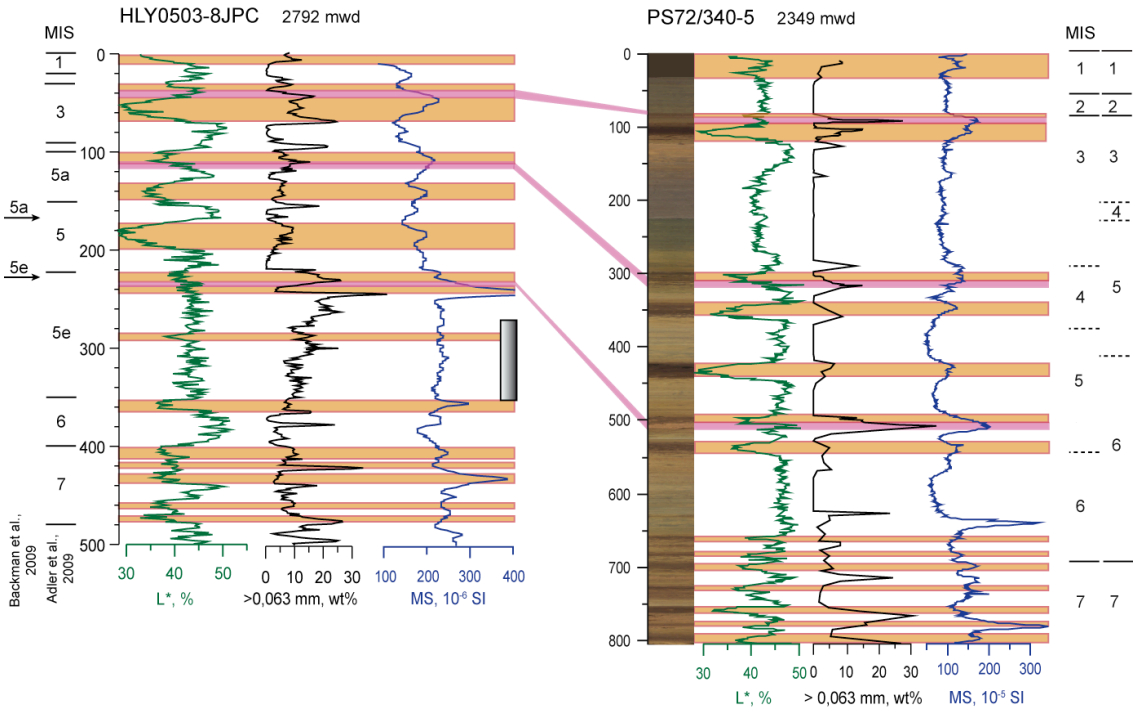

Figure 24. Lithostratigraphic correlation of cores PS72/340-5 and HLY0503-8JPC (Adler et al., 2009; Sellen et al., 2010): L* - lightness, > 0.063 mm - contents of coarse-grained fraction, MS - magnetic susceptibility. In core HLY0503-8JPC, grey shaded bar marks the slump interval, alternative positions of MIS 5a and 5e peaks are shown according to Backman et al. (2009). For core locations see Fig. 8.

Magnetic susceptibility is a good tool for correlation of cores along the Siberian shelves (Stein et al., 2001) and in the central Arctic Ocean (Sellen et al., 2010). Glacial and interglacial modes of sediment deposition are recorded by cyclic variations in bulk magnetic properties as evident in studies of ice-rafted debris and stable isotopic and faunal assemblages in the ACEX cores from the Lomonosov Ridge in the Central Arctic Ocean (O'Regan et al., 2008). MS signal increase in marine sediments is characteristic for periods of higher terrestrial input from the Siberian hinterland where volcanic and indigenous rocks containing ferromagnetic minerals are widely distributed (Stein, 2008; and references therein).

The MS peak corresponding to MIS 6 observed in cores PS72/340-5 and HLY0503-8JPC can be also traced at the base of core PS72/343-1 (Fig. 25). Special attention should be paid to the MS peak in between B6 and B7 units of core PS72/340-5. This peak also seems to appear both in cores PS72/343-1 and PS72/344-1, however, there it is not bound to obvious brown units although other parameters support the proposed correlation scheme along the profile that was suggested by Stein et al. (2010), as will be shown below.

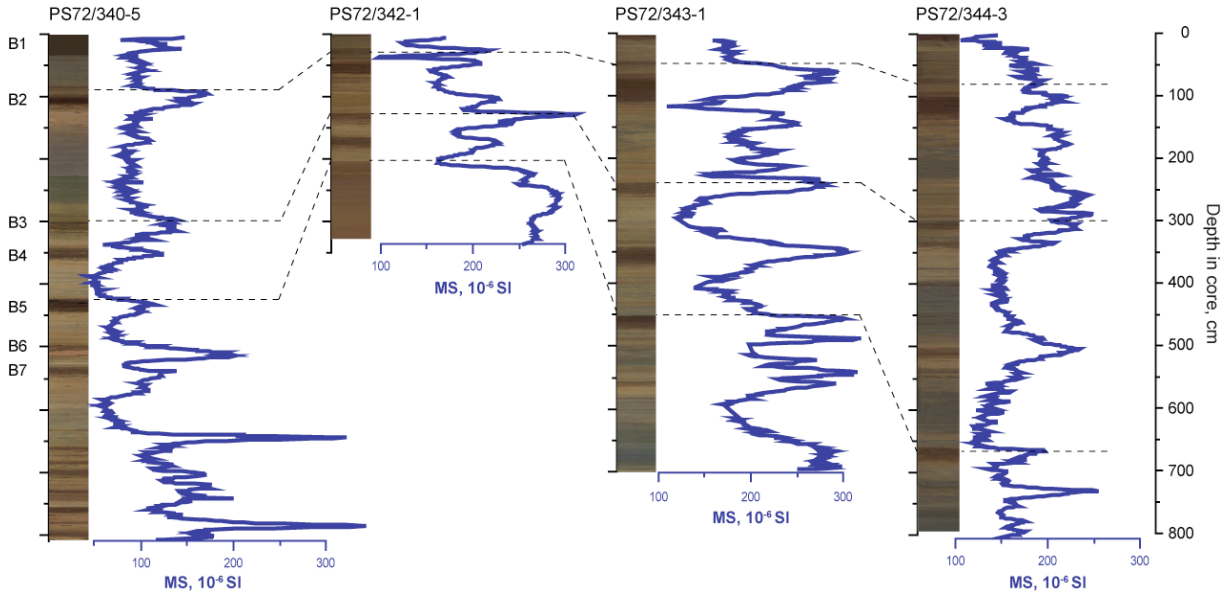

Figure 25. Stratigraphic correlations of cores PS72/340-5, PS72/342-1, PS72/343-1 and PS72/344-3: magnetic susceptibility (MS) measured using the multi-sensor core logger at 1-cm intervals. Brown units are indicated as B1-B7.

That initial correlation was based on shipboard lithological descriptions and colour cyclostratigraphy which can be clearly followed in the lightness records (Fig. 26). On the whole, commonly used counting of manganese-rich brown units in the Arctic Ocean cores works well but other sediment properties should also be taken into consideration for correlation purposes because of possible diagenetic overprints (Löwemark et al., 2008; März et al., 2011).

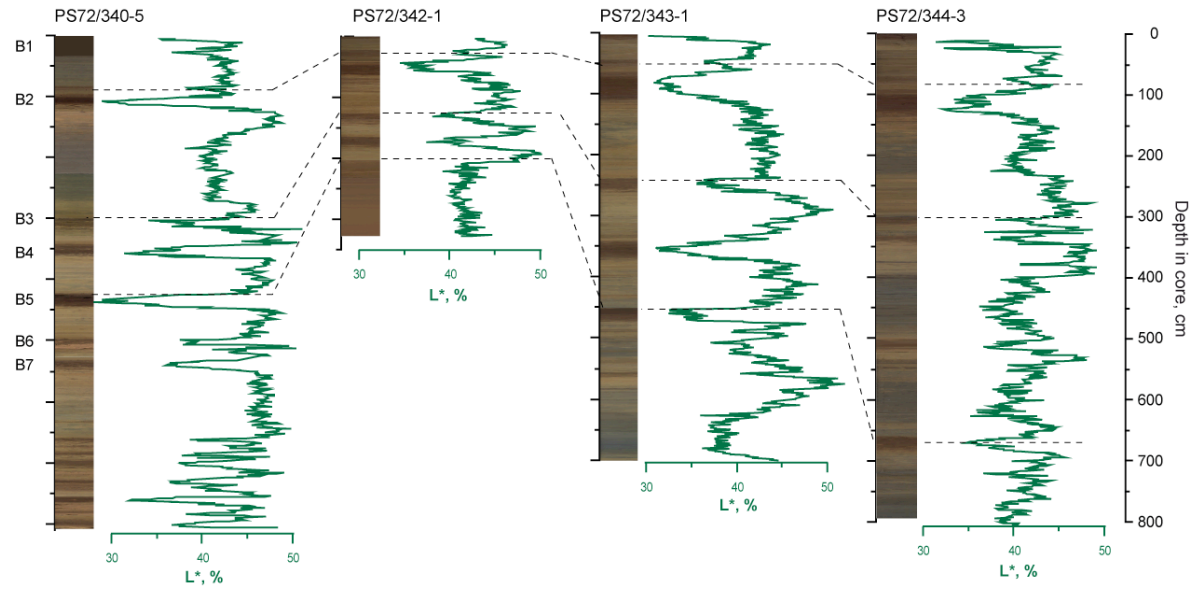

Figure 26. Stratigraphic correlations of cores PS72/340-5, PS72/342-1, PS72/343-1 and PS72/344-3: lightness (L*) inferred from spectral reflectance measured at 1-cm intervals. Brown units are indicated as B1-B7.

A good proxy for development of a stratigraphic correlation is terrigenous sediment composition as it is not much affected by diagenetic processes (Polyak et al., 2009). Build-up and disintegration of ice sheets in the Arctic Ocean periphery are accompanied by increased iceberg discharge to the ocean. The history of iceberg transport of terrigenous material is reflected by the ice-rafted debris (IRD) abundance and variability of its composition (Polyak et al., 2004; Spielhagen et al., 2004). Correlation scheme based on the distribution of coarse-grained material and dolomite is shown in Figure 27.

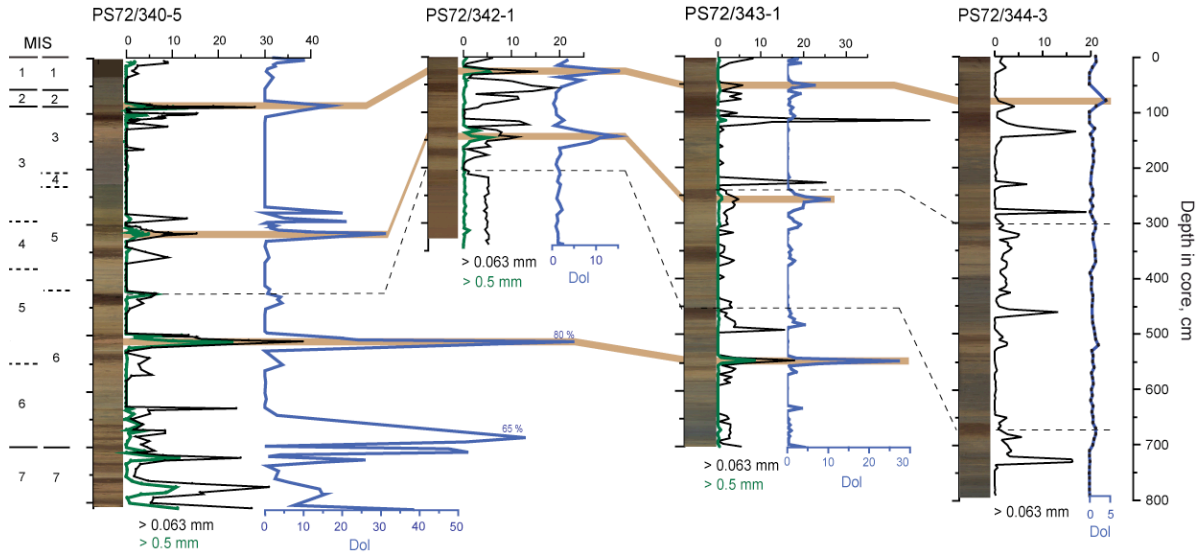

Figure 27. Stratigraphic correlations of cores PS72/340-5, PS72/342-1, PS72/343-1 and PS72/344-3: contents of coarse-grained fraction (wt%) and dolomite (Dol, wt%). Light brown bars mark the most prominent dolomite-rich pink layers. Two age models are shown as discussed in *Chapter 6.5.1*.

6.5.2 Late Quaternary sedimentary paleoenvironments at the Mendeleev Ridge

During the years, a conceptional paleoceanographical model was created for the Arctic Ocean defining lithofacies for glacial, deglacial and interglacial deposition. Cyclic sequences of alternating greyish and brownish layers in the Arctic Ocean are interpreted as resulting from a succession of glacial to interglacial events. In general, interglacial sediments are of brownish and light yellowish colours, characterized by high planktic foraminiferal abundances with low amount of organic carbon, lows in bulk density and p-wave velocity and maxima in magnetic susceptibility, strongly bioturbated. Glacial/interglacial transitions are marked by enhanced deposition of coarse-grained material. On the other hand, glacial sediments are mainly grayish silty muds with low content of foraminifers and increased organic carbon values (e.g. Henrich, 1989; Jakobsson et al., 2000; Norgaard-Pedersen et al., 2007; O'Regan et al., 2008; Polyak et al., 2004; Spielhagen et al., 2004; Vogt et al., 2001). In the work by Jakobsson et al. (2000) a new stratigraphic model was established based on Brunhes-age estimates of geomagnetic inclination reversals, sequential variations in manganese content and color of deep-sea sediments retrieved from the Lomonosov Ridge, tuned to the $\delta^{18}O$ glacial/interglacial global benthic isotope curve, and coccolith assemblages. This age model along with sediment proxies such as physical properties (e.g. sediment density, magnetic susceptibility), IRD contents, biostratigraphy, mineralogical composition, was used to reconstruct paleoceanographic regimes in the Arctic Ocean during the late Quaternary times (e.g. Adler et al., 2009; Norgaard-Pedersen et al., 2007; O'Regan et al., 2008; Polyak et al., 2004; Spielhagen et al., 2004).

Dolomite-rich layers, that often have pinkish colours and therefore referred to as the ‘pink and ‘pink-white’ layers, can be used as regional stratigraphic markers in the Amerasian Basin of the Arctic Ocean (Clark et al., 1980). In our cores, dolomite contents in sediments decrease westwards from core PS72/340-5 to PS72/343-1, possibly indicating the diminishing terrigenous supply from the Canadian Arctic Archipelago, the proposed source area for dolomite dropstones in sediment cores from the Amerasian Basin of the Arctic Ocean (Dalrymple and Maass, 1987; Darby et al., 1989). Pronounced dolomite maxima in our cores are associated with layers comprising gravely (2-10 mm) and coarser material, which can be indicative of iceberg transport for dolomite. On the other side, peaks in the amount of sand (63-125 μm) are mainly consistent with the quartz maxima (not shown here), which is indicative of terrigenous source areas in Eastern Siberia known for the wide distribution of granite rocks (Vinogradov et al., 2008). Separation of these two classes of coarse-grained material (sand and

gravel) derived from different sediment sources, namely North America and Eurasia, was also described by Phillips and Grantz (2001).

Gravel particles associated mostly with dolomite occur in the brown units related to interglacial/interstadial periods. This can be a result of more intensive sea-ice melt-out, with much higher deposition in the ice marginal zone in comparison with perennial ice in the central Arctic. The iceberg melt rate is affected by subsurface circulation in the Arctic Ocean so that periods with enhanced inflow of intermediate, warm Atlantic water to the western Arctic during glaciations were likely characterized with higher sedimentation from icebergs (Phillips and Grantz, 2001; Polyak et al., 2009). In core PS72/344-3, dolomite contents are typically below detection limits (2 wt%) except for the layer above B2 which could be correlated to the first pink layer in the other cores. Location of the coring site PS72/344 on the west flank of the Mendeleev Ridge is not significantly influenced by the modern current circulation system of the Beaufort Gyre (Fig. 11). This implies that the first pink layer was deposited when the material flux from the North American hinterland reached this core location. One possible explanation would be a shift in the surface currents towards the Siberian margin as proposed by Bischof et al. (1996). On the other side, an alternative scenario of higher iceberg discharge should be considered as the IRD can partly settle down before reaching this location because of the iceberg melt-out. Additionally, existence of large ice masses on the ESS shelf in MIS 4-6 (Stein et al., 2010) as well as late Pleistocene glaciations (including the LGM) on the Chukchi margin (Jakobsson et al., 2010; Polyak et al., 2007) could restrict the circulation of surface currents in this region, therefore preventing penetration of the North American ice-rafted material to the ESS margin.

In contrast to the gravel material, sand distribution in cores is not uniform. In PS72/342-1, PS72/343-1 and PS72/344-3, sand also peaks in the transition zones between brown and grey units and within grey beds. As shown by different studies, maxima of coarse-grained material normally correspond to greyish units. These lithofacies are associated with episodes of intensive iceberg rafting during deglaciations (e.g. Henrich, 1989; Jakobsson et al., 2000; Norgaard-Pedersen et al., 2007; O'Regan et al., 2008; Polyak et al., 2004; Spielhagen et al., 2004; Vogt et al., 2001). High contents of sand within brown units in core PS72/340-5 and PS72/342-1 can probably present an artifact as the sampling resolution seems to be not high enough because of lower sedimentation rates in these cores. The relatively high sedimentation rates observed in core PS72/344 can be explained by significant riverine sediment input from the Siberian hinterland (Lisitzin, 2002). In general, the offshore decrease in sedimentation rates

indicates the importance of Siberia and North America as source areas for terrigenous input to the Arctic Ocean. Location of sediment sources (such as river mouths and eroding coasts) and current system at the continental margins, as well as combination of sea-ice concentration and melt-out rates, with much higher deposition in the ice marginal zone in comparison with perennial ice in the central Arctic, determine the sedimentation rates in the Arctic Ocean (Backman et al., 2004; Polyak et al., 2009; Sellen et al., 2010; Spielhagen et al., 2004). Results of the grain-size analysis (*Ch. 6.4.2*) indicate that the Mendeleev Ridge also plays an important role in the sediment distribution as sediments in cores PS72/340-5 (Chukchi Abyssal Plain) and PS72/344-3 (close to the ESS margin) are in general finer than in PS72/342-1 and PS72/343-1 located closer to the ridge crest. Events characterized by strong increase in sand contents are potentially connected to the existence of large ice masses on the ESS shelf in MIS 4-6 (Stein et al., 2010) which was discussed before. In addition, at the same time advance of the large Eurasian ice sheet in West Siberia had a huge impact on the water mass circulation along the Siberian margin reflected in high IRD contents in many sediment cores from the central Arctic Ocean (Spielhagen et al., 2004; Svendsen et al., 2004). However additional information on the IRD provenance is needed to differentiate between potential sediment source areas in Eurasia.

6.5 Conclusions

As evidenced by grain-size and mineralogical data, there were several events of intensified sediment discharge at the Mendeleev Ridge possibly linked to paleoenvironmental changes in North America and Eurasia during the last 200 ka. According to the results of onshore investigations, large parts of North America except for Alaska were covered with ice sheets in glacial times corresponding to MIS 6 and 4-2 (Ehlers and Gibbard, 2007; England et al., 2009). Termination of these glaciations are reflected in the presence of pink (dolomite-rich) layers in cores along the studied transect. NE Russia is believed to have remained mostly ice-free during these two glacial cycles (e.g. Gualtieri et al., 2003), although new geophysical data yield existence of grounding ice masses on the topographical highs and shelves of the Chukchi and East Siberian Seas (Jakobsson et al., 2010; Polyak et al., 2007; Stein et al., 2010), as well as it is suggested that ice cover existed in MIS 6 on the New Siberian Islands (Basilyan et al., 2010). Additional information on the IRD provenance is needed to differentiate between sediment source areas in Eurasia as bulk mineralogical data produced during this study was not sufficient to distinguish between the Chukchi, East Siberian and Laptev seas as potential

source areas for sediment supply. Additional time control is also needed to assign specific ages to the events of iceberg discharge.

6.6 Acknowledgements

We thank captain Stefan Schwarze, his RV "Polarstern" crew and the scientific party onboard for the excellent cooperation during the ARK-XXIII/3 Expedition. This study was carried out within the PhD project of EB supported by the Helmholtz Research School for Polar and Marine Research (POLMAR). We are very thankful to L. Polyak for discussions on the core stratigraphy. Sedigraph grain-size measurements and foraminiferal analysis of core PS72/342-1 were performed at the Otto-Schmidt-Laboratory (AARI, St.Petersburg) in the frame of research grants to EB and SK (projects OSL-11-04 and OSL-12-06). Data supplement is available online at www.pangaea.de.

7 Provenance discrimination in sediments from the Mendeleev Ridge: new insights from the radiogenic Pb and Nd signature of detrital fraction

E. A. Bazhenova, N. Fagel, S. Kostygov, R. Stein

Sediment provenance in the Arctic Ocean was investigated using the isotopic composition of radiogenic lead (Pb) and neodymium (Nd) of detrital clay-size fraction in core PS72/340-5 recovered at the eastern flank of the Mendeleev Ridge. Prior to the geochemical analyses, grain-size distribution in sediments was analyzed and clay fraction was extracted in order to minimize the signals overlapping. For provenance discrimination, results were compared with marine surface sediment data and values for the circum-Arctic subaerial provinces. Based on the isotopic signature and additional mineralogical and geochemical data, potential end-members for the source mixing analysis were determined as the Lena River suspended matter (SPM), Mackenzie River SPM and Okhotsk-Chukotka Volcanic Arc. Late Quaternary sediment supply variability was analyzed using the mixing model constrained by two tracers: $^{207}Pb/^{206}Pb$ and εNd. Our results confirm that over the last 200 ka dolomite-rich pink layers at the southern Mendeleev Ridge were deposited during events associated with intensified iceberg transport from North America. On the whole, sedimentation was mostly controlled by terrigenous input from the Chukchi and East Siberian Seas whereas sediment supply from the Laptev Sea area remained less important and relatively constant at the studied location.

7.1 Introduction

The Quaternary history of the Arctic region comprises cyclical changes in the extension of the land-based ice sheets and sea-ice cover that affected sedimentary environments in the Arctic Ocean (Knies et al., 2000; Polyak and Jakobsson, 2011; Spielhagen et al., 2004). Identification of source areas for the material transported from the hinterland (North America and Eurasia) gives important information about the surface circulation patterns in the Arctic Ocean. Because the landmasses surrounding the Arctic Ocean are composed of different geological terraines, characterized by a very specific mineralogical and chemical signature, relevant data obtained from marine sediments can be used for the determination of the sediment provenance. Whereas today sea ice is the dominant sediment transport agent, during Pleistocene times icebergs from the continental ice sheets surrounding the Arctic Ocean delivered coarse-grained ice-rafted debris to the Arctic Ocean. Based on the petrographical diversity and other characteristics of these rock clasts, information about both past circulation patterns as well as locations where ice sheet existed and calved into the Arctic Ocean, may be obtained (e.g. Bischof et al., 1996; Phillips & Grantz, 2001).

In marine sediment cores from the Amerasian Basin of the Arctic Ocean, especially at the Northwind and Mendeleev Ridges, distinct pink and pink-white carbonate-rich layers with common occurrence of rock clasts are used as lithostratigraphic boundaries (Clark et al., 1980). These layers are enriched in dolomite which was described as a common mineral in surface sediments of the Beaufort Sea, as shown by microscopic and petrographic studies performed on the coarse fraction (e.g. Belov and Lapina, 1961; Bischof et al., 1996). Vast carbonate province of Cambrian-Devonian age outcropping on the Canadian Arctic Archipelago is considered to be the main source for dolomites in the Arctic Ocean sediments (Dalrymple and Maass, 1987; Darby et al., 1989). At the same time, thick Paleozoic carbonate strata were described on the Wrangel, Kotelniy Islands and Severnaya Zemlya archipelago as well as in the Kolyma and Olenek river valleys (Gordeev and Sidorov, 1993; Petrov et al., 1995). Nevertheless, western Laptev Sea, ESS, and Southern Lomonosov Ridge surface sediments do not contain much dolomite (Müller and Stein, 2000; Bazhenova et al., in prep. for MarGeo; Viscosi-Shirley et al., 2003a; 2003b; Vogt, 1997) while glacial samples from the central Lomonosov Ridge and samples from the Morris Jesup Rise cores close to North Greenland do contain high contents of dolomite in the coarse fraction which is suggested to be transported by icebergs as shown by Nørgaard-Pedersen et al. (2007; 1998), Vogt (1996; 1997), Behrends et al. (1999). Therefore, additional mineralogical and geochemical evidence should be found to

confirm the origin of dolomite in the central Arctic Ocean sediments as no detailed comparison of core material with the potential source rocks has been performed yet.

In this study we used sediment core record PS72/340-5 from the Mendeleev Ridge, which spans the last 200 ka, to investigate isotopic composition of radiogenic lead (Pb) and neodymium (Nd) in the clay-size detrital fraction. Obtained results are used to estimate contributions from different sediment sources over time.

7.2 Sampling and analytical methods

7.2.1 Oceanographic setting

The present-day current pattern in the Arctic Ocean (Fig. 28) is determined by interaction of Atlantic and Pacific saline water masses together with the freshwater inflow from rivers draining the Arctic hinterland. Rivers also bring loads of weathering products of the present-day Upper Continental Crust. That is why sediment samples from the large river basins can be used to get an average geochemical signal of subaerial geological terraines surrounding the Arctic Ocean (McLennan, 2001; Millot et al., 2004). The Arctic Coastal Current, forced by winds, river outflows and ice melt, flows from the ESS eastward (Weingartner et al., 1999). The Transpolar Drift leads to the movement of sea-ice away from the Siberian coast, across the Arctic basin, and south through the Fram Strait (Rudels et al., 2004). Pacific water masses enter the Arctic Ocean via the Bering Strait and then penetrate into the Chukchi and Beaufort Seas. In the Canadian Basin, the surface oceanic circulation is dominated by the Beaufort Gyre (e.g. Polyak and Jakobsson, 2011). Distribution of trace elements in the surface waters seems to follow the main systems of the Arctic Ocean currents (Schlosser et al., 1995). Based on the isotopic composition of sediments, changes in continental erosion and oceanic circulation can be reconstructed (Haley et al., 2008; Winter et al., 1997).

Table 7. Locations of surface samples and core PS72/340-5

Sample ID	Depth, m	Latitude	Longitude	Location	Cruise
PS72/287-1	353	74° 15.96' N	90° 59.14' W	CAA	ARK-XXIII/3
PS72/289-1	3533	75° 6.59' N	136° 35.08' W	Beaufort Sea	ARK-XXIII/3
PS72/291-1	1548	71° 16.15' N	137° 10.82' W	Beaufort Sea	ARK-XXIII/3
PS72/340-5	**2344**	**77° 35.19' N**	**171° 32.52' W**	**S Mendeleev Ridge**	**ARK-XXIII/3**
PS72/343-3	1227	77° 18.36' N	179° 2.84' E	S Mendeleev Ridge	ARK-XXIII/3
PS72/344-1	1265	77° 35.99' N	174° 32.41' E	S Mendeleev Ridge	ARK-XXIII/3
G2	49	65° 56.02' N	169° 36.96' W	Bering Strait	RUSALCA-2009
G10	38	65° 35.02' N	168° 7.19' W	Bering Strait	RUSALCA-2009
G25	49	68° 23.80' N	174° 9.13' W	Chukchi Sea	RUSALCA-2009
G27	56	70° 16.95' N	176° 40.04' W	Chukchi Sea	RUSALCA-2009
G33	45	69° 49.38' N	177° 59.35' E	Wrangel Island/CS	RUSALCA-2009
G36	45	72° 25.73' N	174° 0.67' E	East Siberian Sea	RUSALCA-2009
G40	30	71° 39.70' N	179° 30.50' E	Wrangel Island/ESS	RUSALCA-2009

Station locations from the ARK-XXIII/3 Expedition are listed in the cruise report by Jokat (2009), for other stations coordinates and more details can be found in the report of RUSALCA-2009 Expedition (RUSALCA, 2009).

Our study was focused on sediment core PS72/340-5 recovered during the ARK-XXIII/3 Expedition of RV "Polarstern" in 2008. Several surface samples were used in addition to the literature results to investigate the sediment provenance. For coring locations see Figure 28, coordinates are given in Table 7.

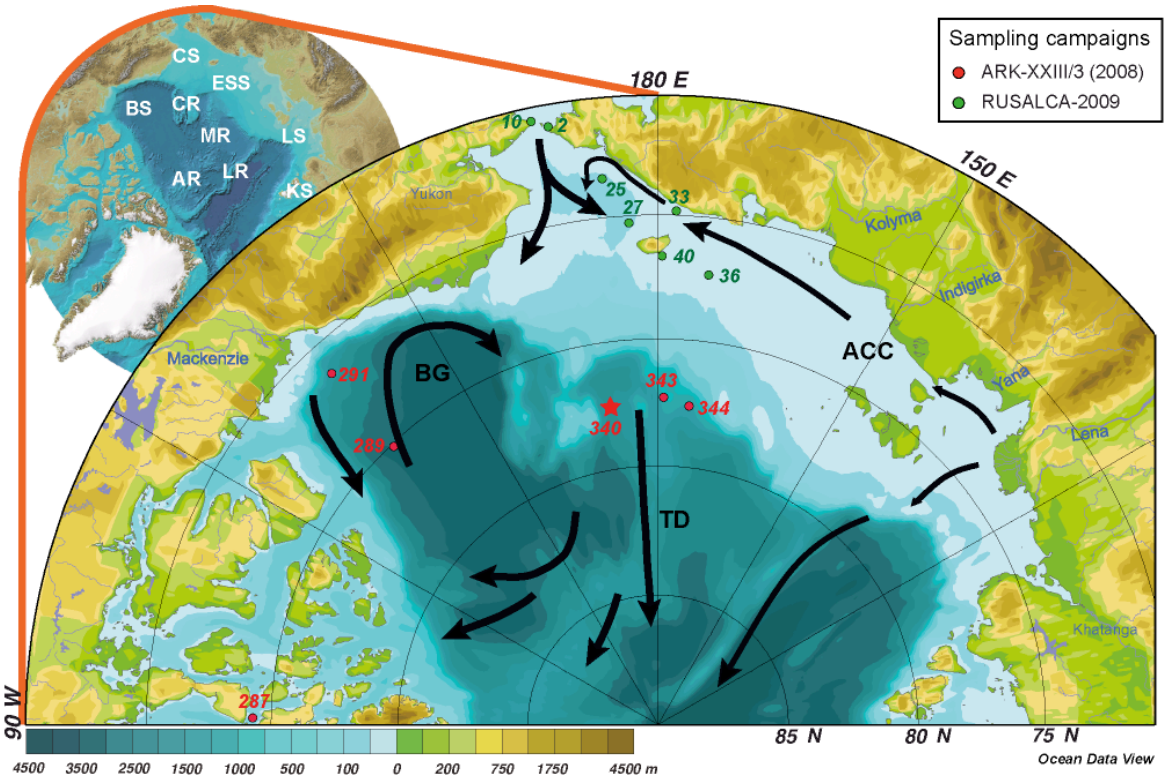

Figure 28. Locations of surface samples used in this study (coordinated listed in Table 9), position of core PS72/340-5 is highlighted by red star. Black arrows mark the directions of major surface current systems: BG – Beaufort Gyre, TD – Transpolar Drift, ACC – Arctic Coastal Current (for details see text). Inlay map shows the Arctic Ocean (CS – Chukchi Sea, ESS – East Siberian Sea, LS – Laptev Sea, KS – Kara Sea, BS – Beaufort Sea, CR – Chukchi Rise, MR – Mendeleev Ridge, AR – Alpha Ridge, LR – Lomonosov Ridge), bathymetry used on both maps is IBCAO (Jakobsson et al., 2008).

7.2.2 Core lithology and stratigraphy

Sediment core PS72/340-5 was sampled at changes in lithology and/or colour to represent all the lithostratigraphic units according to the age model discussed by Bazhenova et al. (*Ch. 6*). The core is mostly composed of various horizontally bedded silty clay units interlaid by a number of diamictons with higher contents of coarse-grained material. According to the commonly used stratigraphy for the Arctic Ocean cores (e.g. Jakobsson et al., 2000), we distinguish between coarse-grained 'brown' units and 'grey' beds, which are of olive to grey colours and very fine-grained. There are also several prominent pink layers enriched in dolomite which are used for correlation of cores in the Amerasian Basin of the Arctic Ocean (Clark et al., 1980).

7.2.3 Grain-size analysis

Prior to the provenance investigations, grain-size distribution in sediments was analyzed. Coarse fraction (>63 μm) was isolated via wet sieving. Grain-size distribution in the fine fraction (<63 μm) was analyzed using a Micromeritics Sedigraph 5100 facility at the Otto-Schmidt-Laboratory (Arctic and Antarctic Research Institute, St.Petersburg, Russia). This technique is meant to measure the gravity-induced settling rates of different size particles in a liquid with known properties. Each sample was tested three times to gain statistically significant data. The output grain-size data represents a set of mass concentrations for the grain sizes from 0.5 to 63 μm measured with increasing step of 0.3 to 3 μm. The cumulative data were recalculated to get absolute weight percentages of size classes. Analytical details and errors are described by Stein (1985), McCave et al. (1995) and Bianchi et al. (1999). To gain a better understanding of the grain-size distribution in sediments, principal component analysis (PCA) of the data was undertaken. This analysis allows us to distinguish grain-size spectral components, which we relate to potential input functions. We included only the fine-grained fraction (0.5-63 μm) into the PCA to avoid the problem of the 'closed array' which occurs when the sum of wt% is normalized to 100 (Andrews and Eberl, 2011).

7.2.4 Isotopic analyses

Sample preparation for the MC-ICP-MS measurements was carried out at the University of Liege (Belgium). Nd and Pb eluates were obtained from the clay fraction (< 2 μm) of core PS72/340-5. This grain size was extracted from the sieved fine fraction (< 63 μm) during sedimentation in water, after the settling time calculated from the Stoke's law. For surface samples, measurements were performed on the bulk ground sediments. All the samples

were treated with HCl 0.1N to remove biogenic carbonates and possible contaminant lead in the case of surface sediments (Gobeil et al., 2001). After that samples were calcined at 550 °C to destroy the organic matter. Following chemical separation took place in the clean laboratory according to the analytical protocol described by Weis et al. (2006). Samples were digested using the mixture of three acids: HF, HNO_3 and HCl. Column chemistry was devided into three steps. Firstly, Pb was separated using the AG 1-X8 anion exchange resin and HBr eluent. After that REE were concentrated using the AG 50-X8 cation exchange resin in HCl environment. Nd was extracted from the REE fraction using the HDEHP adsorbent and HCl eluent.

Isotopic composition of Pb and Nd was measured on a Nu Plasma MC-ICP-MS instrument at the Université Libre de Bruxelles (Belgium). Pb measurements were performed in static wet mode when isotope ratios $^{208}Pb/^{204}Pb$, $^{207}Pb/^{204}Pb$, $^{206}Pb/^{204}Pb$, $^{208}Pb/^{206}Pb$ and $^{207}Pb/^{206}Pb$ were determined. The results were corrected for mass fractionation using internal standard (Tl), as well as for variations in instrumental mass discrimination by common Pb standard (NBS-981) bracketing. Results of 20 NBS-981 measurements ($^{208}Pb/^{204}Pb = 36.7145 \pm 0.0058$, $^{207}Pb/^{204}Pb = 15.4972 \pm 0.0018$, $^{206}Pb/^{204}Pb = 16.9408 \pm 0.0018$) were consistent with the laboratory long term values ($^{208}Pb/^{204}Pb = 36.7149$, $^{207}Pb/^{204}Pb = 15.4969$, $^{206}Pb/^{204}Pb = 16.9402$, n = 608) and with the recommended NBS-981 values of $^{208}Pb/^{204}Pb = 36.7219 \pm 0.0044$, $^{207}Pb/^{204}Pb = 15.4963 \pm 0.0016$, $^{206}Pb/^{204}Pb = 16.9405 \pm 0.0015$ (Galer and Abouchami, 1998). Good reproducibility and representativity of the sample aliquote was confirmed by 8 replicate runs for both Pb and Nd fractions.

Nd fraction was analysed in dynamic dry mode. Measured $^{143}Nd/^{144}Nd$ values were corrected: 1) for mass fractionation using the $^{146}Nd/^{144}Nd$ values; 2) for instrumental drift by standard bracketing using the Rennes Nd standard (University of Rennes, France). The Rennes Nd standard yielded $^{143}Nd/^{144}Nd = 0.511952 \pm 0.000019$ (2σ, n=16), equivalent to $\varepsilon Nd = -13.42 \pm 0.37$, which is consistent with the Rennes value of $^{143}Nd/^{144}Nd = 0.511961 \pm 0.000013$ obtained by Chauvel and Blitchert-Toft (2001). The corrected $^{143}Nd/^{144}Nd$ values were normalized to the chondritic uniform reservoir (CHUR) composition as

$$\varepsilon Nd_{sample} = [(^{143}Nd/^{144}Nd)_{sample}/(^{143}Nd/^{144}Nd)_{CHUR} - 1] \times 10000$$

where $(^{143}Nd/^{144}Nd)_{CHUR} = 0.512638$ (Wasserburg et al., 1981).

Important aspect to note is that the detrital fraction was chosen for investigations. Prior to the column separation, no long-time leaching of sediments was performed. This is of importance for further interpretations and comparison with published values in

leachates/residues (e.g. Arctic Ocean study by Maccali et al., 2012) as 1) reproducibility of measurements for leaching experiments is poorer than for the bulk analysis (Hamelin et al., 1990), and 2) commonly used leaching with HCl can cause changes in the $^{143}Nd/^{144}Nd$ and, consequently, in the εNd values (Innocent et al., 2000).

Obtained isotope ratios were compared pairwise to choose the most representative mixing lines. $^{207}Pb/^{206}Pb$ (which is characterized by high measurement precision) and εNd values were used as the two tracers in a mixing model (shown in *Ch. 7.4*, *Discussion*). A 10%-increment mixing grid was calculated based on the $^{207}Pb/^{206}Pb$ and εNd values following Faure (1986). For each grid point the contribution of the three end-members is determined as $\alpha_{EM1,}$ $\beta_{EM2,}$ $\gamma_{EM3,}$ where $\alpha+\beta+\gamma = 1$. The two additional simultaneous equations are used to calculate the $^{207}Pb/^{206}Pb$ (Pb_{mix}) and εNd (εNd_{mix}) of the mixing:

$$Pb_{mix} = [(Pb_{EM1\ x}\ \alpha_{EM1}) + (Pb_{EM2}\ x\ \beta_{EM2}) + (Pb_{EM3}\ x\ \gamma_{EM3})]$$
$$\varepsilon Nd_{mix} = [(Nd_{EM1\ x}\ \alpha_{EM1}) + (Nd_{EM2}\ x\ \beta_{EM2}) + (Nd_{EM3}\ x\ \gamma_{EM3})]$$

7.2.5 Mineralogical analysis

Mineralogical analysis was performed on oriented aggregates of clay-size material using the Bruker D8 Advance Diffractometer at the University of Liege (Belgium). Routine X-ray diffraction (XRD) clay analyses included the successive measurements: 1) in air-dried or natural conditions, 2) after solvation with ethylene glycol (EG) for 24 hours, and 3) after heating at 500°C for 4 hours. XRD data were processed in the program MacDiff Vers. 4.2.6, applying peak correction using quartz, background correction and smoothing, and counts smoothing (for details on this software see Petschick et al., 1996). Semi-quantitative estimations (±5-10%) for the main clay minerals (illite, chlorite, smectite, kaolinite) were based on the height of diagnostic peaks measured during the EG runs, i.e. at 7Å for kaolinite, 10Å for illite and 14Å for chlorite. The smectite content was deduced by its collapse at 10Å after heating. Intensities of diagnostic peaks were then multiplied by a corrective factor (0.7 for kaolinite, 1 for illite and smectite, 0.34 for chlorite) and values were summed up to 100% (Biscaye, 1965).

7.3 Results

Results of PCA performed on the sedigraph grain-size data (0.5-63 μm) from core PS72/340-5 allowed us to distinguish spectral components (Fig. 29), which could be related to potential input functions. The first five factors were chosen based on the statistically significant factor loadings > 0.7 and explain, cumulatively, 82% of the total variance. In general, results of

the PCA indicate that there are several processes generating the grain-size distribution in core PS72/340-5. The most important feature of the < 63 μm part of the spectra is the distinct separation between the silt- (1st and 2nd factors) and clay-related (3rd factor) modes, which can probably result from different mechanisms controlling the input of these two size fractions. The first factor has a broad peak in the range of 5-10 μm, which can be associated with fine silt (2-10 μm), which is commonly transported in suspension by bottom currents (nepheloid transport, Darby et al., 2009). The second factor is linked with the coarse silt (35 μm), which is likely to be supplied by sea ice (Hebbeln, 2000). The third factor is related to the very fine grain sizes, which is believed to be brought by currents and anchor ice, formed in the shelf zones and containing entrapped clay particles (Darby et al., 2009). Based on the grain-size distribution in sediments, we decided to extract the clay fraction for the isotopic analyses in order to avoid the possible mixing of the source signals. Therefore, the results of isotopic investigations should not be grain-size dependant. In addition to the clay fraction, we performed several measurements on the bulk samples to find out if the isotopic signal shows similar results and to make a guess about the isotopic fractionation and carriers of the obtained signature. In several tests, results yielded slight difference in the Nd and Pb isotope ratios when measured on clay and bulk fractions. Bulk sediments from the pink layers are characterized by less negative εNd and higher $^{207}Pb/^{206}Pb$ values than clay fraction, tending to demonstrate the numbers closer to the range obtained for the brown units, therefore, indicating dilution of the signal. This fact supports the preferential selection of clay fraction for the isotopic analyses.

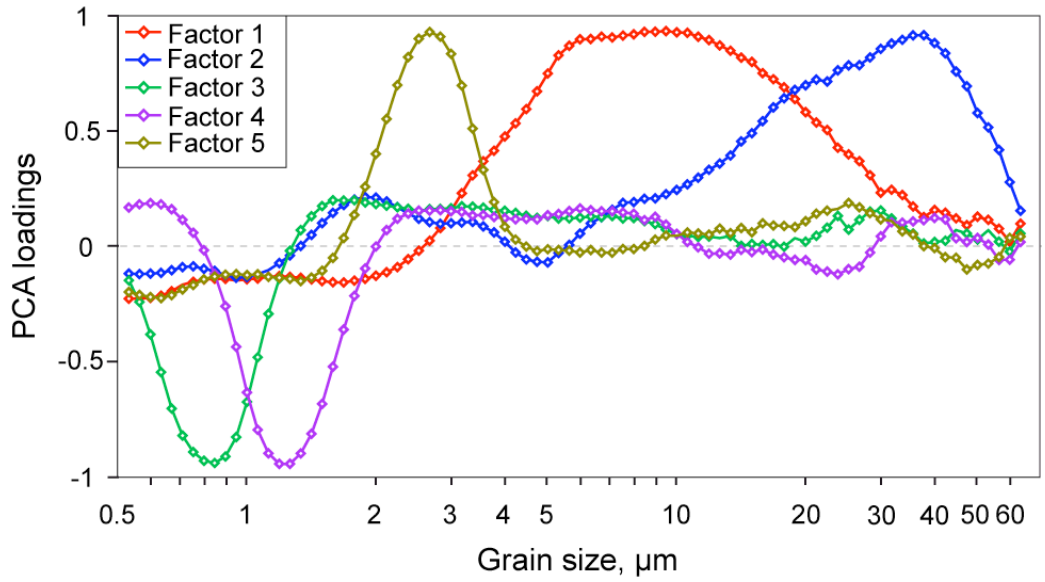

Figure 29. Results of the principal component analysis (PCA) performed on the grain-size data of core PS72/340-5 obtained from the sedigraph measurements (0.5 - 63 μm, logarithmic scale): PCA factor loadings for the first five factors (explaining 82% of the total variance).

Results of Nd and Pb isotope measurements are available online at http://doi.pangaea.de/10.1594/PANGAEA.802671 and http://doi.pangaea.de/10.1594/PANGAEA.802672, respectively. In case of high analytical errors, either a replicate was measured or the obtained values were excluded in further interpretations. Downcore profile of core PS72/340-5 (Fig. 30) displays distinct alterations of sediment colour which is changing along with the grain-size distribution in sediments. The fine-grained grey units are characterized by the highest $^{207}Pb/^{206}Pb$ and εNd (-9 to -8) values in the core. Distinct minima of $^{207}Pb/^{206}Pb$ and εNd (-15 to -17.8) are consistent with the very coarse-grained pink-white layers that occur at the depth of 90, 317 and 510 cm marked by the dolomite maxima. At the same time, relative abundance of smectite in the clay fraction is decreasing down to 0-5 % at 90 and 317 cm core depth while contents of illite increase up to 60% (with the average of 40 % throughout the core). Contents of chlorite and kaolinite remain relatively constant throughout the core (10 and 20-30 %, respectively). However the calculated contents of smectite and chlorite are too low for a good estimation (±5-10%) of clay mineral proportion as the amount of individual components should exceed 20 % (Biscaye, 1965).

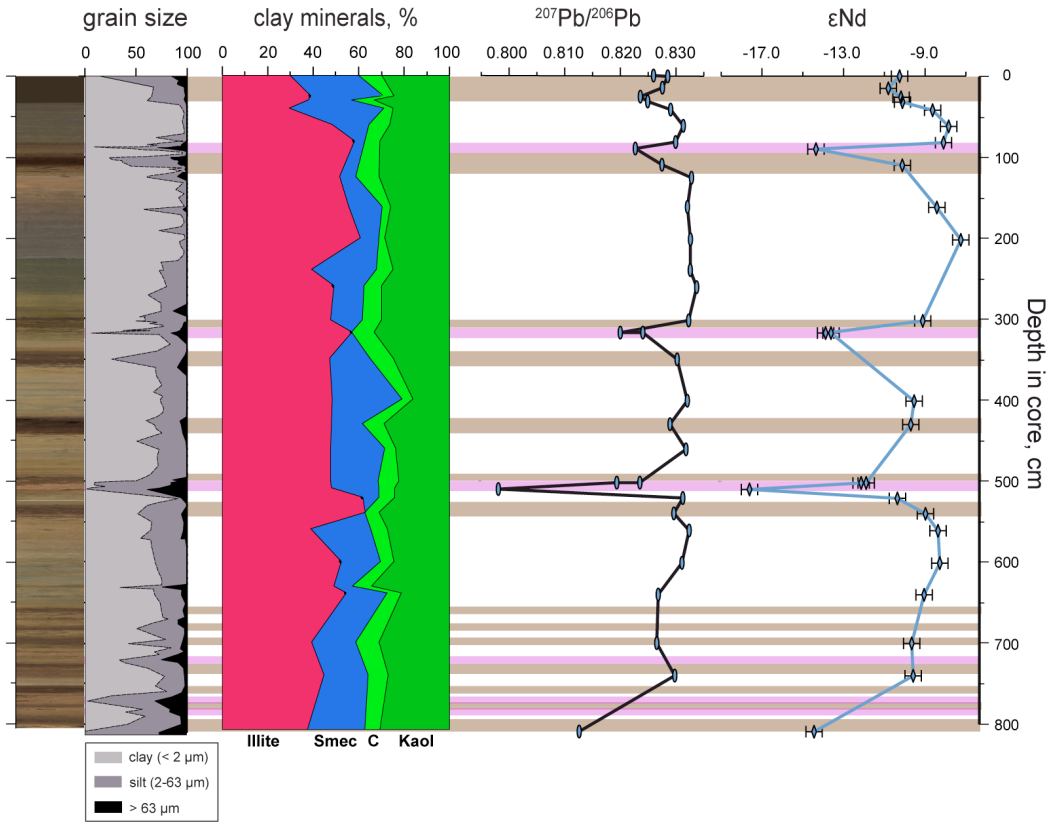

Figure 30. Results of measurements performed on the clay fraction of PS72/340-5 sediments: relative percentage of clay minerals (illite, smectite, chlorite, kaolinite); $^{207}Pb/^{206}Pb$ and εNd (± 2σ=0.4). Results are plotted against the spliced digital core images. Colour bars mark the brown and pink-white lithological units. Lithology and grain-size distribution are described in details in *Ch. 6*.

7.4 Discussion

Obtained sediment isotopic compositions of radiogenic Pb and Nd were compared with the values for the volcanic and magmatic rocks outcropping in the circum-Arctic region (Fig. 31). In this compilation we show provinces of different tectonic settings which are characterized by variable εNd and ratios of different Pb isotopes, also traced in the rivers draining through the land. Marine surface sediments partly inherit the signature of the adjacent terrains but also get the influence of different water masses due to oceanic circulation. Therefore, land-based rocks seem to be a better object for comparison as their signal is more conservative (Asahara et al., 2012; Fagel and Mattielli, 2011).

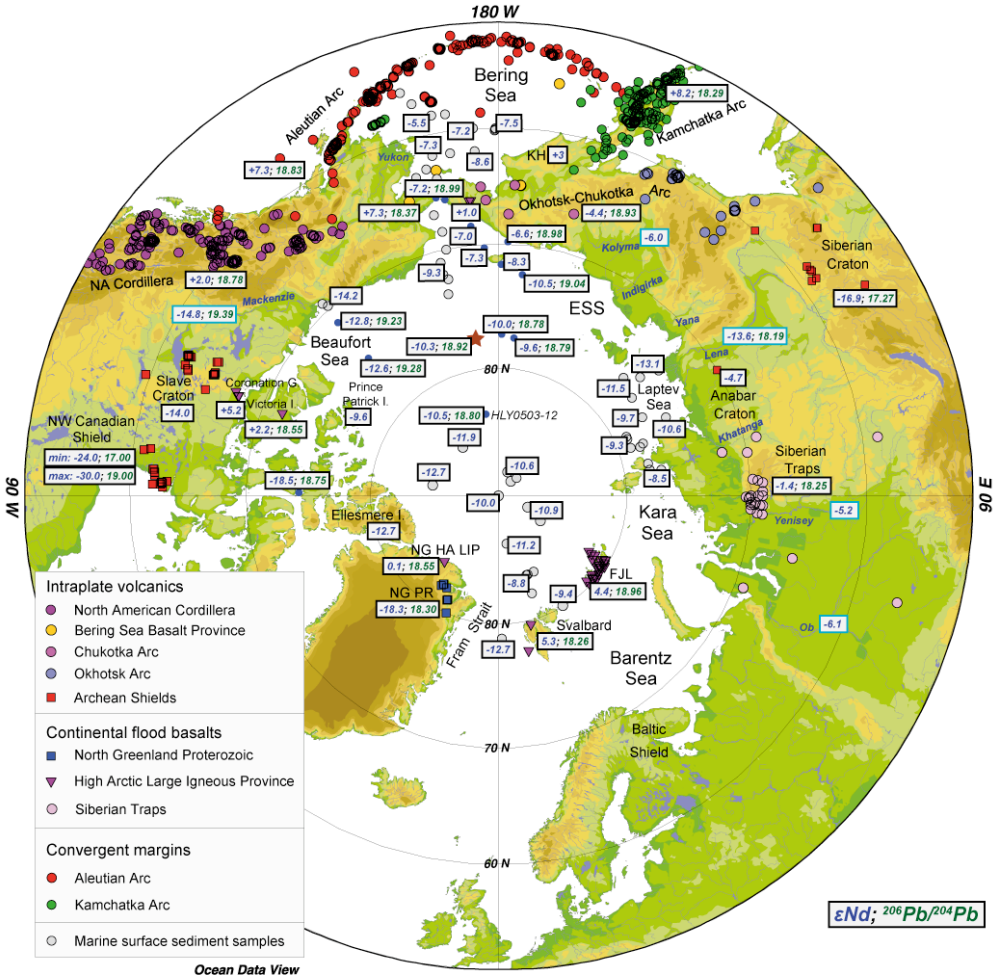

Figure 31. Circum-Arctic values of εNd and $^{206}Pb/^{204}Pb$ (compilation from Fagel et al. (subm.), suppl.). Data for land-based rocks from different tectonic settings are compiled from the GEOROC database (GEOROC, 2003; and references therein). Marine surface sediment values are from published data (Asahara et al., 2012; Eisenhauer et al., 1999; Haley et al., 2008; Tütken et al., 2002; Winter et al., 1997). River water data for Kolyma, Yenisey and Ob are from Zimmermann et al. (2009) and Porcelli et al. (2009). Values for the Mackenzie and Lena rivers suspended matter are from Millot et al. (2004). Dark-blue circles mark the locations of surface samples from this study (see Fig. 25, Table 9 for coordinates) as well as of core HLY0503-12 (Fagel et al., subm.). Location of core PS72/340-5 is highlighted by red star.

In Figure 32 literature data and results from core PS72/340-5 are plotted as $^{207}Pb/^{206}Pb$ versus εNd. Data points from different lithological units are located along a potential mixing line. Dolomite-rich pink layers are characterized by the lowest smectite contents, which can be an additional evidence for the North American sediment source in contrast to the Lena River flowing into the Laptev Sea area, with the eastern part of this basin known for high smectite contents (e.g. Wahsner et al., 1999).

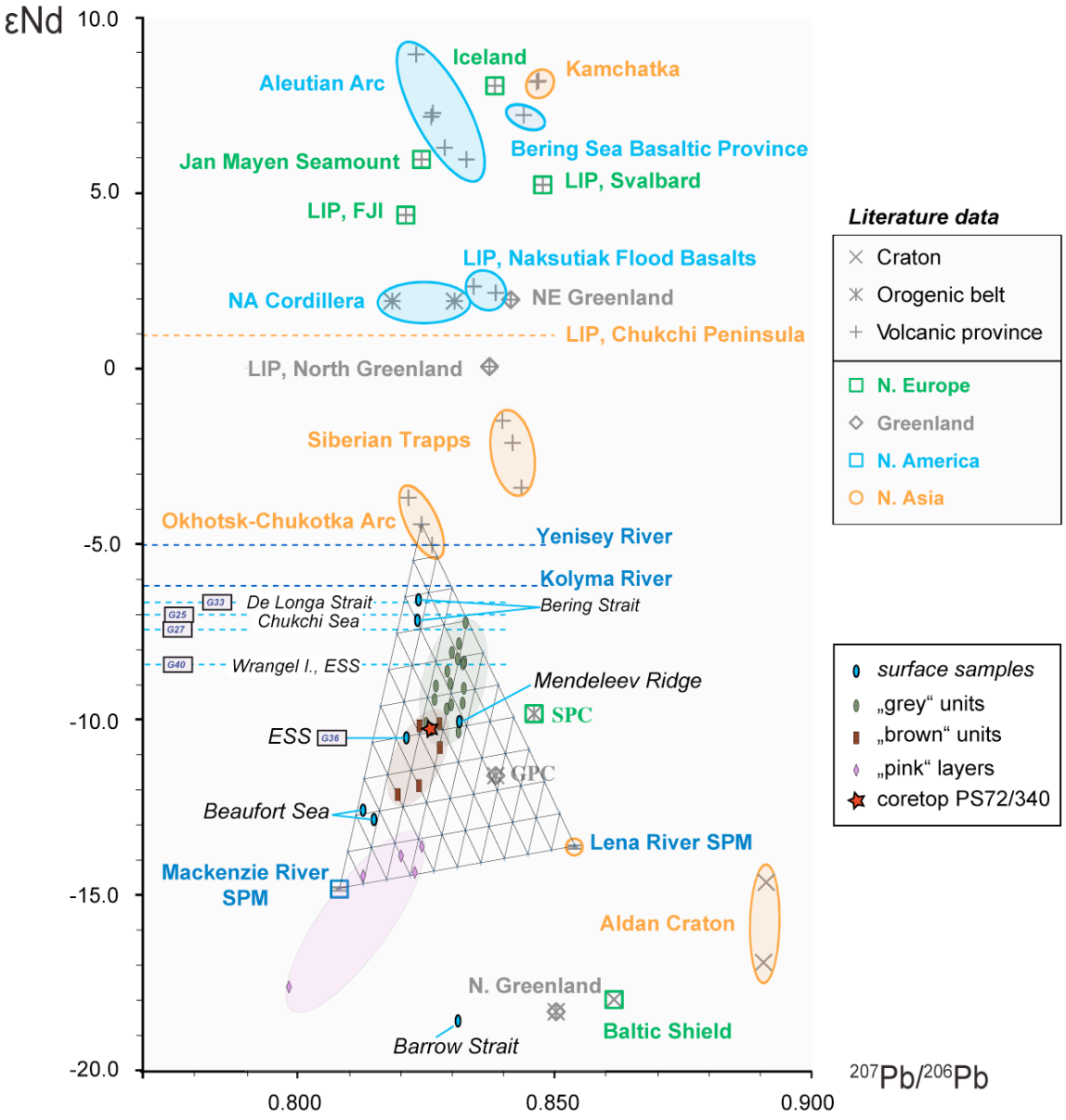

Figure 32. Biplot of $^{207}Pb/^{206}Pb$ and εNd values from the circum-Arctic compilation (Fagel et al., subm.), supplemented by the mixing model for the core PS72/340-5 sediments and surface samples from this study (locations are shown in Fig. 25). Values for literature data are shown for locations from Fig. 28 (see references there). The proposed end-members at the tops of the mixing grid are represented by the Lena River SPM (suspended matter), Mackenzie River SPM and Okhotsk-Chukotka Arc (see text for details).

Taking into account mineralogical composition of various units as well as the isotopic values corresponding to surface sediments from the Arctic Ocean, also shown in Fig. 32, we can suggest that terrigenous material was transported from North American and Eurasian sediment sources. Coming back to the problem of provenance discrimination between the Siberian sediment sources concerning core PS72/340-5 (Bazhenova et al., *in prep*. for QSR, *Ch.* 6), more geochemical evidence is needed to distinguish between the sediment supply areas such as Chukchi, East Siberian and Laptev Seas. However it is rather difficult to decide about the possible sediment provenance only based on the isotopic signatures as geographically widely distributed provinces can have the same geological age and originate from similar magmatic source. Nevertheless, volcanic rocks are the main carriers of Nd while igneous rocks are normally enriched in Pb. To help identify the potential volcanic end-member for the mixing diagram, X-Ray fluorescence (XRF) bulk geochemical data of core PS72/340-5, published by März et al. (2011), were utilized. However it turned out that not all the classification approaches can be used for this purpose, because bulk data plotted as REE spectra and spidergrams (Wood et al., 1979) do not indicate a clear change of the sediment sources with time, in spite of the variable grain-size and mineralogical composition of different time slices, as was also observed in the central Arctic Ocean core HLY0503-12 (location shown in Fig. 31) by Fagel et al. (subm.). At the same time, according to principles of classification of volcanic rocks (e.g. Pearce and Cann, 1973) element ratios can be more useful for provenance discrimination as exemplified by comparison of Rb and Ba concentrations shown in Fig. 33. Here one can clearly distinguish between the fields comprising the isotopic values from Okhotsk-Chukotka Arc versus the Siberian Traps.

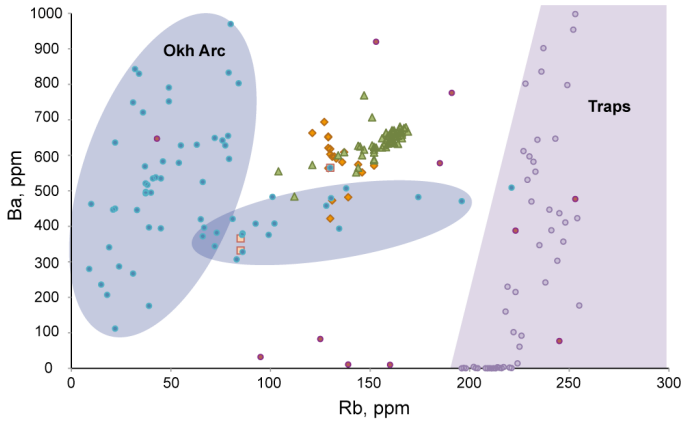

Figure 33. Rb-Ba diagram used for discrimination of the potential volcanic end-members. Data from core PS72/340-5 (pink, brown and grey units; same legend as in the diagram in Fig. 32) show values close to the rocks of Okhotsk-Chukotka Arc (blue and purple dots; same legend used as on the map in Fig. 31), while Rb values for the Siberian Traps are much higher (light-lilac dots).

Based on the isotopic and inorganic geochemical composition of sediments, three end-members for the mixing analysis were set as the Lena River SPM (suspended matter), Mackenzie River SPM and Okhotsk-Chukotka Volcanic Arc. Most of the dots lie along the 2-3 axis, indicating more the less constant contribution from the 1st member. Significant variations in the volcanic compound (εNd) are attributed to changes from the finest to the coarsest (and dolomite-rich) sediments, displaying the provenance shift from the Asian margin to the North American. The outlier belongs to the sample from the depth of 510 cm in core PS72/340-5 corresponding to a prominent pink layer with dolomite contents increased to 80 wt% as evidenced by bulk mineralogical analysis (see *Chapter 6*). This interval also contains several dolomite dropstones up to 10 cm in diameter (Stein et al., 2010). Dolomite was described to be a common mineral in surface samples of the Beaufort Sea (e.g.Belov and Lapina, 1961; Bischof et al., 1996). Vast carbonate province of Cambrian-Devonian age outcropping on the Canadian Arctic Archipelago is considered to be the main source for dolomites in the Arctic Ocean sediments. In core PS72/340-5, the isotopic signal from the pink-white layer at 510 cm cannot be unmixed using only the chosen three end-members, however, this very low εNd value is close to the one obtained for the surface sample from the Barrow Strait (Canadian Arctic Archipelago). Additionally, biomarker tests on the dolomite dropstones from these two locations show similarity (V.Petrova and A.Krylov, VNIIO, unpubl. data), which can be indicative of the same sediment sources.

The proposed end-members were used together with the two tracers in a mixing model (Fig. 32) trying to meet the assumptions that 1) tracers are conservative (no chemical reactions); 2) all components have significantly different concentrations for at least 1 tracer . Based on the calculated grid (see *Methods, Ch. 7.2.4*, for more details), we estimated the relative contribution of the proposed end-members to the $^{207}Pb/^{206}Pb$ and εNd sediment values over time as shown in Figure 34.

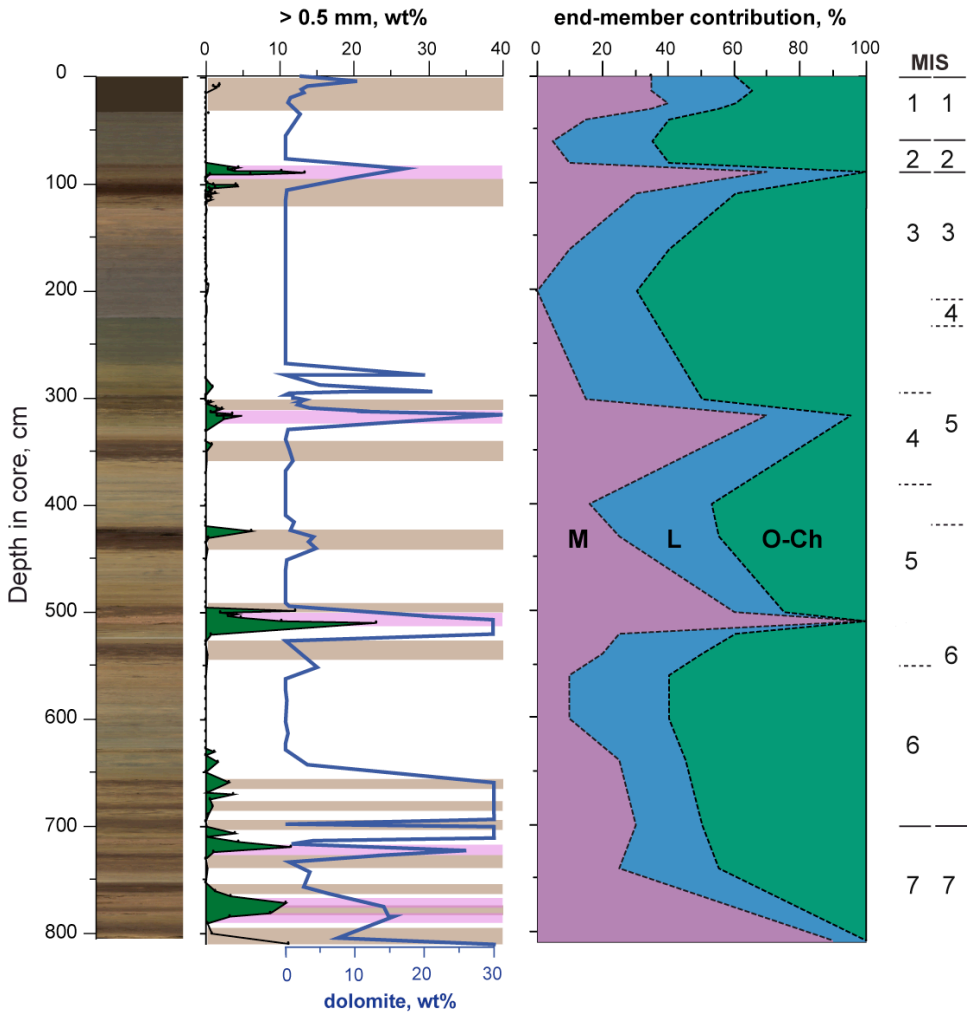

Figure 34. Unmixing of isotopic compositions of Nd and Pb in core PS72/340-5. The three end-members are represented by the Mackenzie River SPM (M), Lena River SPM (L) and Okhotsk-Chukotka Volcanic Arc (O-Ch). Note that signal at 510 cm (corresponding to the third, very prominent, pink layer) cannot be unmixed using only these three end-members (see text for possible explanations). Dolomite and grain-size data are from Bazhenova et al. (*Ch.* 6).

For the last two glacial/interglacial cycles (age model as discussed in *Chapter 6*) signal from North American sources is associated with the coarsest material as displayed by the pronounced maxima corresponding to the pink layers. Supply from the Laptev Sea area remained relatively constant as indicated by the isotopic mixing and lower smectite contents. Therefore, most of the late Quaternary sediment supply variability in core PS72/340-5 can be explained by temporal shifts in sediment transport from North America versus Chukchi and East Siberian Seas (Fig. 35), or by intensification of the former source strength as no quantitative estimations of sediment fluxes can be provided at this stage of study. Further investigations could be done with higher sampling/temporal resolution to provide more implications for the paleoenvironmental reconstructions.

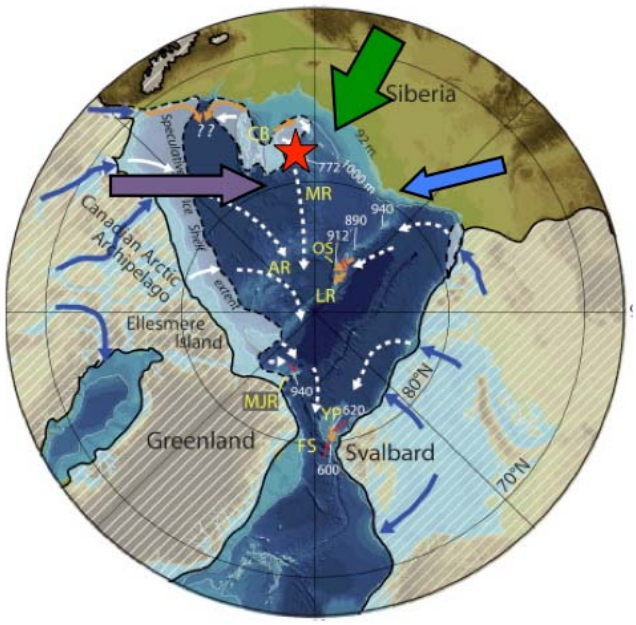

Figure 35. Circum-Arctic map showing tentative reconstruction of MIS 6 ice shelves (Jakobsson et al., 2010; see Fig. 6 for more details). Arrows mark the sediment sources as identified by the $^{207}Pb/^{206}Pb$ and εNd mixing model in core PS72/340-5 (see Fig. 34). Core location is marked with red star.

7.5 Conclusions

As exemplified by the grain-size, mineralogical and Nd and Pb isotope record of core PS72/340-5, the last 200 ka variations of sediment supply at the eastern flank of the Mendeleev Ridge can be mostly attributed to changing contributions from NE Russian vs. North American sources. Over this time period, sedimentation was mostly controlled by terrigenous input from the Chukchi and East Siberian Seas with less prominent but relatively stable contribution from the Laptev Sea. Isotopic signature of radiogenic Pb and Nd confirmed the Canadian origin of material which constitutes the pink dolomite-rich layers in the Amerasian Basin.

7.6 Acknowledgements

We thank the scientific party, the Captain and the Crew on the "Polarstern" ARK-XXIII/3 Cruise (2008). Research stay of EB at the University of Liege was supported by the outgoing scholarship of the Helmholz Graduate School for Polar and Marine Research (POLMAR). C. März is acknowledged for sharing the XRF bulk data for core PS72/340-5. E. Gusev (VNIIO) kindly shared surface samples from the RUSACLA-2009 Expedition. J. Oten is thanked for help with sample preparations in the clean lab at the University of Liege. Grain-size analysis was performed at the Otto-Schmidt-Laboratory in the frame of research grant to EB and SK (grant OSL-11-04).

8 Conclusions and outlook

This PhD thesis focused on sediment records from the Mendeleev Ridge spanning the last 200 ka. One of the main goals of this study was to identify mineralogical and inorganic-geochemical tracers in marine sediments that could be used for discrimination of sediment provenance and consequently for reconstruction of sediment pathways.

During this study, a lot of time was spent on testing the RockJock software developed for quantification of mineral assemblages from the X-Ray diffraction (XRD) data. It was shown that RockJock results for non-clay minerals are quite reliable while contents of clay minerals should be reported cautiously as it is difficult to distinguish some of these minerals without special treatment. Detailed investigations were carried out on a new set of surface samples from the Arctic Ocean to check the possibility of provenance discrimination based on the bulk mineral composition of sediments. Comparison with literature data demonstrated that in provenance studies bulk mineral assemblages should be used along with other indicators for source areas.

Changes of sedimentary settings along the studied transect from the Mendeleev Ridge towards the East Siberian Sea margin were documented for the last 200 ka. As evidenced by grain-size data, there were several events of intensified sediment discharge at the Mendeleev Ridge possibly linked to paleoenvironmental changes in North America and Eurasia. Bulk mineralogical data measured on 4 cores did not provide new insights into the origin of the ice-rafted material. Consequently, new approach was applied for provenance studies using the isotopic composition of radiogenic lead (Pb) and neodymium (Nd) of detrital fraction in core PS72/340-5 from the eastern flank of the Mendeleev Ridge. Sediment supply variability was analyzed using the mixing model constrained by two tracers: $^{207}Pb/^{206}Pb$ and εNd. Our results confirm that over the last 200 ka dolomite-rich pink layers at the southern Mendeleev Ridge were deposited during events associated with intensified iceberg transport from North America.

To provide more insight into the sediment provenance for dolomite-rich layers, several measurements of the biomarker composition were carried out at the AWI and at VNIIOkeangeologia (St.Petersburg, Russia). At VNIIO, the tests were done on dropstones (dolomites), from box corer PS72/287-1 (Barrow Strait), core PS72/340-5 (depth of 510 cm, corresponding to the third, very prominent, pink layer) and core PS72/396-5 (depth of 15 cm) (all the three locations were cored during the ARK-XXIII/3 Expedition, see Fig. 31). Based on

the results for dropstones, all the three samples look similar. However, they are different from the dolomites that were found in the Labrador Sea as dropstones (and H-layers) and in the onshore carbonate formations in the Hudson Area. Although most compounds are similar, those carbonates have a C34/C33 < 1, meaning that the C34 hopanoids dominate over the C33 ones (a very unusual feature) (B.D.A. Naafs, pers. comm.). The three dropstones from the ARK-XXIII/3 Expedition contain less C34 than C33 which is normally the case. We can suggest that the Labrador Sea and the Hudson Area were not the source for our dropstones.

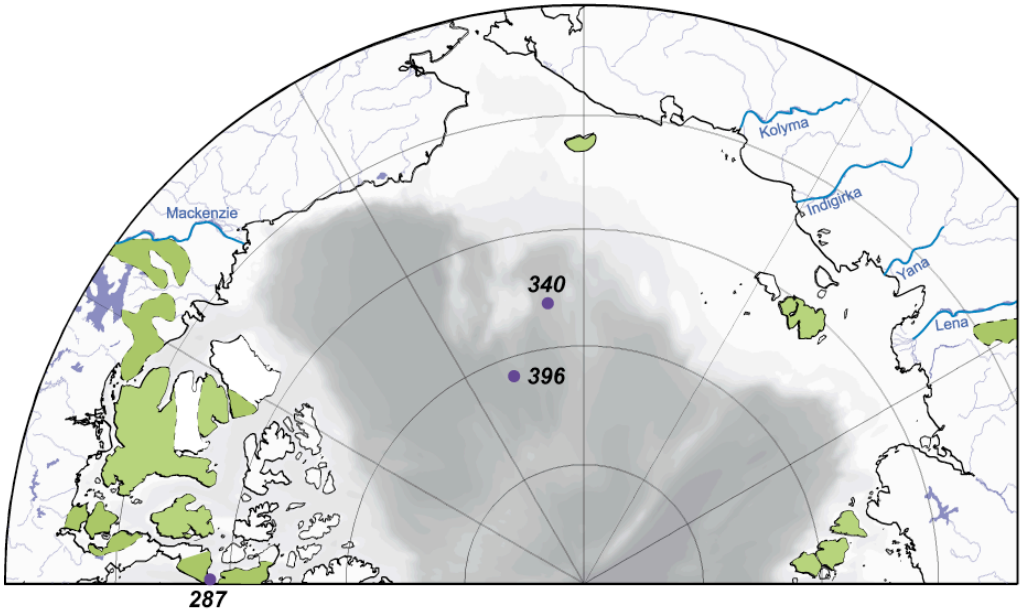

Figure 36. Geographical locations of large-sized dropstones (dolomites) used for biomarker analysis. Cores PS72/2871-1 (287), PS72/340-5 (340) and PS72/396-5 (396) were recovered during the ARK-XIII/3 Expedition (Jokat, 2009). Early Paleozoic carbonate provinces outcropping in North America and Eurasia are marked with green, compilation is based on geological maps compiled by Trettin (1991) and Petrov et al. (1995).

At the AWI, a bulk sample was analyzed from core PS72/340-5 (same depth of 510 cm). Although it is difficult to be sure, this sample also looks a bit different from the analyzed dropstones as it does not contain a lot of hopanes, but this could be related to the fact that this sample was measured in a lower concentration. In addition, the signal of the bulk sample could be diluted in comparison to the pure rock. So we can propose that the pink-white layer in core PS72/340-5 is not purely composed of dolomite from the studied dropstones. Additionally, it seems that the source of the Arctic Ocean detrital layers is different from what was found in the Labrador and North Atlantic. The specific feature of the material in the North Atlantic is that the carbonate formations also contain several organic rich shale formations that give a lot of other very indicative aromatic compounds. The pink-white layer in core PS72/340-5 does not

contain any of those compounds, possibly indicating that the source is made of pure carbonate formations that do not contain organic-rich shales which could be an evidence for input from Victoria and Banks Islands. This area of the Canadian Arctic Archipelago has vast carbonate outcrops of Cambrian-Devonian age which are considered to be the main source for dolomites in the Arctic Ocean sediments (Belov and Lapina, 1961; Bischof et al., 1996; Dalrymple and Maass, 1987; Darby et al., 1989) as discussed in more details in *Chapter 5*. Consequently, more detailed information about these rocks is needed to continue the provenance studies.

9 Data handling

All data presented in this thesis will be publicly available online in the PANGAEA database at https://www.pangaea.de.

10 References

Adler, R. E., Polyak, L., Ortiz, J. D., Kaufman, D. S., Channell, J. E. T., Xuan, C., Grottoli, A. G., Sellen, E., and Crawford, K. A. (2009). Sediment record from the western Arctic Ocean with an improved Late Quaternary age resolution: HOTRAX core HLY0503-8JPC, Mendeleev Ridge. *Global and Planetary Change* **68,** 18-29.

Andrews, J. T., and Eberl, D. D. (2007). Quantitative mineralogy of surface sediments on the Iceland Shelf, and application to down-core studies of Holocene ice-rafted sediments. *J. Sed. Res.* **77,** 469-479.

Andrews, J. T., and Eberl, D. D. (2011). Surface (sea floor) and near-surface (box cores) sediment mineralogy in Baffin Bay as a key to sediment provenance and ice sheet variations. *Canadian Journal of Earth Sciences* **48,** 1307-1328.

Andrews, J. T., and Eberl, D. D. (2012). Determination of sediment provenance by unmixing the mineralogy of source-area sediments: The "SedUnMix" program. *Marine Geology* **291-294,** 24-33.

Asahara, Y., Takeuchi, F., Nagashima, K., Harada, N., Yamamoto, K., Oguri, K., and Tadai, O. (2012). Provenance of terrigenous detritus of the surface sediments in the Bering and Chukchi Seas as derived from Sr and Nd isotopes: Implications for recent climate change in the Arctic regions. *Deep Sea Research Part II: Topical Studies in Oceanography* **61-64,** 155-171.

Backman, J., Fornaciari, E., and Rio, D. (2009). Biochronology and paleoceanography of late Pleistocene and Holocene calcareous nannofossil abundances across the Arctic Basin. *Marine Micropaleontology* **72,** 86-98.

Backman, J., Jakobsson, M., Lovlie, R., Polyak, L., Febo, L. A., and A., L. (2004). Is the central Arctic Ocean a sediment starved basin? *Quaternary Science Reviews* **23,** 1435-1454.

Basilyan, A. E., Nikolskiy, P. A., Maksimov, F. E., and Kuznetsov, V. Y. (2010). Age of cover glaciation of the New Siberian Islands based on 230Th/U-dating of mollusc shells. *In* "Structure and history of development of the lithosphere." pp. 506-514. Paulsen, Moscow*; in Russian.*

Behrends, M., Hoops, E., and Peregovich, B. (1999). Distribution patterns of heavy minerals in Siberian rivers, the Laptev Sea and the eastern Arctic Ocean: an approach to identify sources, transport and pathways of terrigeneous matter. *In* "Land-ocean systems in the Siberian Arctic: Dynamics and history." (H. Kassens, H. A. Bauch, I. Dmitrenko, H. Eicken, H.-W. Hubberten, M. Melles, J. Thiede, and L. A. Timokhov, Eds.), pp. 265-286. Springer, Berlin.

Belov, N. A., and Lapina, N. N. (1961). "Bottom sediments of the Arctic Ocean." Gidrometeoizdat, Leningrad.

Bianchi, G. G., Hall, I. R., McCave, I. N., and Joseph, L. (1999). Measurement of the sortable silt current speed proxy using the Sedigraph 5100 and Coulter Multisizer IIe: precision and accuracy. *Sedimentology* **46,** 1001-1014.

Biscaye, P. E. (1965). Mineralogy and sedimentation of recent deep-sea clay in the Atlantic Ocean and adjacent seas and oceans. *Geological Society of America Bulletin* **76,** 803-832.

Bischof, J., Clark, D. L., and Vincent, J.-S. (1996). Origin of Ice-Rafted Debris: Pleistocene Paleoceanography in the Western Arctic Ocean. *Paleoceanography* **11,** 743-756.

Bischof, J. F., and Darby, D. A. (1997). Mid- to Late Pleistocene Ice Drift in the Western Arctic Ocean: Evidence for a Different Circulation in the Past. *Science* **277,** 74-78.

Blott, S. J., and Pye, K. (2001). GRADISTAT: a grain size distribution and statistics package for the analysis of unconsolidated sediments. *Earth Surface Processes and Landforms* **26,** 1237-1248.

Channell, J. E. T., and Xuan, C. (2009). Self-reversal and apparent magnetic excursions in Arctic sediments. *Earth and Planetary Science Letters* **284,** 124-131.

Channell, J. E. T., Xuan, C., and Hodell, D. A. (2009). Stacking paleointensity and oxygen isotope data for the last 1.5 Myr (PISO-1500). *Earth and Planetary Science Letters* **283,** 14-23.

Chauvel, C., and Blichert-Toft, J. (2001). A hafnium isotope and trace element perspective on melting of the depleted mantle. *Earth and Planetary Science Letters* **190,** 137-151.

Clark, D. L., Whitman, R. R., Morgan, K. A., and Mackey, S. D. (1980). Stratigraphy and glacial-marine sediments of the Amerasian Basin, Central Arctic Ocean. *In* "Special Paper." The Geological Society of America, Boulder, Colorado.

Cronin, T. M., Gemery, L., Briggs Jr, W. M., Jakobsson, M., Polyak, L., and Brouwers, E. M. (2010). Quaternary Sea-ice history in the Arctic Ocean based on a new Ostracode sea-ice proxy. *Quaternary Science Reviews* **29,** 3415-3429.

Cronin, T. M., Smith, S. A., Eynaud, F., O'Regan, M., and King, J. (2008). Quaternary paleoceanography of the central Arctic based on Integrated Ocean Drilling Program Arctic Coring Expedition 302 foraminiferal assemblages. *Paleoceanography* **23**.

Dalrymple, R. W., and Maass, O. C. (1987). Clay mineralogy of late Cenozoic sediments in the CESAR cores, Alpha Ridge, central Arctic Ocean. *Canadian Journal of Earth Sciences* **24,** 1562-1569.

Danzeglocke, U., Jöris, O., and Weninger, B. (2007). CalPal-2007online; http://www.calpal-online.de/

Darby, D. A. (1971). "Carbonate cycles and clay mineralogy of Arctic Ocean sediment cores." Unpublished PhD thesis, University of Wisconsin.

Darby, D. A. (1975). Kaolinite and other clay minerals in Arctic Ocean sediments. *J. Sed. Petrol.* **45,** 272-279.

Darby, D. A., Myers, W. B., Jakobsson, M., and Rigor, I. (2011). Modern dirty sea ice characteristics and sources: The role of anchor ice. *J. Geophys. Res.* **116,** C09008.

Darby, D. A., Naidu, A. S., Mowatt, T. C., and Jones, G. (1989). Sediment composition and sedimentary processes in the Arctic Ocean. *In* "The Arctic Seas: Climatology, Oceanography, Geology and Biology." (Y. Herman, Ed.), pp. 657-720. Van Nostrand Reinhold, New York.

Dudarev, O. V. (2008). Cruise report International Siberian Shelf Study 2008 (ISSS-08). Swedish Knut and Alice Wallenberg Foundation, the Far-Eastern Branch of the Russian Academy of Sciences, the Swedish Research Council, the Russian Foundation for Basic Research, NOAA, and the Swedish Polar Research Secretariat; http://epic.awi.de/28987/1/Dud2008a.pdf

Dyke, A. S., Andrews, J. T., Clark, P. U., England, J. H., Miller, G. H., Shaw, J., and Veillette, J. J. (2002). The Laurentide and Innuitian ice sheets during the Last Glacial Maximum. *Quaternary Science Reviews* **21,** 9-31.

Eberl, D. D. (2003). User guide to RockJock: A program for determining quantitative mineralogy from X-ray diffraction data. U.S. Geological Survey, Washington, DC.

Ehlers, J., and Gibbard, P. L. (2007). The extent and chronology of Cenozoic Global Glaciation. *Quaternary International* **164-165,** 6-20.

Eisenhauer, A., Meyer, H., Rachold, V., Tütken, T., Wiegand, B., Hansen, B. T., Spielhagen, R. F., Lindemann, F., and Kassens, H. (1999). Grain size separation and sediment mixing in Arctic Ocean sediments: evidence from the strontium isotope systematic. *Chemical Geology* **158,** 173-188.

Elverhoi, A., and Ronningsland, T. M. (1978). Semiquantitative calculation of the relative amounts of kaolinite and chlorite by X-ray diffraction. *Marine Geology* **27,** M19-M23.

Emmermann, R., and Lauterjung, J. (1990). Double X-ray analysis of cuttings and rock flour: a powerful tool for rapid and reliable determination of borehole lithostratigraphy. *Scientific Drilling* **1,** 269-282.

England, J. H., Furze, M. F. A., and Doupe, J. P. (2009). Revision of the NW Laurentide Ice Sheet: implications for paleoclimate, the northeast extremity of Beringia, and Arctic Ocean sedimentation. *Quaternary Science Reviews* **28,** 1573-1596.

Fagel, N., Gueibe, J., Not, C., Mattielli, N., Bazhenova, E., Polyak, L., and Hillaire-Marcel, C. (subm.). Glacial/interglacial changes in sediment provenance in the central Arctic Ocean: Mineralogy, trace element and isotope Nd and Pb signature of detrital fraction. (*submitted to QSR)*

Fagel, N., and Mattielli, N. (2011). Holocene evolution of deep circulation in the northern North Atlantic traced by Sm, Nd and Pb isotopes and bulk sediment mineralogy. *Paleoceanography* **26,** PA4220.

Fairbanks, R. G., Mortlock, R. A., Chiu, T.-C., Cao, L., Kaplan, A., Guilderson, T. P., Fairbanks, T. W., Bloom, A. L., Grootes, P. M., and Nadeau, M.-J. (2005). Radiocarbon calibration curve spanning 0 to 50,000 years BP based on paired 230Th/234U/238U and 14C dates on pristine corals. *Quaternary Science Reviews* **24,** 1781-1796.

Faure, G. (1986). "Principles of Isotope Geology." John Wiley and Sons, New York.

Galer, S. J. G., and Abouchami, W. (1998). Practical Application of Lead Triple Spiking for Correction of Instrumental Mass Discrimination. *Mineralogical Magazine* **62A,** 491-492.

GEOROC. (2003). Geochemistry of Rocks of the Oceans and Continents. MPI für Chemie, Mainz, Germany; http://georoc.mpch-mainz.gwdg.de

Gobeil, C., Macdonald, R. W., Smith, J. N., and Beaudin, L. (2001). Atlantic Water Flow Pathways Revealed by Lead Contamination in Arctic Basin Sediments. *Science* **293,** 1301-1304.

Gordeev, V. V., and Sidorov, I. S. (1993). Concentrations of major elements and their outflow into the Laptev Sea by the Lena River. *Marine Chemistry* **43,** 33-45.

Gualtieri, L., Vartanyan, S., Brigham-Grette, J., and Anderson, P. M. (2003). Pleistocene raised marine deposits on Wrangel Island, northeast Siberia and implications for the presence of an East Siberian ice sheet. *Quaternary Research* **59,** 399-410.

Haley, B. A., Frank, M., Spielhagen, R. F., and Fietzke, J. (2008). Radiogenic isotope record of Arctic Ocean circulation and weathering inputs of the past 15 million years. *Paleoceanography* **23,** PA1S13.

Hamelin, B., Grousset, F., and Sholkovitz, E. R. (1990). Pb isotopes in surficial pelagic sediments from the North Atlantic. *Geochimica et Cosmochimica Acta* **54,** 37-47.

Hanslik, D., Jakobsson, M., Backman, J., Bjorck, S., Sellen, E., O'Regan, M., Fornaciari, E., and Skog, G. (2010). Quaternary Arctic Ocean sea ice variations and radiocarbon reservoir age corrections. *Quaternary Science Reviews* **29,** 3430-3441.

Henrich, R. (1989). Glacial/interglacial cycles in the Norwegian Sea: sedimentology, paleoceanography, and evolution of Late Pliocene to Quaternary Northern Hemisphere climate. *In* "Proceedings of the Ocean Drilling Program, Scientific Results." (O. Eldholm, J. Thiede, and E. Taylor, Eds.), pp. 189-232.

Huh, C. A., Pisias, N. G., Kelley, J. M., Maiti, T. C., and Grantz, A. (1997). Natural radionuclides and plutonium in sediments from the western Arctic Ocean: sedimentation rates and pathways of radionuclides. *Deep-Sea Research II* **44,** 1725-1743.

Innocent, C., Fagel, N., and Hillaire-Marcel, C. (2000). Sm-Nd isotope systematics in deep-sea sediments: clay-size versus coarser fractions. *Marine Geology* **168,** 79-87.

Jakobsson, M. (2002). Hypsometry and volume of the Arctic Ocean and its constituent seas. *Geochem. Geophys. Geosyst.* **3**.

Jakobsson, M., Grantz, A., Kristoffersen, Y., and Macnab, R. (2003). Physiographic provinces of the Arctic Ocean. *GSA Bulletin* **115,** 1443-1455.

Jakobsson, M., Løvlie, R., Al-Hanbali, H., Arnold, E., Backman, J., and Mörth, M. (2000). Manganese and color cycles in Arctic Ocean sediments constrain Pleistocene chronology. *Geology* **28,** 23-26.

Jakobsson, M., Macnab, R., Mayer, L., Anderson, R., Edwards, M., Hatzky, J., Schenke, H. W., and Johnson, P. (2008). An improved bathymetric portrayal of the Arctic Ocean: Implications for ocean modeling and geological, geophysical and oceanographic analyses. *Geophys. Res. Lett.* **35**.

Jakobsson, M., Nilsson, J., O'Regan, M., Backman, J., Löwemark, L., Dowdeswell, J. A., Mayer, L., Polyak, L., Colleoni, F., Anderson, L. G., Bjork, G., Darby, D., Eriksson, B., Hanslik, D., Hell, B., Marcussen, C., Sellen, E., and Wallin, A. (2010). An Arctic Ocean ice shelf during MIS 6 constrained by new geophysical and geological data. *Quaternary Science Reviews* **29,** 3505-3517.

Jokat, W. (2009). The expedition of the research vessel "Polarstern" to the Arctic in 2008 (ARK-XXIII/3) / Ed. by Wilfried Jokat with contributions of the participants. *In* "Berichte zur Polar- und Meeresforschung (Reports on Polar and Marine Research)." pp. 266. Alfred Wegener Institute for Polar and Marine Research, Bremerhaven.

Jones, R. W. (1994). "The *Challenger* Foraminifera." Oxford University Press.

Kaufman, D. S., Polyak, L., Adler, R., Channell, J. E. T., and Xuan, C. (2008). Dating late Quaternary planktonic foraminifer Neogloboquadrina pachyderma from the Arctic Ocean using amino acid racemization. *Paleoceanography* **23**.

Kim, B. I., and Slobodin, B. Y. (1991). Main stages of the eastern Arctic shelf history of Russia and Canadian Arctic in Paleogene and Neogene. *In* "Geology of the Circum-Amerasian folded zones." pp. 104-116. SevMorGeologia, St.Petersburg; *in Russian.*

Knies, J., Nowaczyk, N., Mueller, C., Vogt, C., and Stein, R. (2000). A multiproxy approach to reconstruct the environmental changes along the Eurasian continental margin over the last 150.000 years. *Marine Geology* **163,** 317-344.

Kosheleva, V. A., and Jashin, D. S. (1999). "The bottom sediments of the Russia Arctic Seas." VNIIOkeangeologia, St.Petersburg; *in Russian.*

Krylov, A. A., Andreeva, I. A., Vogt, C., Backman, J., Krupskaya, V. V., Grikurov, G. E., Moran, K., and Shoji, H. (2008). A shift in heavy and clay mineral provenance indicates a middle Miocene onset of a perennial sea ice cover in the Arctic Ocean. *Paleoceanography* **23**.

Krylov, A. A., Stein, R., and Ermakova, L. A. (2012). Clay minerals as indicators of late Quaternary sedimentary regimes at the Mendeleev Ridge (Amerasian Basin of the Arctic Ocean). *subm. to Lithology and Mineral Resources*; *in Russian.*

Laj, C., Kissel, C., and Beer, J. (2004). High Resolution Global Paleointensity Stack Since 75 kyr (GLOPIS-75) Calibrated to Absolute Values. *In* "Timescales of the Paleomagnetic Field." (J. E. T. Channell, D. V. Kent, W. Lowrie, and J. G. Meert, Eds.), pp. 255-265. American Geophysical Union, Washington D.C.

Lisiecki, L. E., and Lisiecki, P. A. (2002). Application of dynamic programming to the correlation of paleoclimate records. *Paleoceanography* **17,** 1049.

Lisiecki, L. E., and Raymo, M. E. (2005). A Pliocene-Pleistocene stack of 57 globally distributed benthic d18O records. *Paleoceanography* **20**.

Lisitzin, A. P. (2002). "Sea-ice and iceberg sedimentation in the ocean." Springer.

Loeblich, A. R., Jr., and Tappan, H. (1987). "Foraminiferal genera and their classification." VNR, New York.

Löwemark, L., Jakobsson, M., Mörth, M., and Backman, J. (2008). Arctic Ocean manganese contents and sediment colour cycles. *Polar Research* **27,** 105-113.

Maccali, J., Hillarie-Marcel, C., Carignan, J., and Reisberg, L. C. (2012). Pb isotopes and geochemical monitoring of Arctic sedimentary supplies and water mass export through Fram Strait since the Last Glacial Maximum. *Paleoceanography* **27,** PA1201.

Macdonald, R. W., Barrie, L. A., Bidleman, T. F., Diamond, M. L., Gregor, D. J., Semkin, R. G., Strachan, W. M. J., Li, Y. F., Wania, F., Alaee, M., Alexeeva, L. B., Backus, S. M., Bailey, R., Bewers, J. M., Gobeil, C., Halsall, C. J., Harner, T., Hoff, J. T., Jantunen, L. M. M., Lockhart, W. L., Mackay, D., Muir, D. C. G., Pudykiewicz, J., Reimer, K. J., Smith, J. N., Stern, G. A., Schroeder, W. H., Wagemann, R., and Yunker, M. B. (2000). Contaminants in the Canadian Arctic: 5 years of progress in understanding sources, occurrence and pathways. *The Science of the Total Environment* **254,** 93-234.

März, C., Stratmann, A., Matthiessen, J., Meinhardt, A. K., Eckert, S., Schnetger, B., Vogt, C., Stein, R., and Brumsack, H. J. (2011). Manganese-rich brown layers in Arctic Ocean sediments: Composition, formation mechanisms, and diagenetic overprint. *Geochimica et Cosmochimica Acta* **75,** 7668-7687.

Matthiessen, J., Niessen, F., Stein, R., and Naafs, B. D. A. (2010). Pleistocene glacial marine sedimentary environments at the eastern Mendeleev Ridge, Arctic Ocean. *Polarforschung* **79,** 123-137.

McCave, I. N., Manighetti, B., and Robinson, S. G. (1995). Sortable silt and fine sediment size/composition slicing: parameters for palaeocurrent speed and palaeoceanography. *Paleoceanography* **10,** 593-610.

McLennan, S. M. (2001). Relationships between the trace element composition of sedimentary rocks and upper continental crust. *Geochem. Geophys. Geosyst.* **2**.

Millot, R., Allegre, C.-J., Gaillardet, J., and Roy, S. (2004). Lead isotopic systematics of major river sediments: a new estimate of the Pb isotopic composition of the Upper Continental Crust. *Chemical Geology* **203,** 75-90.

Müller, C., and Stein, R. (2000). Variability of fluvial sediment supply to the Laptev Sea continental margin during Late Weichselian to Holocene times: implications from clay-mineral records. *International Journal of Earth Sciences* **89,** 592-604.

Munsell. (1974). Munsell Soil Colour Chart.

Naidu, A. S., Creager, J. S., and Mowatt, T. C. (1982). Clay mineral dispersal patterns in the north Bering and Chukchi Seas. *Marine Geology* **47,** 1-15.

Naidu, A. S., and Mowatt, T. C. (1983). Sources and dispersal patterns of clay minerals in surface sediments from the continental-shelf areas off Alaska. *Geological Society of America Bulletin* **94,** 841-854.

Norgaard-Pedersen, N., Mikkelsen, N., and Kristoffersen, Y. (2007). Arctic Ocean record of last two glacial-interglacial cycles off North Greenland/Ellesmere Island - Implications for glacial history. *Marine Geology* **244,** 93-108.

Norgaard-Pedersen, N., Spielhagen, R. F., Thiede, J., and Kassens, H. (1998). Central Arctic surface ocean environment during the past 80,000 years. *Paleoceanography* **13**.

Nowaczyk, N. R., Frederichs, T. W., Kassens, H., Norgaard-Pedersen, N., Spielhagen, R. F., Stein, R., and Weiel, D. (2001). Sedimentation rates in the Makarov Basin, central Arctic Ocean: a paleomagnetic and rock magnetic approach. *Paleoceanography* **16,** 368-389.

Nürnberg, D., Levitan, M., Pavlidis, J., and Shelekhova, E. (1995). Distribution of clay minerals in surface sediments from the eastern Barents and south-western Kara seas. *Geologische Rundschau* **84,** 665-682.

O'Regan, M., King, J., Backman, J., Jakobsson, M., Pälike, H., Moran, K., Heil, C., Sakamoto, T., Cronin, T. M., and Jordan, R. W. (2008). Constraints on the Pleistocene chronology of sediments from the Lomonosov Ridge. *Paleoceanography* **23**.

O'Regan, M., Williams, C. J., Frey, K. A., and Jakobsson, M. (2011). A synthesis of the long-term paleoclimatic evolution of the Arctic. *Oceanography* **24,** 66-80.

Omotoso, O., McCarty, D. K., Hillier, S., and Kleeberg, R. (2006). Some successful approaches to quantitative mineral analysis as revealed by the 3rd Reynolds Cup Contest. *Clays and Clay Minerals* **54,** 748-760.

Pearce, J. A., and Cann, J. R. (1973). Tectonic setting of basic volcanic rocks determined using trace element analyses. *Earth and Planetary Science Letters* **19,** 290-300.

Petrov, O., Strelnikov, S., Lopatin, B. G., Koren, T., Shokalsky, S., and Snezhko, V. (1995). Geological map of Russia, 1: 1000000. VSEGEI, St.Petersburg; *in Russian.*

Petschick, R., Kuhn, G., and Gingele, F. (1996). Clay mineral distribution in surface sediments of the South Atlantic: sources, transport, and relation to oceanography. *Marine Geology* **130,** 203-229.

Phillips, R. L., and Grantz, A. (2001). Regional variations in provenance and abundance of ice-rafted clasts in Arctic Ocean sediments: implications for the configuration of late Quaternary oceanic and atmospheric circulation in the Arctic. *Marine Geology* **172,** 91-115.

Polyak, L., Bischof, J., Ortiz, J. D., Darby, D. A., Channell, J. E. T., Xuan, C., Kaufman, D. S., Lшvlie, R., Schneider, D. A., Eberl, D. D., Adler, R. E., and Council, E. A. (2009). Late Quaternary stratigraphy and sedimentation patterns in the western Arctic Ocean. *Global and Planetary Change* **68,** 5-17.

Polyak, L., Curry, W. B., Darby, D. A., Bischof, J., and Cronin, T. M. (2004). Contrasting glacial/interglacial regimes in the western Arctic Ocean as exemplified by a sedimentary record from the Mendeleev Ridge. *Palaeogeography, Palaeoclimatology, Palaeoecology* **203,** 73-93.

Polyak, L., Darby, D. A., Bischof, J. F., and Jakobsson, M. (2007). Stratigraphic constraints on late Pleistocene glacial erosion and deglaciation of the Chukchi margin, Arctic Ocean. *Quaternary Research* **67,** 234-245.

Polyak, L., Edwards, M. H., Coakley, B. J., and Jakobsson, M. (2001). Ice shelves in the Pleistocene Arctic Ocean inferred from glaciogenic deep-sea bedforms. *Nature* **410,** 453-457.

Polyak, L., and Jakobsson, M. (2011). Quaternary sedimentation in the Arctic Ocean: Recent advances and further challenges. *Oceanography* **24,** 52-64.

Porcelli, D., Andersson, P. S., Baskaran, M., Frank, M., Björk, G., and Semiletov, I. (2009). The distribution of neodymium isotopes in Arctic Ocean basins. *Geochimica et Cosmochimica Acta* **73,** 2645-2659.

Rabineau, M., Berne, S., Olivet, J.-L., Aslanian, D., Guillocheau, F., and Joseph, P. (2006). Paleo sea levels reconsidered from direct observation of paleoshoreline position during Glacial Maxima (for the last 500,000 yr). *Earth and Planetary Science Letters* **252,** 119-137.

Roberts, A. P. (2008). Geomagnetic excursions: Knowns and unknowns. *Geophys. Res. Lett.* **35,** L17307.

Rudels, B., Jones, E. P., Schauer, U., and Eriksson, P. (2004). Atlantic sources of the Arctic Ocean surface and halocline waters. *Polar Research* **23,** 181-208.

RUSALCA. (2009). Report on the execution of marine research in the Bering Strait, East Siberian and Chukchi Sea by the Russian-American expedition under the program of "RUSALCA" during the period from 23 August through 30 September, 2009; http://www.arctic.noaa.gov/aro/russian-american/2009/RUSALCA_2009_report.pdf

Schlosser, P., Swift, J. H., Lewis, D., and Pfirman, S. L. (1995). The role of the large-scale Arctic Ocean circulation in the transport of contaminants. *Deep Sea Research Part II: Topical Studies in Oceanography* **42,** 1341-1367.

Sellen, E., O'Regan, M., and Jakobsson, M. (2010). Spatial and temporal Arctic Ocean depositional regimes: a key to the evolution of ice drift and current patterns. *Quaternary Science Reviews* **29,** 3644-3664.

Spielhagen, R. F., Baumann, K.-H., Erlenkeuser, H., Nowaczyk, N. R. N. R., Nшrgaard-Pedersen, N., Vogt, C., and Weiel, D. (2004). Arctic Ocean deep-sea record of northern Eurasian ice sheet history. *Quaternary Science Reviews* **23,** 1455-1483.

Spielhagen, R. F., Werner, K., Sorensen, S. A., Zamelczyk, K., Kandiano, E., Budeus, G., Husum, K., Marchitto, T. M., and Hald, M. (2011). Enhanced Modern Heat Transfer to the Arctic by Warm Atlantic Water. *Science* **331,** 450-453.

Stauch, G., and Gualtieri, L. (2008). Late Quaternary glaciations in northeastern Russia. *Journal of Quaternary Science* **23,** 545-558.

Stein, R. (1985). Rapid grain-size analyses of clay and silt fraction by SediGraph 5000D; comparison with Coulter counter and Atterberg methods. *J. Sed. Res.* **55,** 590-593.

Stein, R. (2008). "Arctic Ocean Sediments: Processes, Proxies, and Paleoenvironment." Elsevier.

Stein, R., Boucsein, B., Fahl, K., Garcia de Oteyza, T., Knies, J., and Niessen, F. (2001). Accumulation of particulate organic carbon at the Eurasian continental margin during late Quaternary times: controlling mechanisms and paleoenvironmental significance. *Global and Planetary Change* **31,** 87-104.

Stein, R., Grobe, H., and Wahsner, M. (1994). Organic carbon, carbonate, and clay mineral distributions in eastern central Arctic Ocean surface sediments. *Marine Geology* **119,** 269-285.

Stein, R., and Korolev, S. (1994). Shelf-to-basin sediment transport in the eastern Arctic Ocean. *In* "Russian-German cooperation in the Siberian shelf seas : geo-system Laptev Sea // Berichte zur Polarforschung (Reports on Polar Research)." (H. Kassens, Ed.), pp. 87-100. Alfred Wegener Institute for Polar and Marine Research, Bremerhaven.

Stein, R., Matthiessen, J., Niessen, F., Krylov, A., Nam, S., and Bazhenova, E. (2010). Towards a better (litho-) stratigraphy and reconstruction of Quaternary paleoenvironment in the Amerasian Basin (Arctic Ocean). *Polarforschung* **79,** 97-121.

Stoner, J. S., Channell, J. E. T., and Hillaire-Marcel, C. (1995). Late Pleistocene relative geomagnetic paleointensity from the deep Labrador Sea: Regional and global correlations. *Earth and Planetary Science Letters* **134,** 237-252.

Svendsen, J. I., Alexanderson, H., Astakhov, V. I., Demidov, I., Dowdeswell, J. A., Funder, S., Gataullin, V., Henriksen, M., Hjort, C., Houmark-Nielsen, M., Hubberten, H. W., Ingylfsson, У., Jakobsson, M., Kjaer, K. H., Larsen, E., Lokrantz, H., Lunkka, J. P., Lyse, A., Mangerud, J., Matiouchkov, A., Murray, A., Mцller, P., Niessen, F., Nikolskaya, O., Polyak, L., Saarnisto, M., Siegert, C., Siegert, M. J., Spielhagen, R. F., and Stein, R. (2004). Late Quaternary ice sheet history of northern Eurasia. *Quaternary Science Reviews* **23,** 1229-1271.

Trettin, H. P. (1991). "Geology of the Innuitian Orogen and Arctic Platform of Canada and Greenland ", Boulder, Colorado.

Tütken, T., Eisenhauer, A., Wiegand, B., and Hansen, B. T. (2002). Glacial-interglacial cycles in Sr and Nd isotopic composition of Arctic marine sediments triggered by the Svalbard/Barents Sea ice sheet. *Marine Geology* **182,** 351-372.

Vetrov, A. A., Semiletov, I. P., and Dudarev, O. V. (2008). Investigations of composition and origin of organic matter in the bottom sediments of the East Siberian Sea. *Geochemistry* **2,** 183-195; *in Russian.*

Vinogradov, V. A., Goryachev, Y. V., Gusev, E. A., and Suprunenko, O. I. (2008). Sedimentary cover of the East Russian Arctic shelf and conditions of its deposition in the land-ocean system *In* "60 years in the Arctic, the Antarctic and the World Ocean." (V. L. Ivanov, Ed.), pp. 63-78. VNIIOkeangeologia, St.Petersburg.

Viscosi-Shirley, C., Mammone, K., Pisias, N., and Dymond, J. (2003a). Clay mineralogy and multi-element chemistry of surface sediments on the Siberian-Arctic shelf: implications for sediment provenance and grain size sorting. *Continental Shelf Research* **23,** 1175-1200.

Viscosi-Shirley, C., Pisias, N., and Mammone, K. (2003b). Sediment source strength, transport pathways and accumulation patterns on the Siberian-Arctic's Chukchi and Laptev shelves. *Continental Shelf Research* **23,** 1201-1225.

Vogt, C. (1996). Bulk mineralogy in surface sediments from the eastern central Arctic Ocean. *In* "Surface-sediment composition and sedimentary processes in the central Arctic Ocean and along the Eurasian Continental Margin." (R. Stein, G. I. Ivanov, M. A. Levitan, and K. Fahl, Eds.), pp. 159-171. Berichte zur Polarforschung (Reports on Polar Research). Alfred Wegener Institute for Polar and Marine Research, Bremerhaven.

Vogt, C. (1997). Zeitliche und räumliche Verteilung von Mineralvergesellschaftungen in spätquartären Sedimenten des Arktischen Ozeans und ihre Nützlichkeit als Klimaindikatoren während der Glazial/Interglazial-Wechel // Regional and temporal variations of mineral assemblages in Arctic Ocean sediments as climatic indicator during glacial/interglacial changes. *Berichte zur Polarforschung (Reports on Polar Research)* **251,** pp. 309.

Vogt, C., Knies, J., Spielhagen, R. F., and Stein, R. (2001). Detailed mineralogical evidence for two nearly identical glacial/deglacial cycles and Atlantic water advection to the Arctic Ocean during the last 90,000 years. *Global and Planetary Change* **31,** 23-44.

Vogt, C., Lauterjung, J., and Fisher, R. X. (2002). Investigation of the clay fraction (<2 μm) of clay mineral society reference clays. *Clays and Clay Minerals* **50,** 388-400.

Wahsner, M., Mueller, C., Stein, R., Ivanov, G., Levitan, M., Shelekhova, E., and Tarasov, G. (1999). Clay-mineral distribution in surface sediments of the Eurasian Arctic Ocean and continental margin as indicator for source areas and transport pathways — a synthesis. *Boreas* **28,** 215-233.

Wasserburg, G. J., Jacousen, S. B., DePaolo, D. J., McCulloch, M. T., and Wen, T. (1981). Precise determination of Sm/Nd ratios, Sm and Nd isotopic abundances in standard solutions. *Geochimica et Cosmochimica Acta* **45,** 2311-2323.

Weingartner, T. J., Danielson, S., Sasaki, Y., Pavlov, V., and Kulakov, M. (1999). The Siberian Coastal Current: A wind- and buoyancy-forced Arctic coastal current. *J. Geophys. Res.* **104,** 29697-29713.

Weis, D., Kieffer, B., Maerschalk, C., Barling, J., de Jong, J., Williams, G. A., Hanano, D., Pretorius, W., Mattielli, N., Scoates, J. S., Goolaerts, A., Friedman, R. M., and Mahoney, J. B. (2006). High-precision isotopic characterization of USGS reference materials by TIMS and MC-ICP-MS. *Geochem. Geophys. Geosyst.* **7,** Q08006.

Winter, B. L., Johnson, C. M., and Clark, D. L. (1997). Strontium, neodymium, and lead isotope variations of authigenic and silicate sediment components from the Late Cenozoic Arctic Ocean: Implications for sediment provenance and the source of trace metals in seawater. *Geochimica et Cosmochimica Acta* **61,** 4181-4200.

Wood, D. A., Joron, J.-L., and Treuil, M. (1979). A re-appraisal of the use of trace elements to classify and discriminate between magma series erupted in different tectonic settings. *Earth and Planetary Science Letters* **45,** 326-336.

Xuan, C., Channell, J. E. T., Polyak, L., and Darby, D. A. (2012). Paleomagnetism of Quaternary sediments from Lomonosov Ridge and Yermak Plateau: implications for age models in the Arctic Ocean. *Quaternary Science Reviews* **32,** 48-63.

Zamoruyev, V. (2004). Quaternary glaciation of north-eastern Asia. *In* "Quaternary Glaciations—Extent and Chronology, Part III: South America, Asia, Africa, Australasia, Antarctica." (J. Ehlers, and P. L. Gibbard, Eds.), pp. 321-323. Developments in Quaternary Science. Elsevier, Amsterdam.

Zimmermann, B., Porcelli, D., Frank, M., Andersson, P. S., Baskaran, M., Lee, D.-C., and Halliday, A. N. (2009). Hafnium isotopes in Arctic Ocean water. *Geochimica et Cosmochimica Acta* **73,** 3218-3233.